Ph.D. Program in Civil, Chemical and Environmental Engineering

Curriculum in Chemical, Materials and Process Engineering

Department of Civil, Chemical and Environmental Engineering

Polytechnic School, University of Genoa, Italy.

Novel products for multilayer coating cycles used as smart strategy to increase energy efficiency and environmental sustainability of buildings: formulation, development and simulation models

Giulia Gaggero

NOVEL PRODUCTS FOR MULTILAYER COATING CYCLES USED AS SMART STRATEGY TO INCREASE ENERGY EFFICIENCY AND ENVIRONMENTAL SUSTAINABILITY OF BUILDINGS: FORMULATION, DEVELOPMENT AND SIMULATION MODELS

BY

GIULIA GAGGERO

Dissertation discussed in partial fulfillment of

the requirements for the Degree of

DOCTOR OF PHILOSOPHY

Civil, Chemical and Environmental Engineering

Curriculum in, Chemical, Material and Process Engineering

Department of Civil, Chemical and Environmental Engineering, University of Genoa, Italy

May, 2022

Adviser(s):
Prof. Rodolfo Botter – Department of Civil, Chemical and Environmental Engineering, University of Genoa, Via All'Opera Pia 15, 16145 Genoa, Italy

Prof. Marina Delucchi – Department of Civil, Chemical and Environmental Engineering, University of Genoa, Via All'Opera Pia 15, 16145 Genoa, Italy

Prof. Silvia Vicini- Department of Chemistry and Industrial Chemistry, University of Genoa, Via Dodecaneso 31, 16146 Genoa, Italy

Ing. Alessandro Beneventi- Boero Bartolomeo S.p.A., R&D "Riccardo Cavalleroni", Strada Comunale Savonesa 9, PST - Blocco F, Rivalta Scrivia, 15057 Tortona (AL), Italy

External Reviewers:

Prof. Irina Smirnova– Institute of Thermal Separation Processes, Hamburg University of Technology, Eißendorfer Straße 38, Hamburg, 21073, Germany

Prof. Alina Sionkowska Department of Chemistry of Biomaterials and Cosmetics, Faculty of Chemistry, Nicolaus Copernicus University in Toruń, 87-100 Torun, Poland

Ph.D. program in Civil, Chemical and Environmental Engineering

Curriculum in, Chemical, Material and Process Engineering

Cycle XXXIV

Giulia Gaggero

Acknowledgements

This PhD scholarship has been granted by the Regione Liguria under the Operational Program Liguria Region - European Social Fund 2014-2020, ASSE 3 "Education and training".

I want to express my deepest gratitude to my supervisors, Prof. Rodolfo Botter, Prof. Marina Delucchi and Prof. Silvia Vicini, for providing me invaluable guidance throughout this PhD work.

I would also like to acknowledge the several collaborators I had during these years:

- Prof. Alberto Lagazzo of the Department of the Department of Civil, Chemical and Environmental Engineering of the University of Genoa for the priceless scientific support.
- Prof. Elisabetta Finocchio of the Department of the Department of Civil, Chemical and Environmental Engineering of the University of Genoa, for the help with the discussion of spectroscopic analysis.
- Prof. Maila Castellano of the Department of Chemistry and Industrial Chemistry of the University of Genova for the precious advice during the first year of this Thesis project.
- Prof. Pavel Gurikov, Laboratory for Development and Modelling of Novel Nanoporous Materials, Hamburg University of Technology, for having granted me the possibility to work and collaborate with his group for six months. I would also like to thank Dr.-Ing. Raman P. Subrahmanyam and Dr. Baldur Schroeter for their scientific supervision.
- Dr. Andrea Dodero and Dr. Davide Clematis for the precious support as friend and as colleague.
- Fabian Canivet of Algaia, France, for having gently provided the alginates employed in this project.
- Zeocell Italia and Zeolite® Italia for having kindly provided the natural zeolites used in this project.

Giulia Gaggero

ABSTRACT

Today, crude oil derivatives are worldwide used as raw materials for the synthesis of carbon-based chemicals. However, the environmental sustainability of their entire life cycles, from the extraction to the application, has been recognized as poor. For what concerns the building sector, synthetic polymers obtained from crude oil are traditionally used inside the coatings formulations. Considering the concern about their environmental impact, it is mandatory and urgent to find more environmentally friendly alternatives. Without any doubt, the most promising alternative to carbon source is biomass, either in its natural state, i.e., biopolymers, or as waste material from agriculture and the food industry. Despite the wide availability of biomass, and the large research on its extraction and modification, the production of bio-based chemicals and the related substitution of the traditional ones is still far to be obtained. Along with the impact of single compounds, another concern about building sustainability lies on the construction processes and the impact of their life cycle. For example, household heating systems mainly depend on fossil fuels and for low thermal insulation building envelopes, the energy consumption in the EU accounts for around 36 % of greenhouse gas emissions.

With these premises, the present PhD Thesis foresees two different goals, namely the development of construction materials for the building sector by using biomass derivatives and recycled components to increase sustainability, and the improvement of energy efficiency for existing and new buildings by enhancing the thermal insulation properties of the building envelopes. The raw materials chosen in this project to replace some of the traditional components are alginate, a biopolymer extracted from seaweed, natural zeolite, naturally occurring porous volcanic rocks, and organic based aerogels from food waste.

For what concerns alginate, the key idea is that its well-known gelling ability, so far mainly used in biomedical and food industries, can be exploited inside coatings formulations as well to improve flow properties during the storage and application phase. The role of its molecular weight, concentration and counterion type has been deeply evaluated through rheological, spectroscopic and tensile tests. According to the obtained results, it can be concluded that such a biopolymer represents a suitable bio-based thickener with an associative like character.

Regarding natural zeolites and organic-based aerogels, they were investigated as a sustainable approach to achieve coating formulations with a low thermal conductivity taking inspiration from highly porous synthetic materials (e.g, synthetic zeolite and silica aerogels). In this context, natural zeolites purchased from national mines and aerogels obtained by recycling food wastes, specifically spent ground coffee and apple pomace, perfectly fit in this research. Considering their natural origin and the lack of literature, the use of these materials as thermal filler inside a coating formulation is ambitious. Moreover, their hydrophilic character does not harmonize with common water based coatings. To overcome this problem, a surface modification of both zeolites and aerogels was carried out to enhance their hydrophobic character.

Thermal properties of both zeolite and aerogel-based plaster were enhanced, with resulting thermal conductivity being lower than that of a standard mineral plaster.

Due to its high novelty, despite the research is still at a preliminary phase, this project can be considered an important step towards the development of coating formulations with a higher amount of bio-based or recycled components and promising thermal insulating properties.

INDEX

LIST OF ABBREVIATIONS

η	Viscosity
η_0	Viscosity at low shear rate
η_{max}	Maximum value of viscosity during the recovery test
γ	Strain
γ_c	Critical strain
τ	Shear stress
τ_0	Yield stress
λ	Thermal conductivity
$\dot{\gamma}$	Shear rate
τ_1	Characteristic time 1
τ_2	Characteristic time 2
σ_{max}	Tensile strength maximum value
$\bar{M}_w$	Average molecular weight
3ITT	Three Interval Thixotropy Test
AA	Ammonium alginate
AG	Apple aerogel
ATR	Attenuated total reflectance
BET	Brunauer, Emmett and Teller theory
BREEAM	Building Research Establishment Assessment Method
CG	Coffee aerogel
CASBEE	Comprehensive Assessment System for Building Environmental
CE	Commercial hydroxypropyl methylcellulose
CHA	Chabazite- zeolite framework
DGNB	German Sustainable Building Council
E	Young modulus
EPS	Expanded polystyrene
ETICS	External Thermal Insulation Composite System

EU	European Union
f	Fitting parameter
FAU	Faujasite-zeolite framework
FDA	Food and Drug Administration
FTIR	Fourier transform infrared
G’	Storage modulus
G’’	Loss modulus
GBRS	Green Building Rating System
GPM	Gas phase method
H-ZCH	Hydrophobic natural zeolite - chabazite
H-ZCL	Hydrophobic natural zeolite - clinoptilolite
HAG	Hydrophobic apple aerogel
HCG	Hydrophobic coffee aerogel
HEC	Hydroxyethyl cellulose
HEU	Heulandite- zeolite framework
HPMC	Hydroxypropyl methyl cellulose
IZA	Zeolite International Association
LCA	Life Cycle Assessment
LEED	Leadership in Energy and Environmental Design
LPM	Liquid phase method
LTA	Linde type A- zeolite framework
LVER	Linear Viscoelastic Range
MC	Methly cellulose
MTES	Methyltriethoxysilane
MTMS	Methyltrimetoxysilane
PA	Potassium alginate
PUR	Polyurethane
q	Heat flux
R	Thermal resistance
SA	Sodium alginate

SAL	Sodium alginate low viscosity
SAM	Sodium alginate medium viscosity
SEM	Scanning electron microscopy
SCD	Supercrticial drying
T	Temperature
tan δ	Damping factor
TEOS	Tetraethoxysilane
TGA	Thermogravimetric analysis
TMOS	Tetramethoxysilane
U	Thermal transmittance
VIP	Vacuum Insulation Panels
VOCs	Volatile Organic Compounds
V_u	Vapor uptake
w_d	Dry weight
w_t	Wet weight after 72 hours
XPS	Extruded polystyrene
ZCH	Natural zeolite - chabazite
ZCL	Natural zeolite - clinoptilolite

Boero Bartolomeo S.p.A.

This Thesis project has been done in collaboration with Boero Bartolomeo S.p.A, an Italian paint manufacturer company. Boero Bartolomeo S.p.A., founded in 1831 in Genoa, is an industrial holding company that formulates, produces and distributes paints for the Architectural and Deco, Yachting, and Marine sectors. It is presented in the Building (Architectural and Deco) sector with brands Boero, Attiva, Rover, and in the Yachting sector with Boero YachtCoatings, Attiva Marine and Veneziani Yachting.

The Gruppo Boero has recently joined forces with the Portuguese coating manufacturer CIN; present in almost 50 countries and recently premium partner of the Italy pavilion at Expo 2020 in Dubai, is a good example of quality and innovation.

INTRODUCTION

The need for sustainable development in the construction sector has become significant in the last decade mostly due to the major resource consumption and contamination that buildings generate, and it deals both with the materials and the construction practices [1].

So far, the terms “Green” and “Sustainable” building have been used interchangeably. However, according to the literature, they do not have the same meaning.

Green building definition is related to using efficiently land and energy, conserving water and other resources, improving indoor and outdoor air quality, and increasing the use of recycled and renewable materials avoiding crude oil derivatives [2].

On the other hand, sustainability is a term well established by the Brundtland Commission in 1987, stating that “sustainable development is a development which meets the needs of the present without compromising the ability of future generations to meet their own needs” [3]. When it comes to sustainable building, the ultimate goal is to develop “environmentally friendly construction practices” that contribute saving energy, water, and raw materials; minimizing water surplus and greenhouse gas emissions; and exploiting reuse and recycle of materials [4].

Today, building energy consumption accounts for approximately 40% of total energy consumption and emits 36% of greenhouse gas emissions in the European Union EU. Approximately 75% of buildings are energy inefficient, and only 1% of them are rehabilitated annually [5]. In this context, enhancing energy efficiency, especially of existing buildings, has become imperative for the architecture, engineering, and construction [6].

The definition of building energy consumption comprises the energy used in the process of building construction, materials production, building demolition, material reuse, and recycling. The main objective of building energy efficiency is to promote the rational use of energy mainly reducing fossil energy consumption by improving the thermal performance of building envelope [7].

Indeed, the EU has established a legislative framework that includes the Energy Performance of Buildings Directive 2010/31/EU and the Energy Efficiency Directive 2012/27/EU. These directives promote policies that will help achieve a highly energy efficient and decarbonized building stock by 2050. In October 2020, the Commission presented its Renovation wave strategy, as part of the European Green Deal. The most important part of this document is an action plan with concrete regulatory, financing, and enabling measures to boost building renovation [8].

For new constructions, the Energy Performance of Buildings Directive requires that EU countries ensure that all the buildings must be nearly zero-emission buildings. Zero energy building has been described as a

building with substantial reduction in energy consumption over duration of service, balancing energy demand from energy sources, reduced carbon dioxide release [9].

With these premises, the source of raw materials used in the construction should be questioned. Specifically, many organic compounds are obtained from crude oil refining process. The non-renewable nature of crude oil and the pollution caused by this process forces the scientific research towards more sustainable alternatives.

Certainly, most of the architectural coatings include organic based compounds. Despite the great number of papers on the use of biomass as carbon source to replicate synthetic polymers, the market is still led by traditional materials and new alternatives are still expensive for paint manufacturers. Moreover, the end-life of all these new products is never mentioned but is reasonable to think that their sustainability only relates to the production phase, whereas during the end-life phase their impact is the same of synthetic polymers.

The goal of this Thesis project is to develop smart multilayer coating cycles with the double aim of increasing sustainability and energy efficiency. To tackle these tasks, traditional components of coatings formulations were replaced with more sustainable materials naturally occurring on earth; then, a modified water-based architectural coating formulation and an innovative plaster formulation were prepared, and optimized to retrofit the interior space of buildings.

Fundamentals

1 SUSTAINABILITY IN THE ARCHITECTURAL FIELD

This Chapter aims to provide a comprehensive description of what does the word sustainable means in the building sector. The attention is focused on the current tools used to evaluate the environmental impact of single products and buildings; specifically Green Building Rating Systems GBRSs and environmental labels are described.

1.1 GREEN BUILDING RATING SYSTEM

Suitable methods and indicators to address the sustainability of resources used in the building sector are relatively new [10]. Recently, the Life Cycle Assessment LCA approach has been used to quantify the environmental impact of many services and products, including buildings. During an LCA study, the environmental impacts of materials and resources are examined all over their life cycle. Architects and engineers can quantify this impact using green building certifications.

Within the green building certification, the green rating systems are established voluntary assessment methods to evaluate the sustainability of construction projects. Currently, the leading rating tools are identified as: LEED (Leadership in Energy and Environmental Design), BREEAM (Building Research Establishment Assessment Method), CASBEE (Comprehensive Assessment System for Building Environmental Efficiency), DGNB (German Sustainable Building Council) [2]. They focus on specific categories like the material used, the indoor air quality and the greenhouse gas emission conferring credits for each category. The global environmental impact depends on the number of the collected credits.

Considering the voluntary nature of these schemes, sustainability labeling has not found its formal systematic place yet. To fulfill the need for a comprehensive and strong framework that would encompass key sustainability indicators and could be used as a reference in all European countries. At the European Commission, the Joint Research Center (JRC) launched Level(s) as a common language of sustainability for buildings within the current European Green Deal [11]. The previously mentioned categories are in this scheme known as macro-aspect for which you can select indicators (materials, energy, resources), and decide the level of accuracy used for their evaluation. Hence, the name Level(s).

1.2 ENVIRONMENTAL LABELS

The interest in the development of sustainable product, in terms of e.g. zero environmental impact and use of renewable sources began in the nineties when the scientific community realized how much the traditional chemistry had a negative impact on human health and on the environment. This new area of study has been denominated Green Chemistry [12]. Nowadays the concern about the environmental impact of products and services is increasing between the populations. Environmental labeling has emerged as a key tool for making sustainable purchasing decisions [13]. Indeed, the sustainability of construction materials can be individually evaluated using environmental labels.

Environmental labels can be classified into two main groups: mandatory or voluntary certifications. Mandatory environmental labeling is generally prescribed by law and appears mainly for specific

performance issues such as water or energy consuming devices. For example, in Europe the entire electrical appliance must have a label containing an A (best performance)–G (worst performance) rating showing its level of energy efficiency.

For what concern the voluntary labels, they are described, and classified by the International Standard Organization into three types:

- Type I
- Type II
- Type III

Type I label, according to ISO 14024 "*Environmental labels and declaration – Type I Environmental labeling – Principles and procedures*", establishes the principles and procedures for developing environmental labeling programs, including the selection of product categories, product environmental criteria and product function characteristics, and for assessing and demonstrating compliance. Type I is a multiple-criteria, third parties certified program based on life cycle considerations [14]. Among them, the EU eco-label, also known as the EU flower, is one of the most famous certifications.

The main objective of EU eco-label is to reduce information asymmetry and guarantee a shopping guideline for customers encouraging them to substitute "conventional" products with eco-labelled ones, which are more resource- and energy-efficient [15].

Type II according to ISO 14021, "*Environmental labels and declarations – Self-declared environmental claims – Type II Environmental labelling"* is based on the self-declarations of the manufacturer. These labels refer to a single characteristic such as recycling and degradability. It is not necessary a third-party certification, but all the information must be true and verifiable otherwise the company may be accused of greenwashing, the practice of making an unsubstantiated or misleading claim about the environmental benefits of a product, service, technology or company practice[16]. Type III according to ISO 14025 *"Environmental labels and declarations – Type III Environmental declarations",* provides quantitative, transparent, verified and comparable information about the life cycle environmental impact in a more extensive report format named Environmental Product Declaration EPD.

2 ENERGY EFFICIENCY IN BUILDINGS

This Chapter shortly introduces the theory of thermal processes in building materials; furthermore, it presents and summarizes the commercially available thermal insulation solutions for the exterior façade and interior space of buildings. Finally, a summary of the most recent innovative solution for the thermal insulation of interior walls is reported.

2.1 THERMAL PROCESSES

Heat transfer is the transport of energy that results from temperature difference. In the building sector, this process must be kept under control as it can lead to undesirable heat loss during wintertime or overheating caused by solar gain. Heat transfer occurs typically by three main phenomena: thermal conduction, thermal convection and thermal radiation. Conduction occurs between different materials in close contact with each other. Convection occurs when there is conduction of heat into the molecules of a fluid. Radiation occurs when a body emits an electromagnetic radiation [17].

Considering the inside of a building, the heat is transferred from the air to the wall, or vice versa, by convective air currents set up by temperature differences between wall and air, by wind or forced ventilation [18]. Various heat exchange processes are possible between a building and the external environment through various building elements such as walls, windows and roofs. There are specific parameters that describe the thermal performances of an object. At a specific temperature, the rate at which this heat transfer occurs through a unit area of a material is called thermal conductivity and is commonly expressed by Fourier's law, Eq. 2.1, as:

$$q = -\lambda \frac{\mathrm{d}T}{dx} \qquad (2.1)$$

where q (W/m^2) is the heat flux, λ (W/m K) is the thermal conductivity and $\mathrm{d}T/\mathrm{d}x$ (K/m) is the temperature gradient. Among the thermal parameters, thermal conductivity is often used to evaluate the thermal insulation properties. Indeed, low values of λ describe a high resistance to conduce heat, thus high insulating properties. The wall opposes a resistance to this heat flow, whose intensity is connected to the materials used. The global thermal resistance of a wall is the result of the combination of each layer and can be calculated as reported in Eq. 2.2:

$$R = d/\lambda \qquad (2.2)$$

Where d is the thickness of the layer (m). Its reciprocal is named thermal transmittance U (W/m^{2}K).

2.2 INSULATION MATERIALS

A common strategy to increase the energy efficiency of buildings focuses on reducing the thermal transmittance through the building envelope employing thermal insulation materials. Typical values of λ for traditional building materials are λ = 0.8 (W/m K) for brick and λ = 1.4 (W/m K) for cement mortar [19]; it is clear that alone, they do not have interesting insulation properties. With this regard, porous materials are commonly used.

The description of the fundamental heat and mass transport phenomena inside porous materials is already well known and has been well described in books [20] . Briefly, porous material can be described as a solid

matrix with a porous structure. Heat transfer in porous materials could be described in a good approximation by the sum of the solid thermal conductivity and the thermal conductivity of the gas within a given porous structure considering the collision of gas molecules inside the pores. Therefore, the thermal conductivity of a porous materials is often called equivalent or effective thermal conductivity. In fact, radiative heat transfer is negligible compared to conduction, and convection does not occur because of the limited free space [21–23].

These materials take advantage of the low thermal conductivity of the gas in the pores, typically air, to increase the overall thermal resistance; in fact, the thermal conductivity of quiescent air λ_{air} at room temperature is low, and estimated about 0.022 W/mK [24].

Several materials are suitable for thermal insulation: fibrous materials, which consist in fibers with small diameter and air within the interspaces, foams and hollow sphere [25].

Among synthetic materials, mineral wool, glass wool, expanded polystyrene (EPS), extruded polystyrene (XPS), polyurethane (PUR) are commonly used with a λ between 0.03-0.06 W/mK. Cork and cellulose on the other hand, are natural materials with well know thermal insulation properties with a λ between 0.04 and 0.05 W/m K [26]. Glass bubble are commercially available as filler with low density and low thermal conductivity λ= 0.04 W/mK [27].

2.2.1. External Thermal Insulation Composite Systems

So far, the most common wall insulation technique involves the refurbishment of the exterior façade of buildings. The External Thermal Insulation Composite Systems, ETICS, has been used in Europe since the 1970s as a major thermal and acoustic insulation method for the building envelope [28].

ETICS is a multilayer system, schematically represented in Figure 2.1, which insulation ability is mainly linked to the presence of a thick insulation board, up to 15 cm, typically made of expanded polystyrene EPS, polyurethane foam, mineral wool or wood fibers to guarantee an increase of thermal performances with λ = 0.03-0.07 (W/m K) [29]. In addition, layers of adhesive, reinforced mesh and plaster are commonly used to build the structure.

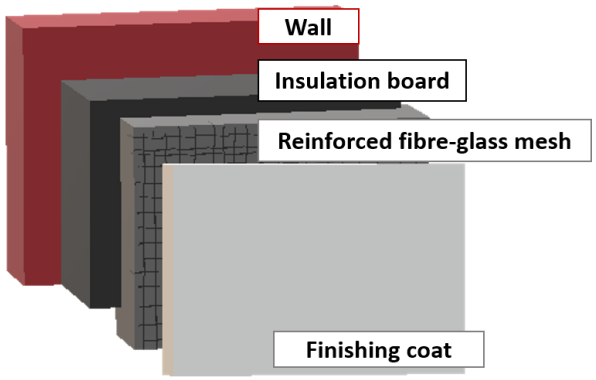

Figure 2.1 External Thermal Insulation Composite Systems, ETICS

The main advantages of ETICS are the reduction of the thermal bridges and global heat losses, no modification of the interior area stealing precious centimeters, increase the facades durability, ease of application.

Furthermore, despite it is true that the ETICSs are used to reduce the energy consumption, considering the additional materials or the larger quantities used they can eventually, increase the environmental impact of this system [30]. Few Life Cycle Analysis studies have been carried out, especially on the single ETICS, but is clear that the choice of insulating materials has the greatest environmental impact [31,32]. Hence, recycled materials have been extensively studied as an alternative to traditional solutions. The global production, consumption and waste management of plastic is of great concern today. Although single use biodegradable plastic is nowadays produced, we still have to dispose of old plastic alternatives. For this reason, reusing plastic waste obtained from shopping bags and water bottles in construction materials has been deeply investigated [33,34]. Another source of recycled materials comes from the paper and textile industries. In fact, paper and textile recycle fibers have been investigated as well as innovative materials for insulation panels [35]. Considering the huge amount of solid wastes that the population produce, waste management finds its new solution inside construction materials [36]. The development of such panels is unfortunately still at the research phase, and the market is still connected to traditional materials.

Despite ETICSs being the most common strategy to increase the thermal insulation of buildings, several disadvantages can be identified. Indeed, EPS is almost the only material used for the production of insulating panels, its synthesis and end-life disposal cannot be considered highly sustainable. Moreover, the high cost of installation, and the restriction within some particular urban center characterized by practical restrictions like narrow streets, and the refurbishment of historical buildings which façade must be kept intact remind the need of alternatives to ETICS.

2.2.2. Internal insulation systems

Whenever it is not possible to place an exterior insulation system, interior insulation can contribute to increase the thermal insulation properties as a valid alternative to ETICS. The thermal insulation of interior envelope also has a great influence on building energy performance. Indeed, it minimizes the heat dissipation and the sound transfer between adjacent rooms [37].

A typical interior wall structure is the result of the stratification of some basic components: bricks, mortar plaster and architectural coating, as shown in Figure 2.2. However, this basic stratification can increase its complexity by adding special elements like insulation panels.

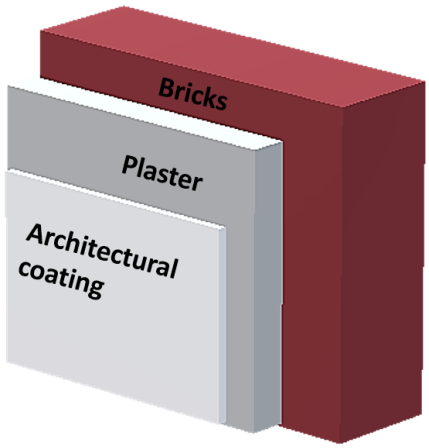

Figure 2.2 Traditional interior wall layers stratification

In this regard, different solutions are available on the market today. Insulation panels similar to those used for ETICS, fiberglass batt and expanded polyurethane foam are the most common methods used as retrofitting methods. They are durable, easy to install at a lower cost. Remarkably, one the biggest disadvantages of these methods are that they can produce dew and they reduce the space, in terms of square meters, inside the rooms.

An innovative solution to overcome these problems relies on the use of thermal plasters. Thermal plaster is a designed material for building surface insulation with various lightweight fillers as barrier insulation materials [38].

Vermiculite, mica, perlite and ceramic hollow sphere are typical fillers for thermal insulation in construction materials like cement or mortar [39]. The main advantages of using a thermal plaster are the easy application and the thin layer, few millimeters, which can be applied on the wall.

Today, the most promising products on the market with the lowest thermal conductivity are silica aerogel plasters and vacuum insulation panels, VIP. Both act as superinsulation materials in small thicknesses: silica aerogel is a low density, highly porous material that can be used as a powder or as mats whereas VIPs consists of evacuated open core materials surrounded by thin laminates, composed of a barrier envelope,

used to maintain the vacuum [40,41]. Even though real simulation showed promising results, aerogel plasters application in real building is limited because of the high cost of the raw material [42,43]. VIPs solutions also seem promising, however the price is not competitive with traditional solutions, and the installation is still difficult because they can be easily damaged and they cannot be cut on site according to the wall structure [44].

3 COATING CYCLES FOR INTERIOR WALLS

This Chapter introduces the reader to the world of building materials. In particular, due to the topic of the present Thesis work, it focuses on architectural coatings and mortar plaster. Traditional components of both the two previously mentioned materials are described along with more sustainable alternatives.

3.1 ARCHITECTURAL COATINGS

Coatings are thin layers that when applied to an object, which is often referred to as the substrate, provide protection and sometimes specific esthetic properties. Architectural coatings are the last layer applied on the wall; usually they are applied with a brush or a roller depending on the product and on the substrate to obtain a thin layer. Specifically, architectural coatings include paints and varnishes (transparent paints) used to decorate and protect buildings, outside and inside [45]. They are complex mixtures of chemical substances that can be grouped into categories such as binders, volatile components or solvent, pigments, fillers, and additives. The list of all the ingredients, which is often expressed in weight percentage, is called paint formulation. Each formulation contains the main ingredients and by tuning their concentration, it is possible to obtain different final products.

The development of a new paint product is a difficult process; a deep knowledge of the single components is required to predict the possible interaction among them.

Binders

The binder determines most of the primary properties of the dried paint film, such as adhesion, various optical and mechanical properties, as well as the resistance against exposure condition [46]. It is the main film forming component and it affects properties such as gloss, flexibility and toughness [47]. Many binders for paints are based on synthetic polymers, drying oils, or natural resins, or combinations of these, and the most important are [48]: acrylic polymers, alkyds polymers, epoxy resins, vinyl polymers, and polyurethanes.

Volatile compounds

Commonly referred to as *solvents* they play a major role in the preparation, mixing, and application of coatings. They are liquids that make the coating fluid enough for application, and they evaporate during and after application. In the past, almost all of the volatile components were low molecular weight organic compounds VOCs. Today, most of the VOCs have been recognized as hazardous chemicals and their use inside paint formulations is strictly regulated by the law (Directive 2004/42/CE). [45].

Pigments

Pigments are insoluble particles that are dispersed in the binder. The selection of the type and the amount of pigment determines not only the color but is also largely responsible for other properties such as the opacity, hiding power, and corrosion resistance of the paint. Indeed, they impart optical properties according to their ability to scatter the incident light. The pigments used inside the coating industry can have both an inorganic and organic origin. As a consequence of that, a wide variety of colors are available. The primary pigments are used to add whiteness and color. Among them titanium dioxide, is the most used white pigment whereas colored pigments are obtained for example from copper and iron based minerals.

Fillers

Fillers are inexpensive materials historically used to reduce the cost of a paint product and to increase or to decrease its density. Moreover, they can provide specific optical, thermal and mechanical properties [49]. Among them calcium carbonate is the most used in water-based architectural coatings. Fine particle size calcium carbonate works by physically spacing titanium dioxide particles improving, optical properties of the dry coating film at lower titanium dioxide contents [50]. Silicates, sulphates and organic fillers are often used as well [51].

Additives

Coating additives are substances added in small proportions to coating compositions to modify certain properties There is a large variety of additives depending on their function i.e. thickening agents, surface active agents and biocides [52].

Thickening agents, also called rheology modifiers, provide the proper consistency to coatings, ensuring the adequate thickness during the application of a coating to a substrate. They influence paints performances all over the life stages providing a viscosity high enough to prevent particle settling and aggregation during the in-can storage, and low enough preventing unwelcome event like spattering and sagging during the application. Quite often, multiple thickeners are required inside a paint formulation to achieve the suitable viscosity.

The major rheology modifier used in coating formulations are:

- non-associative thickener;
- associative thickener;
- inorganic thickener.

Among the first one cellulosic ethers, such as methyl cellulose (MC), hydroxyethyl cellulose (HEC), and hydroxypropyl methyl cellulose (HPMC) have been available for over 30 years, and they continue to be used as thickeners in nearly all latex paints [53]. They are easily available, water soluble with high thickening efficacy by thickening the aqueous phase without interfering with the other components.

Associative thickeners are polymers with hydrophobic ends and hydrophilic chain able to interact with latex particles as their major thickening mechanism in a coating with the formation of transient networks. A typical example are the polyurethane or PUR-thickeners [54,55].

For what concerns the inorganic thickeners, they are mainly clays, like bentonite, often used as secondary thickener to improve sag resistance and thixotropic character.

Surface-active agents are amphiphilic molecules containing both hydrophilic and hydrophobic portions on the same molecule. They can act as wetting agents working on solid/liquid interactions, antifoaming agents tuning the surface tension during mixing process, and dispersing agents preventing settling and particle aggregation [46].

Biocides are substances used to protect coatings from biological attack caused by algae, fungi and other organisms. Biocide agents are available to work both in-can and in the dried film. Considering the dangerousness of this chemicals, their use is strictly regulated by the Biocidal Products Regulation 528/2012 [53].

3.1.1. Sustainable components for architectural coatings

The most recent influences on coating developments are related to environmental considerations, and the need to conform to health and safety legislation. Cost/benefit relationships have also become more important in an increasingly competitive world market and have influenced formulation practice markedly [56]. Specifically, the stringent health and safety legislation, the Circular Economy Strategy and the related Action Plan "Closing the loop" proposed by the European Union in 2014 have been a major driving force on this process of "going green" [57]. This concept focuses on the sustainable, resource-efficient valorization of biomass while also making use of residues and wastes and optimizing the value of biomass over time as best practice to meet the future global climate targets [58].

In recent years, there has been an awakening of interest and awareness of the importance of sustainability in the coatings field. Indeed, many components of paint formulations are derived from crude oil. As we look to the future, coatings will be formulated with completely renewable, recycled and from biomass feedstocks.

Because of that, the last trend in coating sector is the development of "eco-friendly" paint. In these products, it is common to see the substitution of traditional raw materials from crude oil i.e. the binder, with new polymers originated from biomass [59]. Finally, the so called natural paint must be cited; these formulas do not contain chemicals extract from petroleum, only vegetal and inorganic raw materials are allowed; however, the high cost, low in can stability and limited choice of colors are some of the drawbacks that limited the use of natural paints [60].

With these premises, current researches are dedicated to the development of new bio based or waste based components for coatings formulations. However, one of the biggest challenges for the paint industry is the production cost of these new chemicals from biomass thus working with the current technologies make the scaling-up hardly possible. For this reason, most of the research reported in literature belong to university research groups. Bio-based paint market is still small; but it is expected to grow soon. An example of more environmentally friendly alternatives are presented below.

Binders

Bio-based polymers from renewable resources are the most attractive alternative to traditional binders. Preparation of new acrylate polymers from bio-based molecules obtained from either extraction or fermentation of biomass such as glucose, cellulose and lignin is an interesting strategy to synthesize bio-based polyacrylates [61,62]. Polyurethane PU is a well known binder in the coating sector, with many

research reporting the use of bio based raw materials like tannic acid [63] modified soybean oil and castor oil [64] palmitic acid based polyesteramide [65] to synthetize waterborne polyurethane dispersions. Epoxy resins are versatile polymers, however, most of the commercial epoxy resins are derived from petrochemicals and are often suspected of being hazardous; in this sense, the synthesis of a novel highly bio-based vinyl ether monomer from eugenol is a good example of how to use natural resources to obtain a synthetic product [66]

Volatile compounds

Today, most of paints and varnishes formulations are water-based, however volatile organic compounds (VOCs) are still used. The growing concern over VOCs is motivating coating formulators to recycle and reduce traditional solvents, or switch to a more environmentally friendly alternative. Ethyl lactate and D-limonene are a few example of innovative bio-base solvents [67].

Pigment

Despite titanium dioxide TiO_2 has been used for years as white pigment, during the 2017 the ECHA's Committee for Risk Assessment (RAC) classify titanium dioxide as a substance suspected of causing cancer through the inhalation route [68]. Today, only nanosized TiO_2 has been classified as potentially carcinogenic, but due to the lack of data it is hard to say how deeply it affect human health. In particular, since there are still opened questions regarding the toxicity of TiO_2 nanoparticles, at oral and dermal exposure, it is impossible to make a reliable quantitative risk assessment [69].

Beside its potential hazardous the high production cost and low sustainability (due to the chemical processes, the chloride and the sulphate processes, involved in the production) [70], titanium dioxide is still the best solution for coating manufacturer as white pigment;

Direct substitution with another mineral is the easiest way of replacing TiO_2; zinc oxide, zirconia oxide have been extensively studied since they exhibit similar optical properties [71], many types of filler from calcium carbonate to clays have partially replaced titanium dioxide in paint formulations [72].

Alternatively, titanium dioxide can be recovery from different waste materials, such as paint waste. Recovery of TiO_2 might be interest due to the relatively high content of TiO_2 in paint waste, some technique involved pyrolysis of waste material are reported in literature [73]. In the paper industries where TiO_2 is used as much as in coatings sector, the last research are focused on the development of green alternatives such as the use of corn starch in the production of hybrid pigment with calcium carbonate [74].

Fillers

Today calcium carbonate is the most used filler and has not great interest of been replaced since it is a low-cost material, safe for human health, available in nature or as waste product of marble production. Anyway, some attempts to replace calcium carbonate from quarry with waste bio material such as seashells

[75] or eggs [76] have been made. Those studies are not directly connected to the paint industry but they represent a future possibility.

Additives

The research on bio-based alternatives depends on the type of additive. Thickeners for example, can be either bio-based like cellulose derivatives or based on synthetic polymers like PU-based. Considering cellulose thickeners, since the cost of this raw material is extremely low and its origin from biomass, in literature there are very few research on alternative thickeners. However, the global request for cellulosic materials for other purposes and the low environmental friendly process of cellulose transformation, increases the need of finding alternative solutions [77]. Recent studies investigated four types of modified starch in emulsion paints [78], with xanthan gum as well as a potential different polysaccharide based thickener [79]. Potentially, every hydrocolloid with gelling ability can be used as a thickener agent instead of cellulose ethers; agar-agar, alginate, carrageenan, gellan gum have been used for years in the food sector for their gelling ability [80,81].

Surfactants are nowadays mainly synthetic molecules, but natural products have been used for years. By way of example, lecithin obtained from soybean or from egg yolk is one of the most common natural surfactants [82].

3.2 PLASTERS

Plasters are thin layers of mortar, which protect and decorate building walls. From a chemical point of view, a plaster is a mineral coating composed of fine aggregate, sand, a binder, and a specific amount of water. According to the binder use, they can be identified as gypsum, lime, or cement plaster.

It is applied at a thickness that can vary from a few millimeters to a few centimeters, to level off wall surfaces in order to make them even. Plaster has been used for thousands of years as constructive element in buildings, especially in Europe [83]. It was frequently used in Egypt during Pharaonic times, extending back at least 4000 years, and it is found in the construction of the Giza pyramids and back to the Greeks and Romans [84].

3.2.1. Sustainable components for plasters

Mortar can be described in simple terms as a mixture of fine sands, binder and water. Additives are optional mortar ingredients, frequently added to the mixtures to attain or modify specific properties like strength, plasticity or others [85]. In the latest years, environmentally friendly plasters have been studied. Specifically, these research focus on the reuse of waste material and on the use of natural fibers as functional fillers.

Some examples in the literature are of great interest. It is well known that the process of power generation from coal generates two main byproducts fly ash and bottom ash; a composite plaster was developed by replacing up to 60% of fine sand with bottom ash [86]. According to physical features and chemical composition, waste glass is an adequate replacement in cement matrices [87]. Among the diverse types of glasses, soda-lime glass is the most commonly used, such as in bottles, windows and bake ware. This is the reason why most literature focused on its reuse in concretes [88]. Moreover, extensive studies have been conducted on the reuse of recycled plastic in mortars and concrete were raw materials were replaced up to 100% by waste polyethylene terephthalate particles and pulverized glass fiber reinforced plastic waste, respectively [89]. Although the use of recycled plastic seems an effective strategy, we must think about the future disposal, thus the environmental impact of these materials.

The use of natural fibers as reinforcement in plasters is attractive for several reasons. They have a low density, specific properties like thermal insulation, and they are renewable. Agave and hibiscus fibers have been tested as alternative to polymeric fibers in lime-based mortars with promising properties [90]. Rice husk ash is a lignocellulosic material obtained as byproduct form the rice industry (harvesting and processing); several studies have been carried out on the use of rice husk ash as innovative filler in mortar showing promising mechanical and thermal properties [91,92].

4 INNOVATIVE COMPONENTS FOR COATING FORMULATIONS

This Chapter briefly presents the state of the art of the raw materials chosen for this Thesis project. As a matter of fact, they represent promising naturally occurring materials in various application fields. However, their use inside paints and plasters has been not fully investigated. Here, a full description of their characteristics and current use is done.

4.1 ALGINATE

Alginate is a naturally occurring anionic polysaccharide extracted from brown algae, including *Laminaria hyperborea*, *Laminaria digitata*, *Laminaria japonica*, *Ascophyllum nodosum*, and *Macrocystis pyrifera* that has been extensively studied for its biocompatibility, low toxicity, reduced cost, and mild gelation properties in presence of divalent ions [93].

The term alginates usually referred to group of biomolecules comprising alginic acid and its salts; in fact they represent a family of non-repeating unbranched copolymers containing blocks of (1 – 4) – linked β-D-mannuronate (M unit) and α-L-guluronate (G unit) residues. The blocks may be composed of consecutive G-blocks, consecutive M-blocks, and alternating MG-blocks (MG) Figure 4.1 [94].

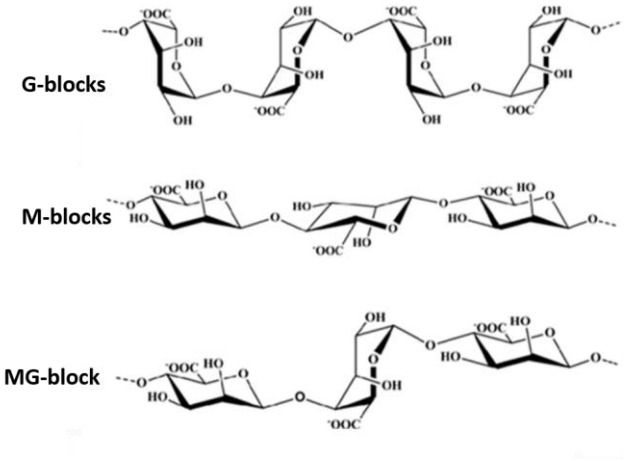

Figure 4.1 Chemical structure of alginates. M: β-D-mannuronate; G: α-L-guluronate units

Extraction of alginate from brown algae is an uncomplicated but multistep procedure, starting with initial treatment with diluted mineral acid to change salts of alginic acid inside the algae into free alginic acid. Either sodium carbonate or sodium hydroxide are used to neutralize the acid and form water-soluble sodium alginate. Precipitation with either calcium chloride or mineral acid can be applied and insoluble calcium alginate fiber or alginic acid gel is then obtained, respectively [95]. Alginate is commonly purchased as salt, for this reason alginic acid is commonly mixed with sodium carbonate or potassium carbonate. Among them, sodium alginate is the most common alginate salt available on the market. The physicochemical properties of alginate are generally influenced by the molecular weight and distribution of MG blocks.

One of the reasons of alginate success is its gelling ability due to specific and strong interactions between long stretches of G units and divalent cations. This gelation process is conventionally called the “egg-box” model, because the divalent cations arrange themselves all around the polymeric chain creating a structure comparable to an “egg shell” [96,97].

Alginates are commonly used in the form of hydrogels: three-dimensional crosslinked network with high water content. Ionic crosslinking, i.e. trivalent and divalent mediated egg box structure and covalent crosslinking are typical technique to form alginate hydrogels [93].

In the past decades, alginate, owing to its biocompatibility, biodegradability, and nontoxicity, has been hugely explored. Thanks to its outstanding properties and relative low cost, it has been largely exploited in the food, biomedical, and pharmaceutical industries.

Alginate has become one of the most interesting environmentally safe alternatives for food packaging. In fact, alginate films can be used as a vehicle for bioactive components, producing active packaging reducing microbial growth [98,99]. Furthermore, the dietary fibers contained in seaweed can adsorb sodium in the gastrointestinal tract avoiding sodium accumulation known to cause hypertension, followed by organ disorder [100]. Along with wound dressing and tissue engineering, the development of drug delivery systems based on alginate is continuously growing. For example, alginate capsules were used to encapsulate and then sustaining the release of antimicrobial, anti-inflammatory, antifungal agents. Moreover, they show promising results as nanocarriers in target cancer therapy [101]. It is worth mentioning that sodium alginate is used in the cosmetic industries as well. Many cleansing products contain abrasive agents to improve skin condition. These abrasive agents are beads commonly made of synthetic polymers; considering the recent concern about micro plastic pollution, alginate beads represent a valid alternative solution for abrasive agents [102,103].

In this project, alginate was investigated as thickener inside coatings formulations. According to its biological origin, naturally occurrence, and outstanding gelling ability it represents a valid alternative to standard thickeners.

4.2 ZEOLITE

Zeolites, literally derived from Greek words “Zeo” and Lithos” which means boil and stone, respectively [104] are microporous crystalline aluminosilicate minerals of the tectosilicate family. They have a three dimensional framework of interconnected tetrahedra mainly composed of aluminum, silicon and oxygen atoms. The crystalline structure is originated from $[AlO_4]^{5-}$ and $[SiO_4]^{4-}$, linked together to form a structure where all four oxygen atoms located at corners of each tetrahedron are shared with adjacent tetrahedral crystals. In zeolite structures, some of the silicon cations (4+) are replaced by aluminum (3+) into a tetrahedral unit, giving rise to a deficiency of positive charge. The so developed charge is balanced by the presence of IA or IIA metal ions, like Li^+, Na^+, Mg^{2+}, Ca^{2+}. Moreover, the broad structural cavities and the inlet channels contain water molecules differently bonded to the zeolite framework [105]. The empirical formula for zeolites is $M_{2/n}O{\cdot}Al_2O_3{\cdot}ySiO_2{\cdot}wH_2O$, in which *n* corresponds to the valence electrons of the cations, *y* value is between 2-200, and *w* is the water trapped in the channels of zeolite cages [106]. Zeolites

can either occur in natural environment or be synthetized in laboratories. Synthetic zeolites are prepared from materials with a high content of silicon and aluminum. Among them, clay minerals and coal fly ash have been frequently used to synthesis zeolite A, zeolite X, zeolite Y, and zeolite P [107].

Natural zeolites are volcanic sedimentary rocks spread all over the world; over 40 types of natural zeolite are identified. Precisely, the common forms are clinoptilolite, mordenite, phillipsite, chabazite, stilbite, analcime, and laumontite, and others are rare such as offretite, paulingite, barrerite, and mazzite [107,108].

According to the Zeolite International Association IZA, more than 200 zeolite frameworks exist. The most common frameworks are reported in Figure 4.2. Considering the zeolite used in this project, a short description of clinoptilolite and chabazite will be given.

Clinoptilolite is one of the most common natural zeolites, easily obtained from mines, suitable as a sorbent due to its natural characteristics [109]. Clinoptilolite belongs to the heulandite family, which tetrahedra bind over all four apexes with the formation of a honeycomb-like three-dimensional framework [110].

Chabazite is one of the most ubiquitous natural zeolites with a variable composition. Its framework structure is built up by double 6-rings linked by tilted four-membered rings to form one cavity per unit cell. Each cavity is connected to six neighboring by sharing 8-ring windows. Exchangeable cations and water molecules in chabazite are located in various sites whose location and occupation depends on the cation [111,112].

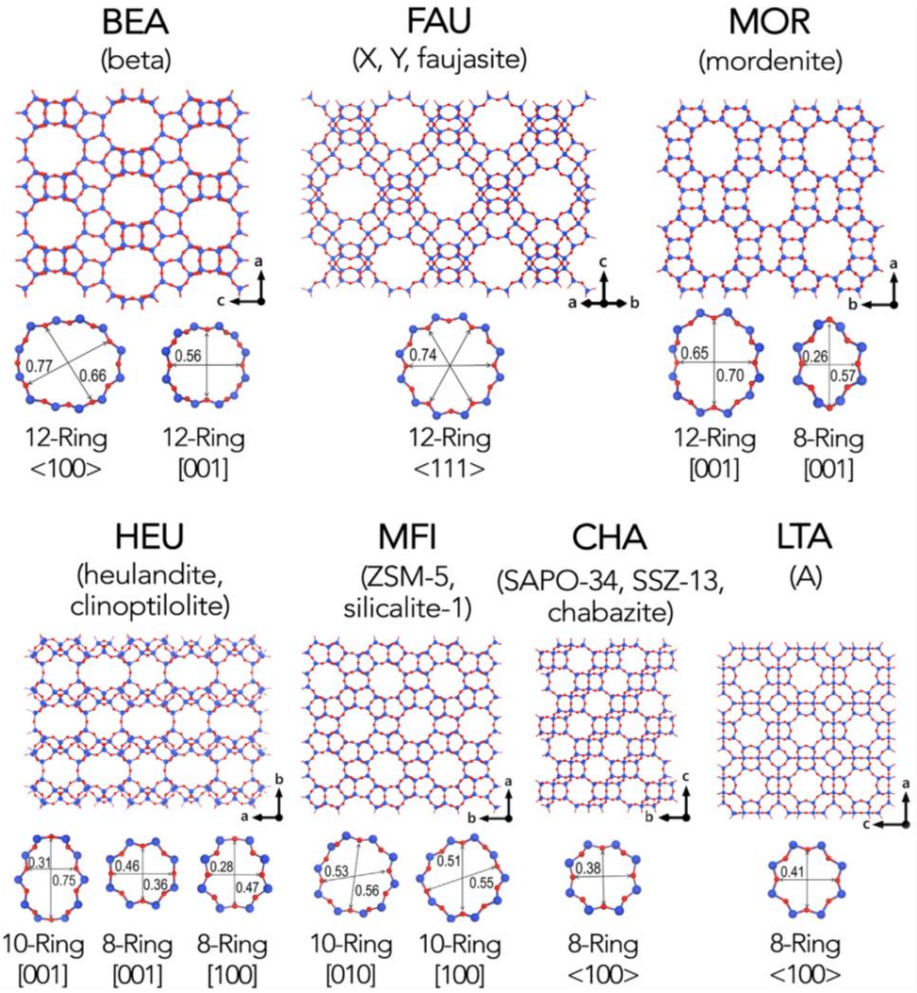

Figure 4.2 Zeolite framework types. Published with the permission of [113]

Zeolites are versatile minerals; their interesting physicochemical properties, such as cation exchange, molecular sieving, catalysis and sorption allow them to be extensively used in a wide range of application. The use of zeolite as catalyst is well known in the oil refining and petrochemical industry, including catalytic cracking, hydrocracking and alkylation [114]. Their catalytic activities descend from the presence of their active sites (bronsted acid) on OH bridging framework between silicon and aluminum channel [115]. Thanks to the extended literature on zeolite synthesis, the optimization of zeolite design lead to the possibility of using it as catalysts for biomass valorization into fuels and chemicals answer to one of the biggest challenge of reducing the fossil fuel as raw materials for fine chemistry [116,117].

Remarkably, cation exchange is one of their most important properties, which has allowed the use of zeolite as adsorbent This property allows removing and recovering the cations from very low concentration in solutions [118]. Heavy metal or dye removal are one of the most famous example of zeolite adsorption properties in waste water treatment [107,119]. The adsorption and ion exchange properties have been used also in gas phase in fact, zeolites with their honeycomb like structures have been widely studied as air purifiers. To improve treatment efficacy, some functional molecules like activated carbon, silver

nanoparticles or photo catalytic agents are often added to zeolite [120]. Furthermore, they have been successfully used for VOC capture in various industries because of their good positive response to low pressure drop, and temperature swing desorption [121].

Despite the continuous research on zeolites, they are commercially available. In agriculture zeolites have numerous applications: they work as heavy metal removers, they improve soil properties acting as macro nutrient supplement and as source of water increasing crop yield and they slowly release fertilizer thereby saving costs [115,122].

In the last decades, a growing interest on the possible exploitation of zeolites for human health has been depicted. Zeolites are edible, biocompatible, and possibly non-toxic substances with already mentioned unique properties. Hence, these properties account for their new applications in several medical areas. With their small cavities, zeolites are perfect matrix for drug release system. In fact, anti-inflammatory and antimicrobial medicine have been loaded inside zeolites and tested for drug delivery. Some research on encapsulation of anti-cancer drugs were carried out as well. Moreover, composite materials prepared with zeolites and polymers have been tested for biosensing, wound healing and as scaffold for cellular growth [123,124].

In this project, natural zeolites were investigated as thermal insulating filler inside coatings formulations. According to their naturally occurrence, and peculiar porous microstructure they represent a valid alternative to a standard thermal insulating filler.

4.3 SILICA AND ORGANIC-BASED AEROGEL

Aerogels are unique lightweight nanoporous materials with an open pore structure and exceptional properties i.e. low density, large porosity, high surface area, and very good thermal insulation properties [125]. Different materials can be used but silica is the most common and well-known raw material for aerogel production. Discovered in 1930s by S. Kistler they have been forgotten for almost 30 year due to a complex synthesis procedure [126].

Today, aerogel production process is divided in 3 steps: gel formation, aging and drying. During the initial step of wet gel preparation, the Si-based precursor is dispersed in water or organic solvent to initiate gelation in the system via hydrolysis and polycondensation reactions. The resulting siloxane bridges (Si-O-Si) provide backbone to the formation of silica matrix and are found to be porous in nature with solvent filled pores. Tetraethoxysilane (TEOS), tetramethoxysilane (TMOS), , or methyltriethoxysilane (MTES) which are initially involved as monomers, are commonly used as precursor [127]. At the end of the gel formation step, the obtained gel is fragile, and the solution typically contained unreacted species, thus an aging step before drying increases the mechanical strength of the silica network. The drying step is crucial

because the entrapped solvent must be removed without the collapse of the network. Ambient pressure drying APD, freeze drying FD, and supercritical drying SCD are the procedure mainly used to obtain aerogels. Among the three processes, SCD is the most effective and promising method; it consists on the extraction of the solvent inside the gel using a supercritical fluid by increasing the temperature as well as pressure above its critical point [126,128]. Supercritical drying by CO_2 extraction has been recognize as safe and environmental friendly procedure. Moreover, the drying step is faster in comparison with ADP and FD and is characterized by a negligible value of surface tension, avoiding the collapse of the structure. If the initial gel is formed in a water media, a solvent exchange phase is required before the drying. Indeed, water has a low solubility in supercritical CO_2 thus its removal is difficult and inefficient; ethanol and acetone have better solubility and are used as solvent for SCD [129].

Due to their unusual characteristics, a greater attention has been given to aerogels in recent years and various applications were investigated. For example, in environmental applications, aerogels demonstrated to be effective in air purification, VOCs removal and wastewater treatment. Furthermore, they can be used in the biomedical field as drug carriers, biosensing, wound healing and as scaffolding materials. Many other applications are known for aerogels, as catalyst for example, or heat storage devices [127,130].

Above all, the physical property that made aerogels famous is the low thermal conductivity, with λ=0.014 W/m K at ambient pressure [131]. In particular, the nanopore size of aerogels is smaller than the mean free path of free gas molecules (70 nm for air at atmospheric pressure); for this reason, the gaseous thermal conductivity within aerogels is smaller than the thermal conductivity of air [132]. Despite their outstanding thermal and acoustic insulation properties [133], the high manufacturing cost limited their spreading in the building sector.

Without any doubt, silica precursors are the most studied and used substances for commercial aerogel manufacture. However, they can be prepared from other sources both inorganic, like oxide and organic like carbon based. Organic based aerogels can be distinguished in two different types of product: bio-based and waste-based.

Among the organic, biopolymers like cellulose, alginate, chitosan, lignin and pectin have been effectively used for bio-based aerogels preparation [134]. Biocompatibility and low toxicity are adding values to the already mentioned physical properties. The synthesis of bio-based aerogel involved three steps: gel formation, solvent exchange and drying. In this case, gel formation depends on the type of biopolymer used as starting material: ionic and covalent crosslinking, pH induced gelation and temperature induced gelation are the most common methods to obtain gels. Considering that most of these gelation methods are carried out in water solutions, solvent exchange step is crucial and delicate because of significant shrinkage that can destroy the porous structure. Drying step follows the same rules described for silica aerogels [135].

Biomedical and environmental applications are the future of bio-based aerogels, alone or with grafted molecules; several example are already available as scaffold [136], drug carriers [137] and metal sorption materials [138].

Waste based aerogels are a good example of how the scientific community work on sustainable alternative of traditional process. Inside this group of materials, it is possible to identify two main branches: recycle based and organic waste-based aerogel. The basic principle is that they exploit the lignocellulosic content of waste to produce aerogels. For example, textile and paper industries are the important sources of cellulosic waste material that can be regenerated and use to obtain aerogels [139,140]. Nevertheless, waste biomass valorization is attracting many scientist; banana [141], watermelon [142], and pomelo peel [143] were used as carbon source for aerogel preparation as well.

Although the research is still at its beginning, waste-based aerogels are a potential solution for developing sustainable porous materials. However, the manufacturing process involved chemicals and energy consumption. An alternative solution to reduce the preparation steps is to use the pure biomass, reducing the chemicals and thermal or mechanical process involved. For example, spent ground coffee represents a valid raw material that can undergo directly to solvent exchange phase; biodegradable hybrid coffee-cotton aerogel has been successfully developed by means of freeze-drying [144].

In this project, organic waste-based aerogels were investigated as new thermal insulating filler for coatings formulations. According to their biological origin as recycled materials, peculiar porous structure, and unconventional use, they represent a valid alternative to standard thermal insulating filler.

Experimental

5 EXPERIMENTAL METHODOLOGIES

.

This Chapter aims to shortly present the theory behind the main experimental methodologies employed in the present Thesis work to help the reader understanding of the following discussions.

5.1 RHEOLOGICAL ANALYSIS

The term rheology was invented in 1920 by Professor Eugene Bingham at Lafayette College in Indiana USA and describes the deformation of matter resulting from the application of a force. According to their rheological behavior, the matter can be divided in three families. Ideal solid materials where the energy required for the deformation is fully recovered once the force is removed, ideal liquids or pure viscous materials where the deformation is irreversible and the energy required for the deformation is dissipated and visco-elastic materials where a combination of both the previous behaviors can be detected [145,146].

Consider two parallel plates divided by a small gap with liquid in between; when a shear stress, τ (Pa), is applied to the upper plate, there is a continuous change in velocity across the small height of the liquid, from a constant value of the upper plate to zero at the lower plate. The speed drop across the gap size is called shear rate, $\dot{\gamma}$ (s^{-1}) [147] . The ratio between the shear stress and the shear rate is called viscosity, η (Pa s) and describes the resistance of a material to flow Eq. 5.1.

$$\eta = \frac{\tau}{\dot{\gamma}} \qquad (5.1)$$

Ideal fluids have a constant viscosity and are so called Newtonian fluids. When the viscosity depends on the shear rate or the shear stress applied during the deformation, the fluid behaves as a non-Newtonian material. Commonly observed flow curves under rotational conditions of non-Newtonian materials are reported in Figure 5.1. Typically, steady state viscosity measurements are conducted by applying an increasing shear rate at a fixed temperature to evaluate the sample flow behavior.

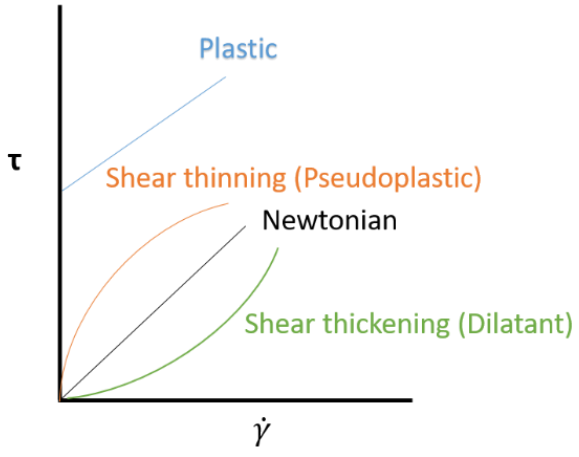

Figure 5.1 Commonly observed shear stress and shear rate relationships for both Newtonian and non-Newtonian fluids

The most common non-Newtonian fluids are the so-called shear thinning or pseudoplastic fluids where the viscosity decreases increasing the shear rate or the shear stress. Particulate dispersions, polymer

colloids, and polymer solutions can display this behavior. When this decrease of viscosity occurs after a specific value of stress, known as yield stress τ_0, they are called viscoplastic or Bingham fluids. All these viscosity profiles are time-dependent and involve a structural deformation. Some materials are able to recover their original microstructure when the applied shear is removed; this dependency on the shear history is also called thixotropy [148]. For thixotropic fluids, like coatings, the investigation of the structural regeneration over time is fundamental to evaluate the final application and appearance on the wall. In many coating applications, generating a smooth defect-free surface is crucial [149]. A bad leveling with the presence of brush or roller marks, and poor anti-sagging properties with drops of paint on the wall are unpleasant events that can be avoid by evaluating the application properties performing specific rheological test when formulating a coating product.

Three interval thixotropy test, 3ITT, is a common rheology test to evaluate the structural regeneration of a material. In fact, it has the power to predict the material recovery after a structural breakdown by simulating the application process in three intervals: the first and the latter intervals simulate the behavior at rest, and the middle interval simulates the structural breakdown that occurs during application, Figure 5.2. If the structural regeneration occurs too quickly this leads to poor surface leveling. On the other hand, if the regeneration is too slow, the coating will sag [150].

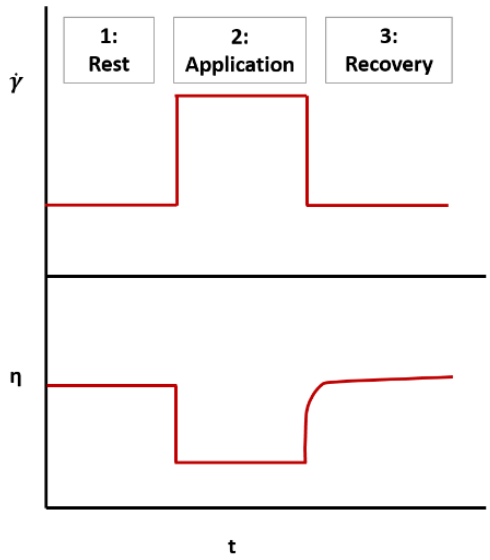

Figure 5.2 Graphic description of the Three Interval Thixotropy Test

Paints and coatings are complex materials, understanding their rheological behavior is difficult but it has a key role in the development of a successful product. By studying the rheological profile, it is possible to obtain information about all the life stages of a paint: from storage to application as reported in Figure 5.3.

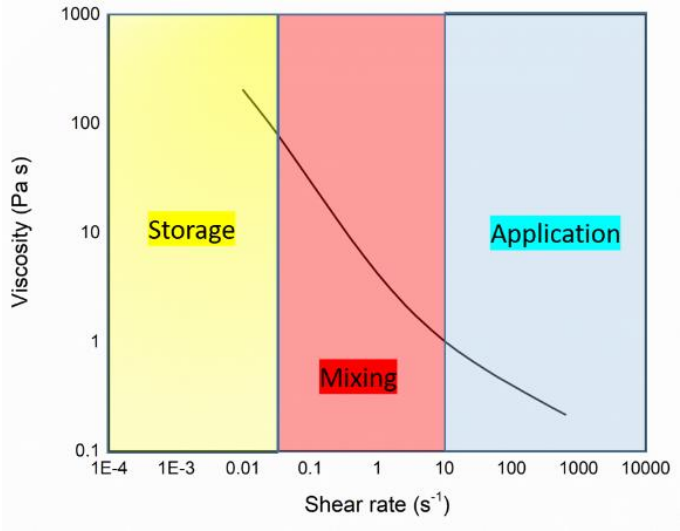

Figure 5.3 Typical viscosity profile of a water based paint describing the shear rate ranges connected to the storage, mixing and application processes

The rheological profile of a non-Newtonian material is incomplete considering only rotational test. The viscoelastic nature of a material is often characterized under sinusoidal deformation. Dynamic tests provide data on viscosity and elasticity related to the frequency applied; in fact, this test mode relates the assigned angular velocity or frequency to the resulting oscillating stress or strain [146].

Considering that viscoelasticity is a combination of two idealized behaviors, Hookean elasticity and Newtonian viscosity, a simple mechanical model can be used to describe this character. Here the most important viscoelastic parameters are G', the storage or elastic modulus, and G'', the loss or viscous modulus. The ratio between G'' and G' is called damping factor, tan δ, and for coatings represents the particle settling ability. For high content solid dispersion, the higher the solid character the better is the anti-settling property resulting in good in –can storage stability [148].

Amplitude sweep test where the strain γ varies at a fixed low frequency is used to investigate the linear viscoelastic range (LVER) where both the storage modulus (G') and the loss modulus (G") are independent from the strain, running parallel to each other Figure 5.4. Amplitude sweep test enhances the more solid or liquid like character of a coating depending on which modulus predominates inside the LVER and allows the determination of other viscoelastic parameters like the critical strain, γ_c at which the microstructure collapse when G'=G'' [151].

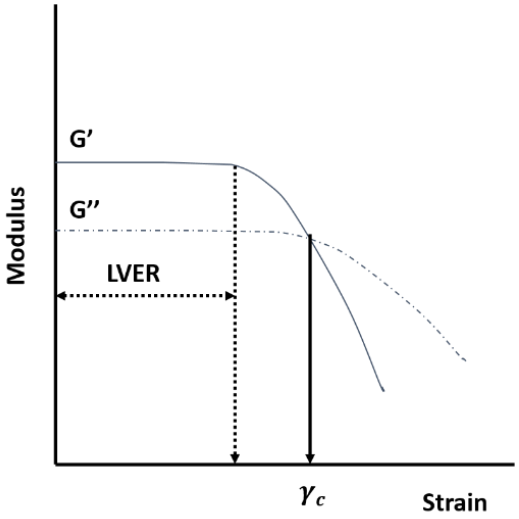

Figure 5.4 Commonly observed viscoelastic behavior of a coating performing an amplitude sweep test

5.2 SPECTROSCOPIC ANAYLSIS

Fourier transform infrared spectroscopy (FTIR) is a non-destructive technique used to characterize the chemical composition of a sample. The technique is based upon the identification of functional groups within molecules where such groups vibrate (either through stretching or bending) when irradiated with specific wavelengths of light [152]. The raw data acquired by the instrument are transformed by a mathematical procedure called Fourier transformation and plotted as absorption of the specific wavelengths against the wavenumber to obtain the IR spectrum.

The infrared region of the electromagnetic spectrum lies between 10 and 12500 cm^{-1} and can be divided into three regions: near-IR, mid-IR and far-IR.

In the mid-IR range (400–4000 cm^{-1}), there are several extremely important and useful classes of bonds that can be studied [153]. The mid-IR spectrum is divided into four regions: the single bond region (2500-4000 cm^{-1}), the triple bond region (2000-2500 cm^{-1}), the double bond region (1500-2000 cm^{-1}), and the fingerprint region. The latter describes unique molecular vibration extremely specific for each compound [154].

In this work, infrared spectroscopy has been used as qualitative analysis to characterize the raw materials and to evaluate their surface modification with specific chemicals.

5.3 WETTING ABILITY

The primary measure of wetting of a liquid on a surface is the equilibrium contact angle θ and it is described by Young's relation, Eq. 5.2.

$$\cos\theta = \frac{\gamma_{SV} - \gamma_{SL}}{\gamma_{LV}} \qquad (5.2)$$

Where γ is the interfacial tension between solid, liquid and vapor phases respectively [155].

As a matter of fact, static and dynamic contact angle measurements are commonly employed to study the wetting, dewetting, and adhesion characteristics of surfaces. According to the wetting ability, a surface is hydrophobic when its static water contact angle θ is >90° and is hydrophilic when θ is <90°. Superhydrophobicity is reached when the contact angle is higher than 145°, as reported in Figure 5.5 [156].

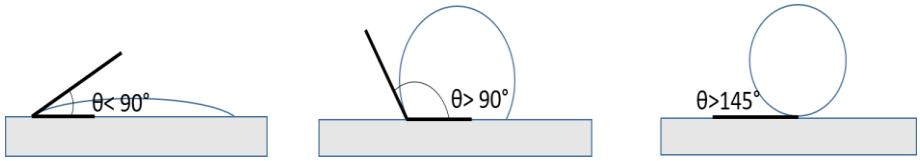

Figure 5.5 Schematic contact angle description from highly hydrophilic to super hydrophobic surface

Due to its relative simplicity, it is a useful technique to investigate surface modifications.

In this work, the static sessile drop method was used to investigate the wettability of the new fillers.

5.4 THERMOGRAVIMETRIC ANALYSIS

Thermogravimetric analysis (TGA) is an analytical technique used to determine the thermal stability of materials by monitoring the weight change that occurs as a sample is heated at a constant rate. The measurement is usually carried out in air or in an inert atmosphere [157]. Each weight loss describes the degradation step of a specific compound.

In this work, TGA was used to evaluate the thermal stability of the new fillers. Furthermore, it was used as quality assessment of the presence of specific molecules on the filler surface after chemical surface modification.

5.5 TENSILE TESTS

The investigation of the mechanical characteristics of a material is an important tool to evaluate the application conditions and durability of a specific material. In a tension test the sample is typically subject to a uniaxial extension that elongates the sample at a constant rate of elongation [158]. Tensile tests measure the force required to break a specimen and the extent to which the specimen elongates before the breaking

point. The force is converted to tensile stress considering the initial section area of the sample, and a stress-strain diagram is then plotted where the initial slope of the curve is Young's modulus, E [159].

Tensile properties of thin coatings are rarely evaluated because requires a challenging sample preparation method. Free films are needed in either the classical "dog bone" shape or rectangular stripes, Figure 5.6, as a consequence of that non uniform thickness, breaks on the edges and clamps slipping can occur decreasing the reproducibility. However, according to the literature, by taking into account the highest value of the tensile properties it is possible to reduce the error on the measurement and obtain reasonable results [50].

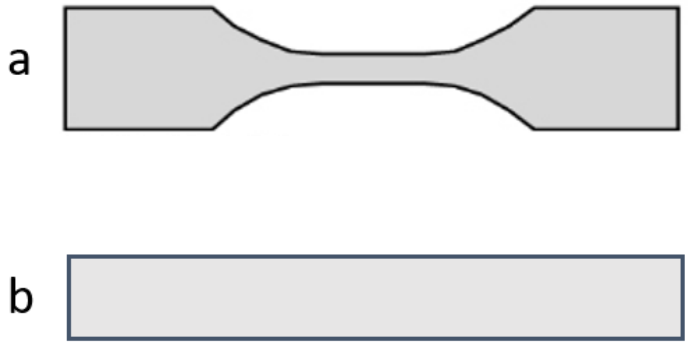

Figure 5.6 Tensile test sample shape: a) "dog bone", b) rectangular stripe

5.6 THERMAL PROPERTIES INVESTIGATION

Heat transfer is the transport of energy that results from temperature difference. For the occupied space, this heat transfer may be undesirable, as in the heat loss through the walls of a heated building in winter or the heat gained through the windows of a car on a hot summer's day.

Thermal conductivity, λ (W/m K), thermal transmittance U (W/m^2 K), and total thermal resistance, R_{tot}, are the most important thermal properties for construction materials.

According to European standards, there are two different procedures to determine the thermal properties of a masonry wall. The first procedure is based on the hot box measurement following either EN ISO 8990 or EN 1934 and the second one foresees two- and three-dimensional numerical calculations according to EN1745 [160].

In this work, an experimental set up based on UNI EN ISO 1934 was used. The instrument consists of two boxes, called cold chamber and hot chamber, separated by the sample to be tested. On both sides, a forced convection is induced. A uniform distribution of air is achieved close to the specimen surface. Between the two chambers a temperature difference of at least 20°C is established, which induced a heat flow through the sample. The insulating properties of the specimen are evaluated through the measurement

of heat flow and temperature differences between the hot and cold sides. The heat flow is measured using a standard heat flow meter (HFP01, Hukseflux, The Netherlands) while the temperature of air and surfaces of the specimen in both chambers are measured using ten type T thermocouples [161].

6 ALGINATE AS THICKENER FOR ARCHITECTURAL COATINGS: CHARACTERIZATION AND OPTIMIZATION OF AN ALGINATE BASED COATING FORMULATION

In the previous Chapters, traditional architectural coatings formulations were presented. Recent bio-based alternatives were shown as well. The main idea of this project is to replace traditional components with unconventional ones for the building sector.

As such, in the present Chapter, we deeply investigate the role of alginate as thickener for a water based coating formulation. Considering its molecular weight and counter ion type, a systematic approach to evaluate the feasibility of this polysaccharide to develop a successful product was followed.

6.1 DEVELOPMENT OF A COATING FORMULATION: BASIC CONCEPT

The main goal of this Thesis work is to study the feasibility of using non-conventional materials inside a paint formulation. In the previous chapter, the use of alginates in a wide range of fields has been well established. However, little about the use of this material in the architectural field is known. For this reason, a step-by-step approach was followed during the experimental campaign of this project. Raw materials were characterized and added inside the formulation gradually increasing the total number of components.

As previously described, the development of coatings formulation requires four general components: solvent, binder, additives and fillers. Moreover, it needs to meet specific requirements; considering both the market demand and the environmental regulations.

To help the reader throughout the reading of the next chapters, a brief introduction to the traditional single components used in this work is done. All these materials were of commercial use and were supplied by Boero Bartolomeo S.p.A. Italy:

- Solvent: tap water
- Binder: a copolymeric emulsion of a vinyl-based polymer with a 50 % wt. solid content
- Additives: antifoam, dispersant, wetting agent and biocide are fatty acid or polyacrylic based chemicals
- Traditional thickener: hydroxypropyl methylcellulose
- Filler: calcium carbonate
- Pigment: titanium dioxide

Coating formulations are expressed as percentage by weight, wt. %.

The preparation process involves two phases: the gel preparation, at low speed, where the thickener and the solvent are mixed, and the dispersion or grinding phase where a higher speed is required to achieve a homogeneous dispersion of the solid components.

6.2 THE ROLE OF ALGINATE MOLECULAR WEIGHT AND CONCENTRATION ON ITS THICKENING ABILITY IN COATING FORMULATIONS

Part of the content of this chapter was published as:

Gaggero, G.; Delucchi, M.; Allegretta, G.; Vicini, S.; Botter, R. *Interaction of sodium alginate thickener with components of architectural water-based coatings.* Progress in Organic Coatings, 151, 106116, **2021**.

Sodium alginate is a seaweed derived polysaccharide whose gelling ability is well-known in biomedical and food industries. Its widespread use in biomedical and food research is due to its biocompatibility, non-toxicity and ability to easily form a gel structure by ionic cross-linking with multivalent cations [162,163]; in addition, considering its role as thickener in other fields, sodium alginate has potential application in printing paste in the textile industry.

Food grade alginate can be used as thickener and stabilizer ingredient in food recipes. Sodium alginate as E401 is edible, safe and approved by the Food and Drug Administration (FDA). Its thickening properties are not limited to pudding and yoghurt preparation. For example, in textile printing the thickener not only affects rheological properties but also the correct color, design definition, evenness, and softness. Synthetic thickeners have been historically used but some attempts have been made on using alginate as thickener for printing paste. Alginate alone and alginate mixed with aloe Vera showed some good printing qualities [164,165]. When it comes to architectural coatings, suppliers suggest alginate as a suitable thickener for paints; however, it is hard to find scientific literature related to this topic. To our knowledge the most relevant example of alginate paint is a patented ecological paint based on plant and marine components that work as thickener [166]. However, little is known about the influence of alginate on paint properties.

In this chapter, sodium alginate was studied as potential thickeners for the development of water-based coatings for the architectural field. In particular, the influence of its molecular weight, concentration and type of alginate salt was investigated. The suitability of alginates for the specified scope was verified evaluating the occurrence of interactions between the polysaccharide and the main components of the formulation (water, binder, powder pigment and filler). This aim was achieved through a step-by-step approach, using rheological and spectroscopic analysis on increasingly complex samples, i.e., from aqueous solutions consisting of water and thickener to complete paint formulations.

6.2.1. Materials

A commercial hydroxypropyl methylcellulose (CE) with methoxy content of 19-24 wt.%, hydroxypropoxy content of 4-12 wt.% and viscosity 7000÷8000 mPa·s at 2% in H_2O at 25°C, was used as

benchmark thickener. Two sodium alginates (SA) purchased from Sigma Aldrich were used as experimental thickeners to investigate the role of the molecular weight $\bar{M}_w$:

- a low viscosity alginate (SAL), viscosity 4 – 12 mPa·s at 1% in H_2O at 25°C, M/G ratio of 1.56
- a medium viscosity alginate (SAM), viscosity ≥ 2000 mPa·s at 2% in H_2O at 25°C, M/G ratio of 1.56.

The other components used to prepare the final coating described in Section 6.1: solvent, binder, cellulose or the selected polysaccharides as thickener, pigment and filler are commercial products provided by Boero Bartolomeo S.p.A.

6.2.2. Samples preparations

A step-by-step investigation of the interaction between the polysaccharides and the surrounding system was carried out selecting the ingredients for the preparation of different samples and assessing the properties of the prepared formulation at each step:

- Step 1 samples, called aqueous solutions, were prepared by gently adding the thickener to tap water under magnetic stirring, at room temperature, to avoid the formation of lumps;
- Step 2 samples, called binder emulsions, were prepared by adding the binder and the small concentration of additives to the aqueous solution containing the thickener under magnetic stirring at low speed to promote a homogeneous distribution inside the sample;
- Step 3 samples, called solid dispersions, were prepared by adding the solid powder, either calcium carbonate or titanium dioxide, and the additives to an aqueous solution of sodium alginate and binder under magnetic stirring.
- Step 4, called complete formulations, were prepared mixing all the previous investigated components by using a high-speed disperser, Dispermat, equipped with a stainless-steel dispersion impeller; low speed was set during the mixing phase, while high speed was set during the grinding phase.

According to the company know-how, the concentration of cellulose thickener was fixed equal to 0.4 wt. % of the total formulation, i.e., the weight of all the components, as in a standard wall paint formulation.

Since the viscosity of the alginates differs from that of cellulosic thickener, multiple concentrations were tested: 0.4 wt. %, i.e., the standard concentration of CE and 0.2 wt. % as attempt concentrations.

An alphanumeric code was used to identify the different samples: the first letters describe the type of thickener, the first number is the weight percent of thickener and the last number corresponds to the step involved in the analysis. For step 3, the final letters describe the powder investigated, i.e., “cc” for calcium carbonate and “t” for titanium dioxide.

Step 1, 2 and 4 were prepared considering the real concentration, wt. %, of the total formulation; samples composition is reported in Table 6.1 and Table 6.3.

Step 3 was prepared with a lower concentration of calcium carbonate, compared to the total formulation, to ensure a good dispersion because no grinding phase was involved; samples composition is shown in Table 6.1. The solid-gel mixture, made of alginate, water and solid component, was stirred for 30 minutes and then left overnight at rest. The mixture was moved into a centrifuge tube, centrifuged at 8,000 rpm for 5 minutes, washed with demineralized water, and centrifuged again. After that, the powder was placed in an oven at T= 50°C for 48 hours.

Table 6.1 Samples compositions expressed in grams of aqueous solutions (step 1) and binder emulsions (step 2)

Step	Sample code	Thickener (g)	Water (g)	Binder + Additives (g)	Pigment + Filler (g)	Total (g)
1	CE04_1	0.4	23.0			23.4
	SAL02_1 and SAM02_1	0.2	23.2			23.4
	SAL04_1 and SAM04_1	0.4	23.0			23.4
2	CE04_2	0.4	23.0	10.6		34.0
	SAL02_2 and SAM02_2	0.2	23.2	10.6		34.0
	SAL04_2 and SAM04_2	0.4	23.0	10.6		34.0

Table 6.2 Samples compositions and preparation methods of solid dispersions (step 3)

Step	Sample code	Composition
3	SALcc_3 and SAMcc_3	0.25 g calcium carbonate added to 20 ml of a 2.5 wt.% aqueous solution of sodium alginate
	SAMt_3	0.25 g titanium dioxide added to 20 ml of a 2.5 wt.% aqueous solution of sodium alginate

Table 6.3 Samples compositions expressed in grams of the complete formulations (step 4)

Step	Sample code	Thickener (g)	Water (g)	Binder + Additives (g)	Pigment + Filler (g)	Total (g)
4	SAL02_4 and SAM02_4	0.2	23.2	10.6	66.0	100.0
	SAL04_4 and SAM04_4	0.4	23.0	10.6	66.0	100.0

6.2.3. Characterizations techniques

Rheological measurements were performed with an Anton Paar Physica MCR 301 rheometer using two different geometries: a cone-plate, with cone angle α=2° for step 1 and step 2 samples, and a parallel plate d=50 mm for step 4 samples. A Peltier plate and a PTD 200 temperature control system were used to keep a constant temperature of 23°C.

Steady-shear flow behavior was evaluated by varying the shear rate from 0.01 to 1000 s^{-1}. A resting time of 60 s was fixed after loading the samples before starting the measurement. Non-equilibrium flow curves were investigated through a logarithmic shear stress ramp by recording the viscosity every 60 seconds only for the complete formulations. The shear stress range was chosen specifically for each sample. To ensure data reproducibility, the curves shown in this work are the average curves of two replicates.

Amplitude sweep tests, where the frequency is fixed and the strain amplitude increases, were performed to identify the linear viscoelastic region, LVER, where the storage and loss modulus are independent from the deformation and the network structure is not destroyed [50]. The strain γ ranged from 0.01 to 100% at constant frequency of 1 Hz.

Infrared spectra were recorded on a NICOLET 380 FT-IR spectrometer and acquired by accumulating 100 scans at 4 cm^{-1} with a resolution between 400–4000 cm^{-1}. Pellets were prepared by potassium bromide dilution technique; sample concentration inside each pellet was 1 wt. %.

6.2.4. Results and discussion

Step 1

The first step involved the characterization of aqueous solutions of the polysaccharides; the importance of this step is linked both to understanding the thickening efficacy with aqueous media, and to identifying the rheological profile of the raw materials. Viscosity curve of aqueous solution are reported in Figure 6.1.

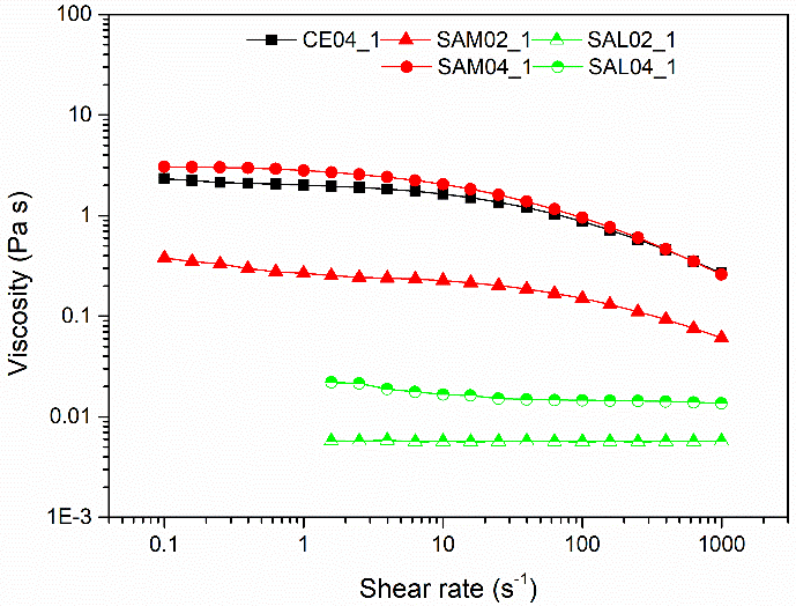

Figure 6.1 Viscosity curves of aqueous solutions; step 1

CE04_1 has an initial constant value of viscosity, followed by a viscosity drop as the shear rate is increased; SAM samples have the same trend; specifically, they exhibit a Newtonian plateau at low shear rates and a power law region at higher shear rates; this is typical evidence of the so called shear thinning behavior. SAL samples show a Newtonian behavior, with constant values of viscosity over shear rate. Considering the overall viscosity profile, SAM04_1 shows almost a perfect overlapping with CE04_1 while SAM02_1 have a lower viscosity than CE04_1 at the same shear rate, respectively. On the other hand, all the SAL samples exhibit lower values compared to those of CE04_1 in the whole range of shear rates.

This difference is strongly correlated to the chemical nature, the concentration and the average molecular mass $\bar{M}_W$ of the thickener.

Considering the chemical nature, CE is a non-ionic polymer, without charge on its backbone, and it has a thickening effect only interacting with the aqueous phase due to its large hydrodynamic volume capable of immobilizing water molecules [50]. On the other hand, SA acts in water as a polyelectrolyte because it carries a negative charge due to the presence of a carboxyl group in each monosaccharide unit. Hence, it interacts with water molecules through its first hydration shell, with the existence of large water pools confined between polysaccharide chains, and its conformation might be affected by electrostatic interactions with the negative charges [167].

Moreover, polymer-chain behavior in solution depends on their molecular mass and concentration. CE is a commercial product, so the direct information on its average molecular weight $\bar{M}_W$ is not known, but according to the literature it is reasonable to assume a value higher than 500 kg/mol [168]. On the other hand, in a recent work, the $\bar{M}_W$ of SAM and SAL was calculated as 490±60 kg/mol and 145±2 kg/mol,

respectively [169]. For these reasons, CE04_1 and SAM04_1 exhibit similar behavior, with higher viscosity than SAL04_1, due to the formation of a thicker secondary structure made by entanglements.

Finally, considering the concentration, it is well known that, in good solvents, three concentration regimes exist: a diluted, a semi-diluted and a concentrated one. Among them, a further classification considers the occurrence of overlapping chains, with the formation of entanglements, both in the semi-diluted and the concentrated regime [170]. By observing the molecule conformation, CE has a semiflexible chain, and reaches the semi-diluted entangled regime at lower concentrations than alginate [171]. SAM samples belong to the semi-diluted entangled regime, i.e., the long chains create a network of entanglements. According to the literature, SAL, in these concentrations, behaves almost like a neutral polymer in a semi-diluted unentangled regime [169]; the short chains cannot build a strong network and the predominant interaction is probably with water molecules.

Step 2

The polymeric binder provides film formation and adhesion to the substrate; it can interact with the thickener in the case of polymers that contain hydrophobic groups capable of association, i.e. associative thickener. Thus, the evaluation of possible interactions between the polysaccharide and the binder is fundamental to understanding the properties of the final product [47,50].

The viscosity curves of the binder emulsions are reported in Figure 6.2.

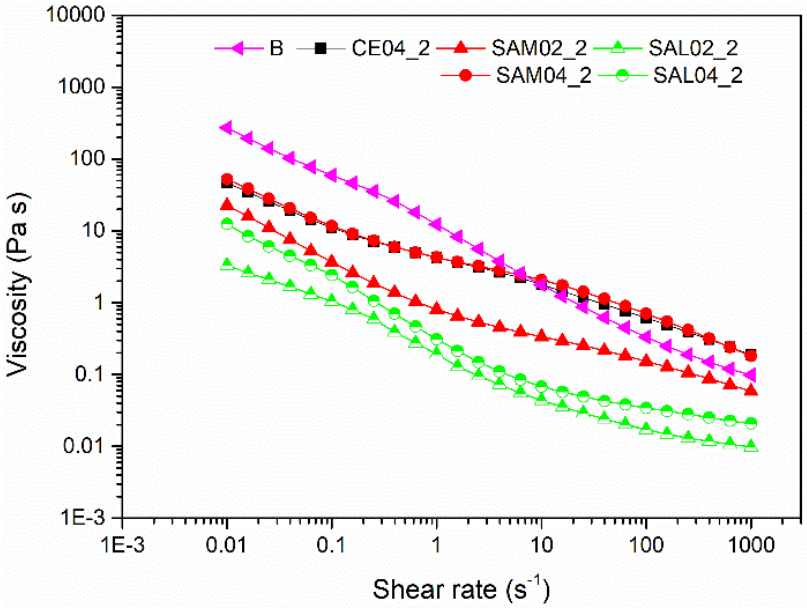

Figure 6.2 Viscosity curves of binder emulsions; step 2

The viscosity curve of the pure binder emulsion (binder raw material, B in Figure 6.2) is added for comparison.

It is worth noticing that at low shear rate, the entire set of samples exhibit a drastic decrease of viscosity increasing the shear rate, and the previously observed Newtonian plateau is absent. This behavior is typical of shear-thinning materials, inclined to a solid-like character. At higher shear rates, the curves tend to overlap the corresponding step 1 curves; this occurs for all the concentrations involved and is more evident for CE and SAM, i.e., medium viscosity samples, rather than for low viscosity samples.

In order to understand these behaviors, it is important to clarify that the binder is an emulsion, thus polymer particles are stabilized in a water phase. At low shear rates, the emulsion droplets or particles are closely packed, acting like a high-concentrated-solid dispersion, exhibiting high values of viscosity. Increasing the shear rates, viscosity sharply decreases, showing a non-Newtonian character, typical of the binder raw material. At higher shear rates the architecture of the emulsion is disrupted, because of the deformation, elongation and alignment, of the particles occurring under shear forces [172,173]. CE04_2 shows the presence of two distinctive regions: at a lower shear rate the rheological behavior is driven by the binder's rheology while at a high shear rate by the aqueous gel rheology. Considering the SAM samples, the same behavior of CE appears: a critical shear rate value characterizes the transition from the solid-like binder behavior (low shear) to the polysaccharide shear thinning behavior, due to the detangled- and oriented-chain morphology (high shear). The stiffer the gel network, the higher the concentration of alginate and the lower this critical value is. SAM04_2 and CE04_2 exhibit the same behavior, and since it is well known that cellulosic ethers do not interact with the binder [174], it is possible to assume that also the alginates do not chemically interact with the binder. On the other hand, SAL samples, due the weaker network build-up of the polysaccharide chains in water, do not exhibit an evident transition, but behave as solid-like materials, reaching the lowest value of viscosity imposed by the aqueous gel.

Step 3

It is well known that alginate interacts with divalent cations in aqueous solutions by means of egg-box mechanism; here the possible interaction of SA with the cations on the surface of calcium carbonate and titanium dioxide was investigated through FTIR spectroscopy. The interaction between alginate and calcium carbonate, the is shown in Figure 6.3. Considering that SAM and SAL showed the same spectra, only SAM is reported in Figure 6.3.

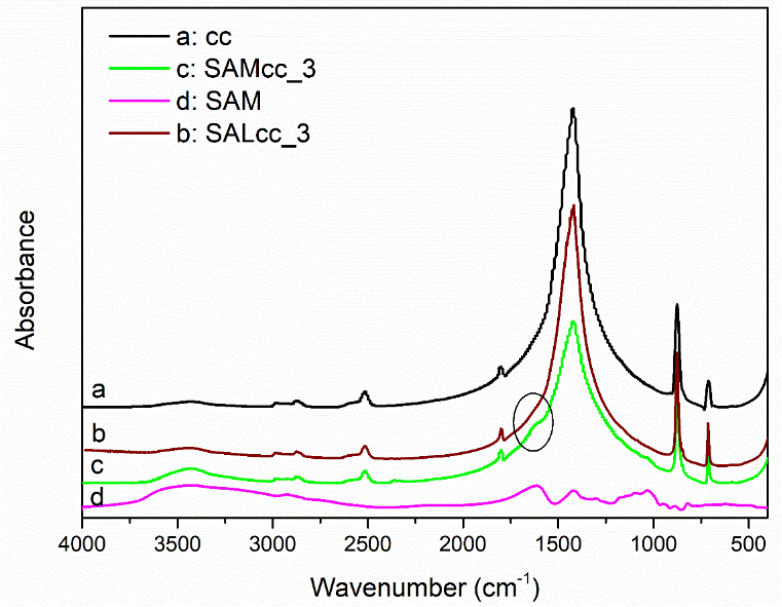

Figure 6.3 FTIR spectra of a) calcium carbonate, b) mixture of calcium carbonate and low viscosity alginate, c) mixture of calcium carbonate and medium viscosity alginate d) medium viscosity alginate

The most representative absorbance peaks of calcium carbonate are at 1430 cm^{-1} corresponding to the asymmetric stretching vibration of CO_3^{2-}, at 875 and 713 cm^{-1} corresponding to the symmetric stretching vibration and the out-of-plane bending vibration of CO_3^{2-} [175]. In the IR spectrum of SAM, the most important peaks are the OH stretching broad band at 3435 cm^{-1}, and partially overlapped with vibrational modes of molecularly adsorbed water, the stretching vibration of CH at 2925 cm^{-1}, the COO^- asymmetric stretching vibration of at 1617 cm^{-1}, and the corresponding COO^- symmetric stretching vibration at 1419 cm^{-1}. A few complex bands in the range of 1000-1200 cm^{-1} are due to CO and CC stretching modes of the organic chain [176]. The mixture sample presents at low wavenumbers all the calcium carbonate peaks, namely the strong band at around 1400 cm^{-1} containing both the vibrational modes of CO_3^{2-} and COO^- groups and a shoulder at around 1600 cm^{-1}, even more evident in the spectrum of the mixture carbonate/SAM as can be seen in the circle.

It is known that the FTIR analysis of calcium alginate, prepared by immersing a solution of sodium alginate in a calcium chloride bath, gives rise to displacements of the COO^- peaks [177]. Less immediate is the analysis of a spectrum where the calcium ions available for chelation are not in solution but are part of a mineral such as calcium carbonate, few works are available in the literature where alginate is used as a depressant or as an additive during the crystallization of calcium carbonate [178,179]. To highlight the presence of alginate in the sample spectrum, a subtraction between the spectrum of pure calcium carbonate and that of a mixture was performed. The OH broad band shifted from 3435 cm^{-1} to 3450 cm^{-1}, because the hydroxyl groups of the polysaccharide chain are no longer free but occupied and influenced by the formation of the chelated structure by hydrogen bonding. The shift of the carboxylate peak (asymmetric

stretching) from 1617 cm^{-1} to 1622 cm^{-1} reveals the presence of chelation with calcium. Therefore, the ionic exchange between the sodium of SAM and the calcium on the carbonate surface, is suggested by the shifting of peaks of the carboxylate group typical of the alginate [180]. In fact, by changing the counter ion, the surroundings of the carboxyl group change, in particular sodium and calcium being different in ionic radius, charge, charge density and atomic weight. However, the effect on the electric field around the carboxylate group is reduced due to the presence of molecules of water, therefore the displacement is minimal.

Considering the mixture with SAL, the same method was followed to evaluate the presence of alginate peaks. In this case, the OH broad band shifted from 3435 cm^{-1} to 3447 cm^{-1} while the asymmetric COO^- stretching band shifted for from 1617 to 1630 cm^{-1} demonstrating again an interaction between the two materials.

IR spectra of titanium dioxide, SAM and the mixture sample are depicted in Figure 6.4.

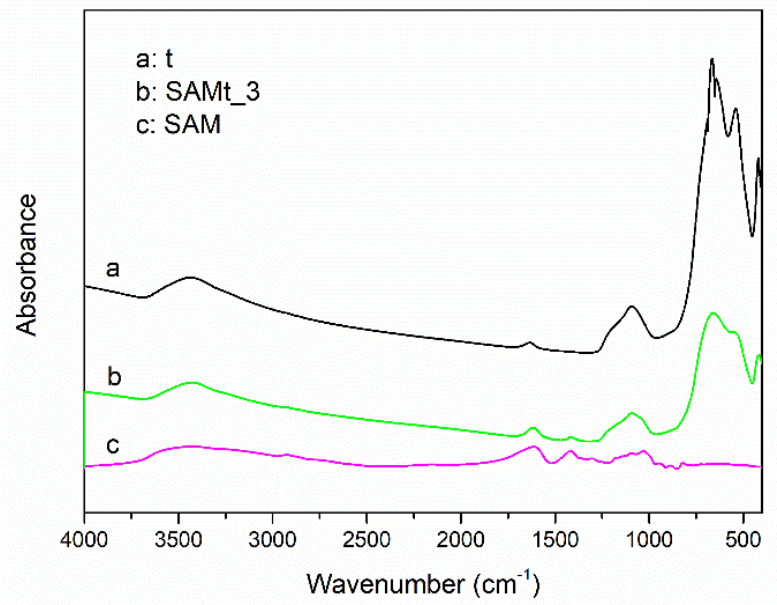

Figure 6.4 FTIR spectra of: a) titanium dioxide, b) sodium alginate medium viscosity, c) mixture of titanium dioxide and sodium alginate medium viscosity

The FTIR spectra of titanium dioxide show a main complex absorption in the range of 400–700 cm^{-1}, related to bending and stretching mode of Ti–O–Ti [181]. Broad and weaker bands at 3440 and 1633 cm^{-1} are indeed due to molecularly adsorbed water. The mixed sample exhibit all the titanium peaks, almost unchanged. As further proof, the subtraction spectrum only show a small peak correlated to the symmetric stretching vibration of COO^- due to the presence of a small amount of alginate slightly shifted from its original position. No clear information can be obtained from an analysis of the peak at 1630 cm^{-1}, because it includes both the signal related to the asymmetric COO^- stretching mode and to the deformation mode of adsorbed molecular water, strongly overlapped. According to this analysis, the alginate adsorbed to the titanium dioxide surface results in a small amount; according to the neutral pH condition of the samples the

surface charge of TiO_2 is negative thus only repulsive interactions took place [182]. The occurrence of shifts can be due to the interaction with some impurities or with water molecules surrounding the mineral.

Step 4

The last step involved the rheological investigation of the complete formulation. Understanding the flow behavior is fundamental for the development of a successful product. Here, both a controlled shear rate and a controlled shear stress approaches were used. In a shear rate ramp test, the low shear rate region describes the storage condition, the medium shear rate region describes the processability and the high shear rate region describes the application processes [183]. In a shear stress ramp test, it is possible to evaluate the yield stress, thus the minimum stress requires to flow. The viscosity curves of the complete formulations are reported in Figure 6.5.

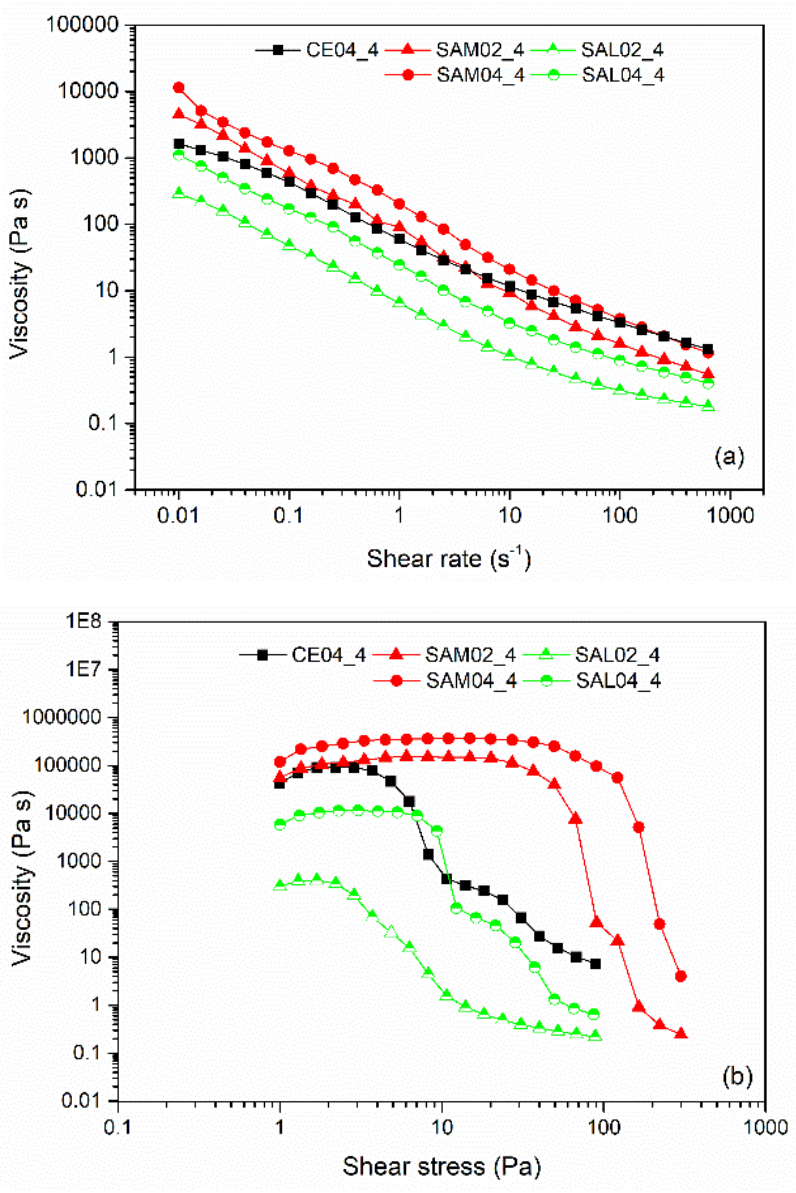

Figure 6.5 Viscosity curves of complete formulations step 3: (a) shear rate ramp, (b) shear stress ramp

All the samples exhibit a non-Newtonian, shear thinning behavior. Furthermore, considering the whole shear rate range of the experiments Figure 6.5 (a), the rheological behavior is typical of high solid content dispersions i.e., coatings, with the absence of a low shear viscosity plateau and a steep decrease in viscosity. In particular, when the test input is the shear stress, Figure 6.5 , they show a yield stress τ_0, i.e. a critical value of stress below which the material does not flow. For this reason, they are sometimes called viscoplastic materials or Bingham fluids.

The low shear rate region, thus lower than 0.1 s^{-1}, describes the storage conditions; considering that all the rheological tests were performed after 60 seconds of conditioning time, it can be assumed that the data obtained are a good prediction of the storage condition. Both the SAM02_4 and SAM04_4 samples, when compared to CE04_4, exhibit higher values of viscosity, demonstrating that they have good anti-settling properties. On the other hand, the SAL02_4 and SAL04_4 curves do not reach CE04_4; these low values of viscosity, especially for SAL02_4, are a sign of possible syneresis or sedimentation during time, events that are often unwelcome in commercial products.

Shear rate between 10 and 1000 s^{-1} is often referred to the mixing and pumping process; it is possible to evaluate the processability of the formulations through the flow curves. As experimental evidence, SAM04_4 was too “thick” and exhibited problems of powder dispersion in the mixture. On the contrary, SAL02_4 was too “thin” to be processed without spattering in the grinding phase.

Considering the high shear rate region, which describes the application process, it is interesting to notice that at about 700 s^{-1} SAM04_4 exhibits the same behavior as CE04_4, with an overlap of the two curves. Differently, SAM02_4 has a lower value of viscosity, but still not low enough to be applied, thus all three samples need to be diluted before application. On the other hand, SAL samples already have a sufficiently low value of viscosity that potentially allows them to be applied without dilution.

According to the most recent literature, controlled shear stress should be the correct approach to evaluate paint rheology, especially because the application process is a stress driven phenomenon rather than a shear rate driven one [184]. In any case, since the equilibrium time was too long at low shear stresses, carrying out a steady state, shear stress-controlled viscosity measurement was not possible. For this reason, non-equilibrium flow curves with a shear stress ramp were performed and are reported in Figure 6.5 (b).

It is worth noticing that after 24 hours of rest, all the alginate samples exhibit an initial solid-like character that increases with the average molecular mass and the concentration involved in the formulation and disappears after mixing. This stiff gel structure, absent in the cellulosic paint, can be compared to a “pudding” and it was stiffer for SAM_4 samples than SAL_4 samples.

Even though they are non-equilibrium curves, the results obtained are in good agreement with the shear rate-controlled measurements obtained in the steady state conditions of Figure 6.5 (a), demonstrating a shear thinning behavior. The low shear stress region, as well as the low shear rate region, is the rheological

representation of the condition at rest; by considering the plateau, SAM04_4 has the highest viscosity thus, the best anti-settling properties. SAM02_4 and CE04_4 overlap, leading to a similar behavior during the storage condition; SAL04_4 exhibits a fairly high viscosity, assuring sufficient anti-settling properties; SAL02_4 has the lowest viscosity, thus the worst anti-settling properties. Increasing the shear stress, all the samples exhibit a drop-in viscosity, which appears in two clearly different steps for CE04_4, SAM02_4, SAL04_4, and less evident for SAL02_4. SAM04_4 exhibits only one inflection point, probably because the investigated range of shear stress was not high enough to see the possible second one. This discontinuity reminds us of the so called "structure point" found in food rheology characterization and can be described as the stress at which the destruction of a tertiary structure occurs. From a structural point of view, this means that there are aggregates structures that collapse in different moments of the analysis, because of their dimension and degree of energy dissipation [185]. Since these formulations have high solid contents and are characterized by synergistic interaction among the components, it is reasonable to think that the microstructure collapses in more than one-step, with a remarkable rheological effect of the microaggregates in the system. This behavior can also be associated with the minimum stress that a material needs to overcome to begin to flow, commonly known as apparent yield stress, τ_0 [186]. In fact, paints are structured materials, and it is not unusual that they behave like a solid at rest and require a stress to begin to flow. The determination of τ_0 is controversial; it depends on the sample pre-treatment and on the method that is used to calculate it, for example evaluation through extrapolation from the flow curve, creep tests or amplitude sweep tests [187]. For this reason, the absolute value could differ among the tests, but it will be an efficient tool to predict the plastic behavior. In this work, τ_0 is determined by the intersection point between the linear section at low shear stress and the inflectional tangent at the beginning of the viscosity drop in the non-equilibrium flow curve of Figure 6.5 (b). No fitting models were used due to the peculiar shape of the curves.

The curves show that CE04_4 has a low apparent yield stress around 5 Pa, both SAM samples exhibit a very high value of τ_0, over 50 Pa; SAL04_4 has the closest value compared to CE04_4, 8 Pa, and SAL02_4 has the lowest value of τ_0, 2 Pa.

The peculiar behavior of both the alginates can be attributed to the chemical nature that distinguish hydroxypropyl methylcellulose from sodium alginate. CE is an organic, non-associative thickener, which does not interact with the surrounding system but causes an increase in viscosity through a hydrodynamic mechanism and the formation of polymeric entanglements. Sodium alginate has become famous in biomedical, food and textile industries because of its gelling ability with multivalent cations via a chelating effect; the so-called egg-box model [188]. Paint formulation is a complex mixture of chemicals, it cannot be excluded that, sodium alginate, with its anionic nature, interacts with one or more components of the paint. Evidence of interaction between sodium carboxymethylcellulose, another anionic polysaccharide, and calcium carbonate demonstrated the possible association between the two components [189]. For this

reason, great attention was paid to the solid components, in this case calcium carbonate and titanium dioxide; in fact, a recent work studied the role of alginate as depressing agent to separate minerals, including calcite, in a flotation test through the chelating effect of its carboxyl group on superficial metallic ions [178,190]. Moreover, step 3 spectroscopic investigations showed an interaction between calcium carbonate and alginate. For these reasons, the ability to endure higher stress before deformation, as seen in Figure 6.5, is due to the formation of a gel structure that cannot be linked only to the formation of entanglements. Considering that both the alginates have the same M/G ratio i.e., the number of chelating sites, the stiffness of the network has to be related to the concentration and the molecular mass of the thickener. Thus, increasing the concentration, the number of chelating sites increases; in addition, increasing alginate molecular mass the chain length increases, so the probability of chain/calcite-particle interaction rises. Differently, low viscosity alginate, acting almost as a neutral polymer in this environment, does not have enough chelating sites adjacent to build up a strong 3D network and behaves as the non-ionic cellulose. After all these considerations, the gel appearance is reasonably the result of both the semi-diluted entangled regime and the interaction with the superficial calcium ions of calcium carbonate and titanium ions of titanium dioxide.

Paints are viscoelastic materials, whose properties are evaluated through two parameters: the storage modulus, G', representing the elastic component, and the loss modulus, G'', representing the viscous portion of the material. Amplitude sweep tests are reported in Figure 6.6.

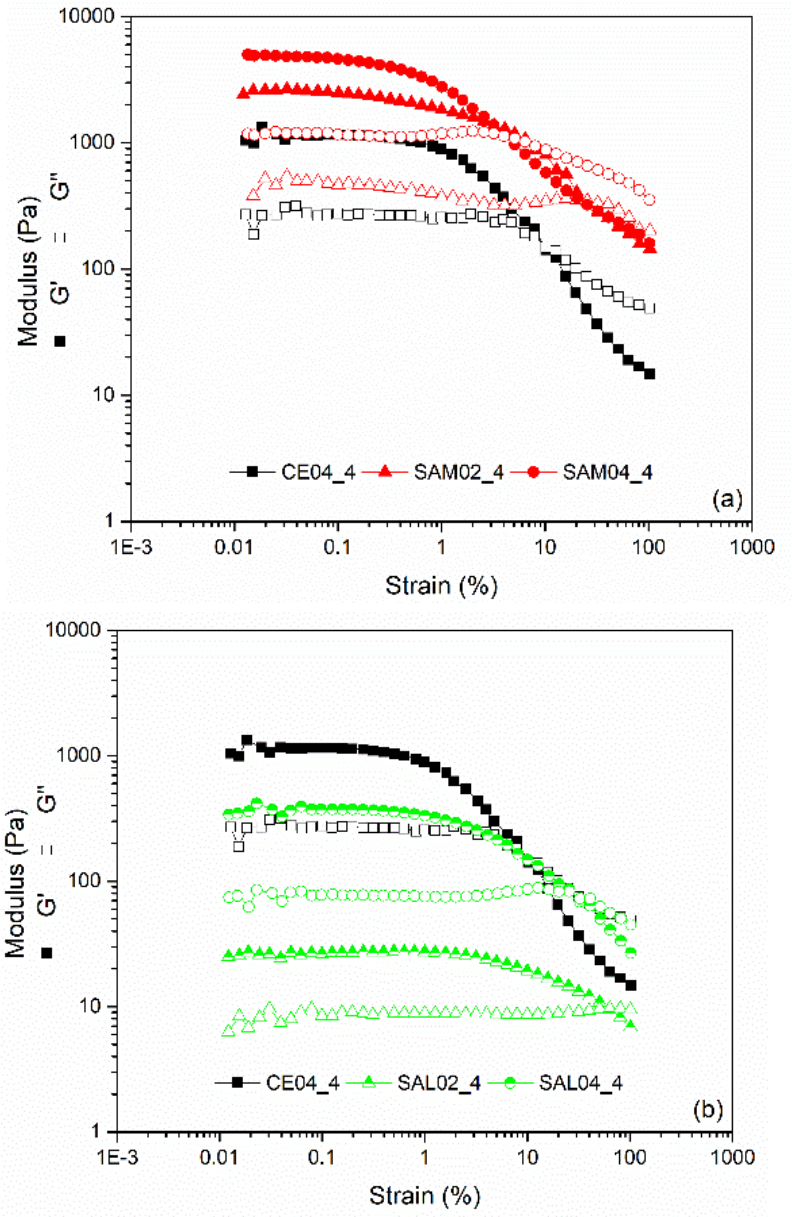

Figure 6.6 Amplitude sweep test of the complete formulations performed at f=1 Hz; a) CE04_4 compared with Sodium alginate medium viscosity, b) CE04_4 compared with sodium alginate low viscosity

It is readily visible that G' results higher than G'' for all the specimens and for the whole range of considered strains; then the solid part prevailed on the liquid part of the samples. Both SAM02_4 and SAM04_4 exhibit a higher value of both G' and G'' compared to CE04_4. On the other hand, SAL02_4 and SAL04_4 show a lower value of both the viscoelastic parameters throughout the whole curve. The linear viscoelastic region occurs at low strain; it indicates where the material response is independent from the deformation and the network structure does not break-down. At the end of the linear region, when both G' and G'' lose their independency from strain, the yielding region occurs. In this region the crossover point identified with a critical strain γ_c, where G'=G'', need to be investigated. At the crossover point the

solid like character changes to a viscous like one, with a breakdown of the internal microstructure. The crossover point can be used to predict anti-settling properties; the higher the strain at which the crossover occurs, the more elastic the network, the better the anti-settling properties [191]. The ratio between G'' and G' is called the damping factor, tan δ, and represents the dominant portion of the viscoelastic behavior [192]; the lower the value of tan δ, the higher the solid-like behavior, the better the anti-settling properties. Table 6.4 reported the viscoelastic parameters extrapolated from the amplitude sweep test.

Table 6.4 Viscoelastic parameters, critical strain, and damping factor obtained from the amplitude sweep test

	γ_c (%)	tan δ
CE04_4	9	0.23
SAM02_4	25	0.21
SAM04_4	5	0.29
SAL02_4	63	0.32
SAL04_4	24	0.29

CE04_4 shows a low value of the critical strain and a short linear viscoelastic regime, LVER, as the result of a weak gel structure. SAM02_4 has a higher value of γ_c then SAM04_4. This behavior is likely attributed to the fact that increasing the concentration of alginate, the material has a higher solid-like character, as demonstrated by G' being higher than G''; thus a higher brittleness is reasonably attributed to this network. Indeed, lower strain are required to induced structural transition [193]. SAL02_4 exhibits the highest γ_c according to the long LVER and the extremely low value of G' resulting in a very weak structure.

Moreover, all the samples have a tan δ < 1, this confirms the solid-like character and good anti-settling properties.

6.2.5. Conclusions

The possible use of anionic sodium alginates as thickeners in wall-paint formulations was evaluated analyzing their interaction with water, binder, pigment and filler; in particular, the effect of average molecular mass and concentration was investigated. A comparison with cellulose ether was made, and it indicated that:

- Rheological measurements of aqueous solutions established the presence of a stiff network for CE and SAM samples; this is due to the presence of entanglements; on the other hand, SAL samples, did not exhibit an organized molecular architecture due to their shorter chains and lower $\bar{M}_W$. Considering the binder emulsions, viscosity curves indicated that the gel structure remained

undisturbed for all the samples, highlighting the non-associative nature, in the general terms of association between thickeners and binders, of the alginates. Considering the complete formulations, the presence of pigment and filler increased the overall viscosity and the shear thinning nature of the samples leading to the characteristic Bingham like flow behavior. According to the rheology profile, for our purpose SAM samples exhibited a strong gel structure and only the 0.2 wt. % concentration of SA resulted suitable for future formulation. SAL samples exhibited a weak gel structure, evidenced by the low value of apparent yield stress and by the amplitude sweep test.

- FTIR spectra demonstrated that the gel stiffness could be related to the presence of a chelating effect between the carboxyl group of alginate chains and the superficial calcium ions of the calcium carbonate; no evidence of chelation was found for the titanium dioxide.

6.3 EVALUATION OF THE EFFECT OF ALGINATE COUNTERIONS ON THE DEVELOPMENT OF A COATING FORMULATION FROM STORAGE TO APPLICATION PHASE

Part of the content of this chapter was published as:

Gaggero, G.; Delucchi, M.; Di Tanna, G.; Lagazzo, A.; Vicini, S.; Botterp, R. *Effect of different alginate salts on the rheological and tensile properties of waterborne paints.* Progress in Organic Coatings,163, 106676, **2022**.

Sodium alginate has proved to be a suitable thickener for water-based coatings formulations. Its thickening mechanism is linked to both the effect of its molecular weight and a weak chelating interaction between the superficial ions of calcium carbonate, i.e., the filler. Acting as an associative-like thickener, alginate has a great potential inside paints formulations.

In this Chapter, three different types of alginates salt were analyzed as possible substitutes of a standard thickener, i.e., soluble cellulose: sodium alginate, potassium alginate and ammonium alginate. In fact, little is known about the gelling ability dependency on the alginate salt counterion. In addition, the work is related to the investigation of the influence of the alginate counterions on the stability and applicability of tailored basic formulations through a combination of several rheological and mechanical measurements. Moreover, this investigation has been made in all the different life stages of the paint formulation: from wet to dry state and from storage to application conditions. According to the results obtained in Section 6.2, 0.2 wt. % was chosen as optimal concentration for the development of a water-based alginate coating. However, samples at 0.4 wt.% were tested as well and the result are shown in Appendix A.

6.3.1. Materials

A commercial hydroxypropyl methylcellulose (CE) with methoxy content of 19-24 wt.%, hydroxypropoxy content of 4-12 wt.% and viscosity 7000÷8000 mPa·s at 2% in H_2O at 25°C, was used as benchmark thickener.

Sodium alginate, SA, potassium alginate, PA, and ammonium alginate, AA, were gently provided by Algaia. No information about the molecular weight was available; however, viscosities data and a common M/G ratio of 1.3 were available as technical information:

- Sodium alginate, SA, viscosity 350-550 mPa s in 1% water at 20°C
- Potassium alginate, PA, viscosity 450-650 mPa s in 1% water at 20°C
- Ammonium alginate, AA, viscosity 350-450 mPa s in 1% water at 20°C.

6.3.2. Samples preparation

Considering the different testing condition reported in the technical data sheet from the different suppliers, a viscosity curve was investigated for each raw material. Aqueous solutions were prepared according to the cellulose concentration used in the total formulation: i.e., 0.4 g of thickener and 23.0 g of water.

Waterborne paints were prepared starting from a standard formulation developed in Section 6.2 formulation using organic and inorganic components. The organic part includes a vinyl copolymer emulsion as binder, a thickener and several other additives; the inorganic part includes titanium dioxide and calcium carbonate as pigment and filler, respectively. Tap water is used as solvent.

Cellulose was kept as reference thickener at 0.4 wt. % while alginate, according to our previous results was kept at 0.2 wt. %. An alphanumeric code was used to identify the different samples were the letters describe the type of alginate salt and the set of numbers the concentration used; for example SA02 means sodium alginate at 0.2 wt. %. All the sample compositions are reported in Table 6.5.

Considering the importance of understanding the applicability of alginate as thickener, samples were tested as basic, diluted and dry formulations. This was done in order to estimate the coatings behavior and the counterion influence through all the different life stages.

Table 6.5 Composition expressed in grams of Sodium SA, potassium PA and ammonium AA alginate based coatings

Sample code	Thickener (g)	Water (g)	Binder + Additives (g)	Pigment + Filler (g)	Total (g)
SA02, PA02 and AA02	0.2	23.2	10.6	66.0	100.0

6.3.3. Characterizations techniques

Rheological measurements were performed with an Anton Paar Physica MCR 301 rheometer using a parallel plate geometry, d = 50 mm. A Peltier plate and a PTD 200 temperature control system were used to keep constant temperature at 23 °C. Before each experiment, after loading the sample, a waiting time of 60 seconds was fixed. All the tests were repeated at least twice to obtain good data reliability.

Steady-shear flow behavior was evaluated by varying the shear rate from 0.01 to 1000 s^{-1}. Non-equilibrium flow curves were investigated through a logarithmic shear stress ramp by recording the viscosity every 60 seconds only for the complete formulations. The shear stress range was chosen specifically for each sample. To ensure data reproducibility, the curves shown in this work are the average curves of two replicates.

Amplitude or strain sweep tests, where the frequency is fixed and the strain amplitude increases, were performed to identify the linear viscoelastic region, LVER, where the storage and loss modulus are independent from the deformation and the network structure is not destroyed [50] and viscoelastic parameters such as the critical strain and the flow point. The strain γ ranged from 0.01 to 100% at constant frequency of 1 Hz.

Then, rheological tests were performed on diluted samples, obtained with the addition of 30% V of water to the basic formulation, according to the practical application conditions. Steady-shear viscosity tests were performed varying the shear rate from 0.01 to 1000 s^{-1}.

Three interval thixotropic test, 3ITT, was used to evaluate the paint thixotropy and the application process. Samples were subjected to three rotational steps. In the first step, the shear rate was fixed at 0.1 s^{-1} for 40, in the second step the shear rate was fixed at 1000 s^{-1} for 2 s, and the in the third step the shear rate 0.1 s^{-1} for 200 s. Typically, the percentage of regeneration achieved in the third interval at specific time, i.e., after 20 s or 60 s from the high load step, is used to analyze the structural rebuilding.

Mechanical characterization of free-standing dry paints was performed on basic formulations, i.e., undiluted samples. A Zwick Roell Z0.5 Materials Testing Machine was used to evaluate the elastic modulus and the tensile strength of thin dry paint films, with thickness of about 100 μm, at T= 23 °C. All the samples were applied on polypropylene foils using a film applicator. After three days of air drying at room temperature, rectangular stripes were carefully hand cut with a scalpel. The grips were manufactured specifically for the testing of thin films, the gauge length varied between 2.5 and 4 cm. A pre-load of 0.1 N was set to standardize the starting point, strain rate was set at 1 mm/min and minimum three replicates were tested to obtain good data reliability.

6.3.4. Results and discussion

Aqueous solutions

A steady state flow curve was performed to have a fair comparison between the viscosity values of the thickeners, and it is reported in Figure 6.7. Considering the standard concentration of cellulose Table 6.5, only 0.4 wt. %, over the total weight of the formulation were tested as aqueous solutions to compare the four thickeners in the same conditions. Samples were named considering the same alphanumeric codification adding the "aq" to describe their nature of aqueous solutions.

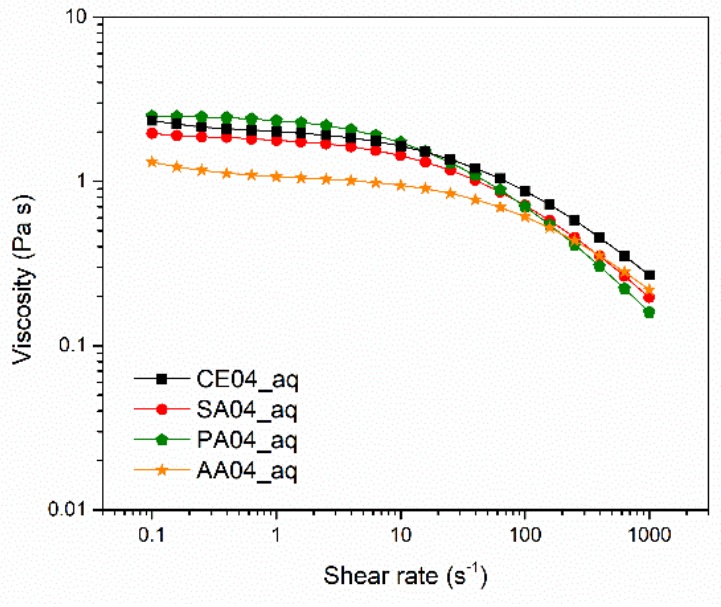

Figure 6.7 Comparison between viscosities curves of alginates and cellulose aqueous solutions considering the thickener concentration inside the formulation (0.4 wt. %)

A typical shear thinning curve is depicted in Figure 6.7 with a Newtonian plateau at low shear rates and a power law region at higher shear both for cellulose and alginates sample. Moreover, it is clear that the four thickeners have a comparable viscosity profile.

Basic formulation

Rheological profile of CE04, SA02, PA02 and AA02 was investigated under rotational conditions, Figure 6.8

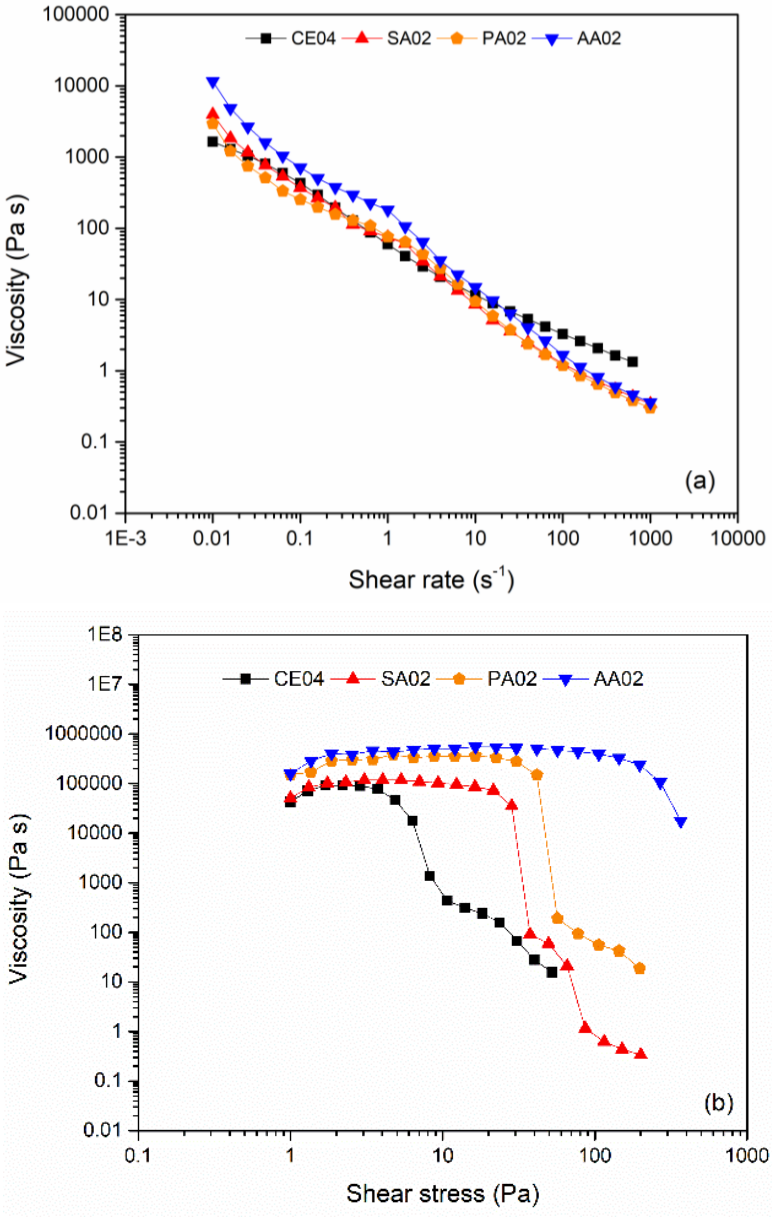

Figure 6.8 Viscosity curves of paint formulations containing cellulose CE04, sodium alginate SA02, potassium alginate PA02 and ammonium alginate AA02: (a) shear rate ramp, (b)shear stress ramp

All the samples exhibit a non-Newtonian, shear thinning behavior with a rise of the overall viscosity. Furthermore, considering the whole shear rate range of the experiments, the rheological behavior is typical of high solid content dispersions, i.e., coatings, exhibiting a Bingham like flow behavior.

At low shear rates, all the alginates samples exhibit a good rheological profile, almost overlapping with CE04 enabling good in-can stability properties. No specific influence of the counterion is detected here.

Non equilibrium viscosity curves are depicted in Figure 6.8 (b). The low shear stress region, as well as the low shear rate region, is the rheological representation of the storage condition. At low shear stress all the samples exhibit a plateau with a viscosity value high enough to prevent particles settling. By increasing

the shear stress, CA04, SA02 and PA02 exhibit a two-step decrease of the viscosity. This behavior is linked to the presence of aggregates that breaks in different moment of the process, showing a discontinuity in the curves. Considering AA02 an initial decrease in viscosity can be seen from Figure 6.8 (b), however the shear stress range investigated was not wide enough to appreciate the drop-in of viscosity. Yield stress τ_0, was evaluated through the shear stress ramp. The curves show that CE04 has a low apparent yield stress around 5 Pa, while all the alginate samples have a very high value of τ_0. A different viscosity profile is depicted; among the alginates AA02 exhibits the highest value of τ_0 followed by PA02 and SA02. The counterion affects the rigidity of the network built up by the alginate during its thickening phase. According to these results, ammonium alginate seems to create a stronger network.

Paints are viscoelastic materials, whose properties are evaluated through two parameters: the storage modulus, G', representing the elastic component, and the loss modulus, G'', representing the viscous portion of the material. Figure 6.9 shows the strain sweep tests performed to investigate the viscoelasticity and to determine the time-dependent deformation of paint systems.

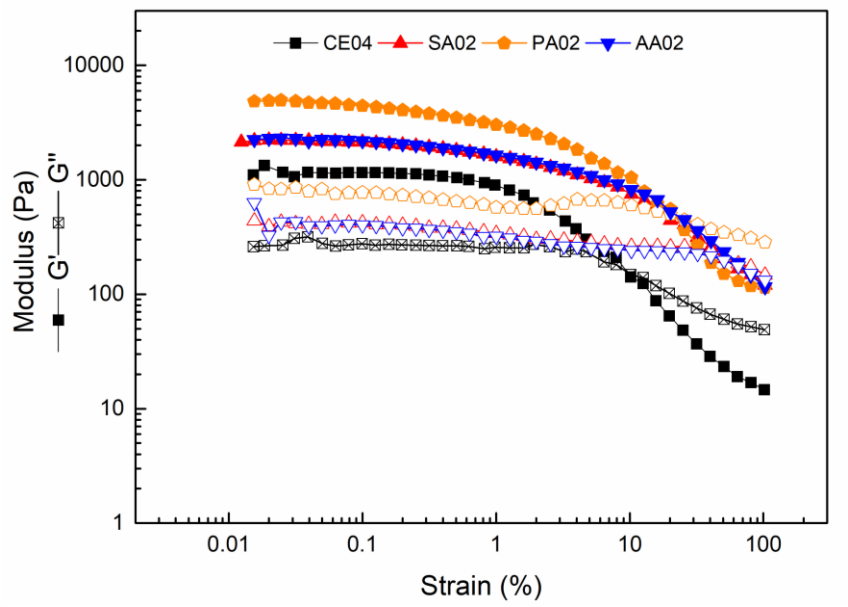

Figure 6.9 Amplitude sweep test of paint formulations containing cellulose CE04, sodium alginate SA02, potassium alginate PA02 and ammonium alginate AA02. ■ G' = storage modulus, □ G''= loss modulus

It is clear that G' results higher than G'' for all the specimens then the solid part prevailed on the liquid part of the samples. The linear viscoelastic region, LVER, occurs at low strain; it indicates where the material response is independent from the deformation and the network structure does not breakdown. It is clear that also, the molecular weight affects the strain sweep curves; however, considering the comparable viscosities of the technical data sheet and the experimental viscosity curve of the aqueous solutions, it is possible to assume that inside the formulations the difference among the molecular weights is hardly detectable.

From Figure 6.9 it is possible to see that all alginates sample exhibit a higher value of both G' and G'' compared to CE04. Considering the absolute value of G' inside the LVER, PA02 has the highest value of G', while SA02 and AA02 almost overlapped. According to the amplitude sweep test, the alginate counterion has a little effect on the absolute value of G' and G''.

The ratio between G'' and G' is called the damping factor, tan δ, and represents the dominant portion of the viscoelastic behavior [192]; the lower the value of tan δ, the higher the solid-like behavior. According to the raw data reported in Table 6.1 inside the LVER tan δ decrease following the order: CE04-AA02-SA02-PA02. These results are in good agreement with the strain sweep tests and highlighted a general more elastic behavior of alginates compared to cellulose.

At the end of the linear region, when both G' and G'' lose their independency from strain, the yielding region occurs. In this region the crossover point, where G'=G'' is the point in which the solid like character changes to a viscous like one, with a breakdown of the internal structure. The crossover point can be used to predict anti-settling properties; the higher the strain at which the crossover occurs, the more elastic the network; the better the anti-settling properties [191]. Table 6.6 reports the crossover strain and tan δ for the tested materials.

Table 6.6 Viscoelastic parameters obtained from amplitude sweep test; critical strain and damping factor for cellulose CE04, sodium alginate SA02, potassium alginate PA02 and ammonium alginate AA02 samples

	γ_c (%)	tan δ
CE04	9	0.23±0.03
SA02	42	0.19±0.02
AA02	72	0.20±0.04
PA02	20	0.18±0.03

CE04 exhibits the lowest values of the critical strain followed by PA02, SA02 and AA02. Because of a general stiffer gel network and a more solid-like structure, γ_c is considerably higher for all the alginate samples when compared to CE04. In particular, it is strongly affected by the type of alginate salt. According to the literature, sodium and potassium alginates with the same molecular weight have a counterion dependence on Ca^{2+} linkage, PA alginates generally display a faster sol/gel transition compared to the SA alginates and this fact can be deduced from a reduced elastic moduli of SA alginate with respect to one of PA alginates [194]. In fact, the internal network of PA02 shows higher brittleness (γ_c = 20%) compared to AA02 (γ_c = 72%), and SA02 which shows intermediate properties. Considering that sodium alginate weakly interacts with the superficial calcium ions of calcium carbonate [178,195], it is possible to assert that

potassium and ammonium alginates interact as well. Furthermore, all the samples exhibit low tan δ, ensuring good anti-settling properties.

According to the amplitude sweep test, inside LVER the effect of the counterion is not clear considering only the absolute value of G' and G''; while the differences of the other viscoelastic parameters such as γ_c and tan δ, highlight a trend connected to type of alginate salt used.

Dry samples

Mechanical properties of architectural coatings are not usually directly measured because of the difficulties encountered during the free-standing film preparation, thus the low reproducibility of the data [196]. Anyhow, it was interesting to analyze if the alginate counterions affect the mechanical properties of dry paints. Tensile strength, $\sigma_{max,}$ and Young modulus, E, were investigated to describe the mechanical properties of the samples; strain elongation was not considered due to the high dependency of this parameter on inner defects, such as air bubbles, lumps of filler and jagged edges, in the samples. All the stress/strain curves are shown in Figure 6.10

Low values of both the tensile parameters were attributed to the presence of defective units. For this reason, only the highest value of σ_{max} and E account for the best result; all the data are reported in Figure 6.10.

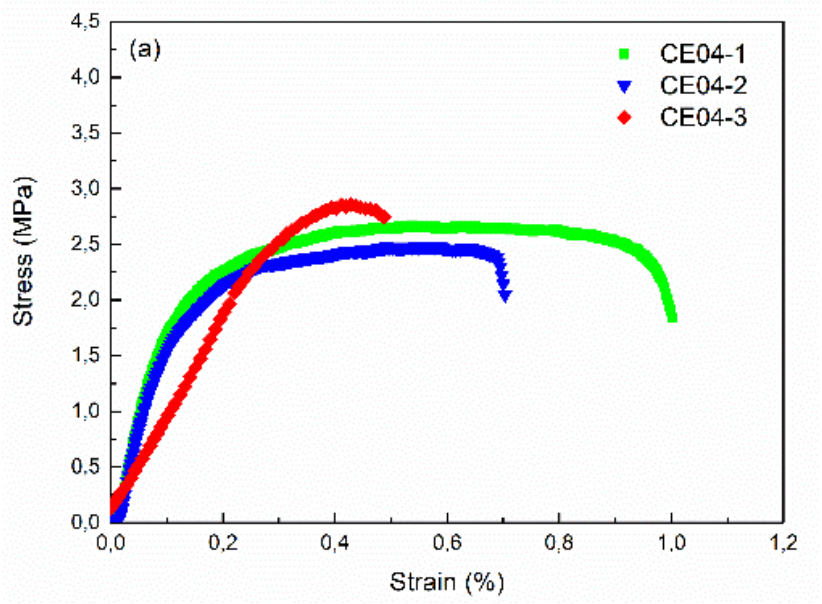
(a)
CE04-1
CE04-2
CE04-3
Stress (MPa)
Strain (%)
0,0
0,5
1,0
1,5
2,0
2,5
3,0
3,5
4,0
4,5
0,0
0,2
0,4
0,6
0,8
1,0
1,2

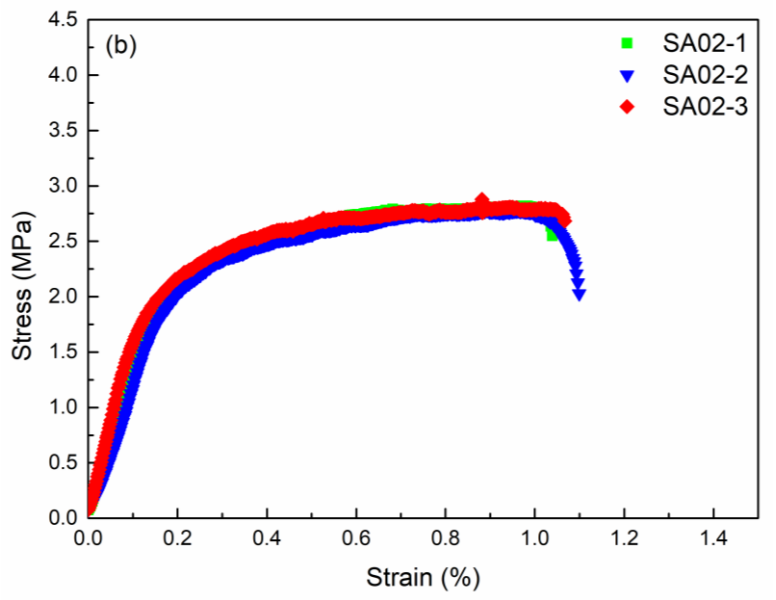
(b)
SA02-1
SA02-2
SA02-3
Stress (MPa)
Strain (%)
0.0
0.5
1.0
1.5
2.0
2.5
3.0
3.5
4.0
4.5
0.0
0.2
0.4
0.6
0.8
1.0
1.2
1.4

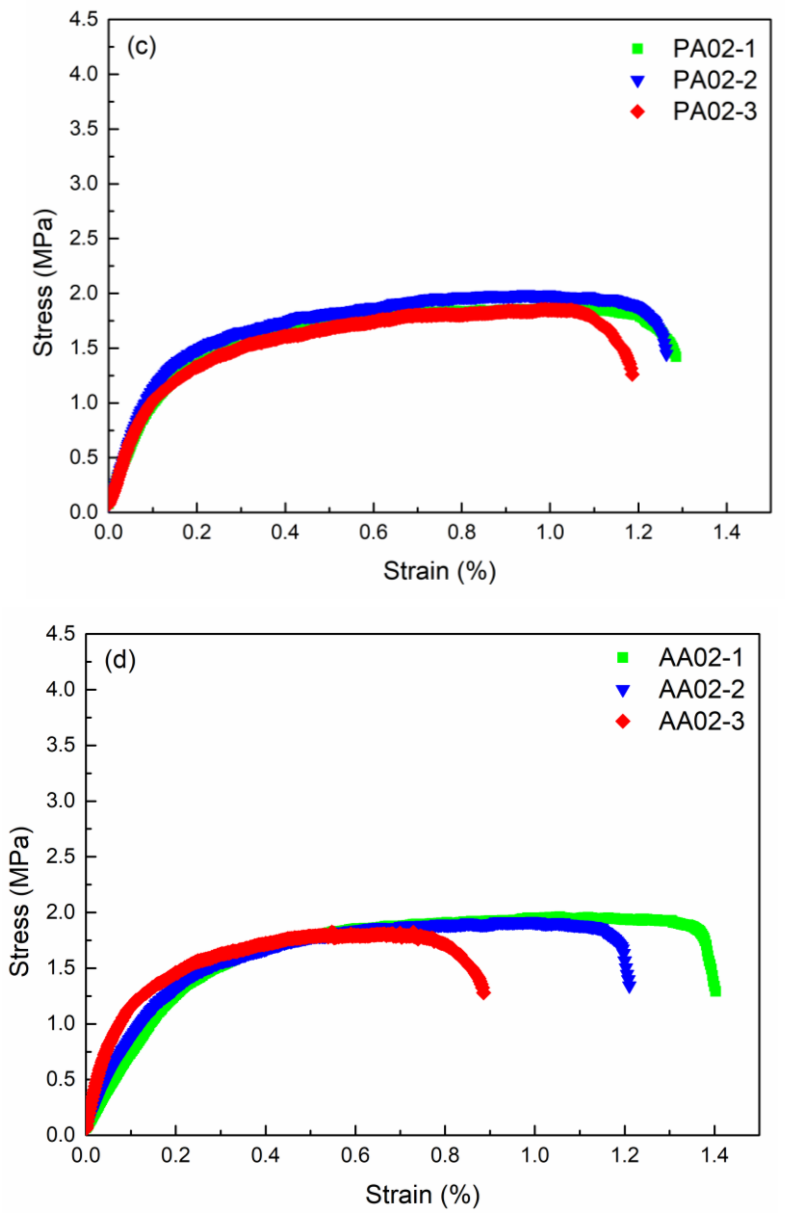

Figure 6.10 Tensile test, stress vs strain curves of standard cellulose based formulation and alginate based formulation: a) cellulose CE04, b) sodium alginate SA02, c) potassium alginate PA02, and d) ammonium alginate AA02

Comparing the standard CE04 with all the alginate 0.2 wt. % samples, SA02 exhibits the same value of σ_{max} while AA02 and PA02 exhibit a lower value. Considering the σ_{max} values, SA02 samples have the highest σ_{max}, followed by AA02 samples and PA02 samples. Observing the E values, AA02 has the highest value followed by SA02 and PA02. This is strongly connected with the homogeneity of the dispersion. The counterion affects the tensile properties; the more uniform is the paint, the higher the tensile strength and the Young moduli. From the results reported in Table 6.7 it appears that the use of potassium alginates

leads to a lower homogeneity followed by ammonium alginate. Sodium alginate on the other hand, lead to a more uniform dispersion. All the tensile test results are in good agreement with the rheological test.

Table 6.7 Tensile test results: maximum tensile strength and Young's modulus

Sample	σ_{max} (MPa)	E (MPa)
CE04	2.48	2.73
SA02	2.47	2.23
AA02	1.89	2.81
PA02	1.85	1.27

Diluted samples

Rheological evaluation of diluted samples is fundamental to understand and predict the application phase. Viscosity curves are reported in Figure 6.11. The test was performed only in a shear rate controlled system to focus on the application process.

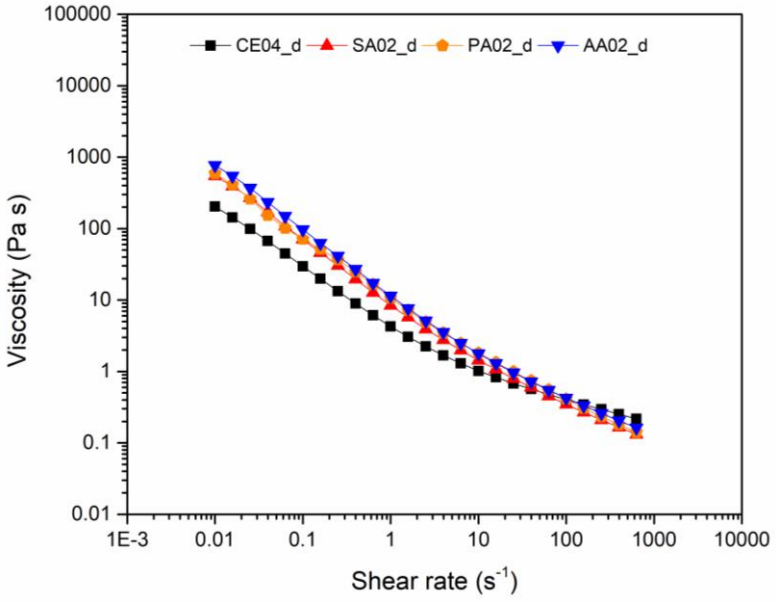

Figure 6.11 Flow behavior during application: viscosity curves of 30 % V diluted sample cellulose CE04, sodium alginate SA02, potassium alginate PA02 and ammonium alginate AA02

All the samples, according to their nature of highly solid dispersions, exhibit a shear-thinning behavior, with a smoother decrease of viscosity as shear rate increases compared to the not diluted samples.

At low shear rates all the alginate samples show higher viscosity values than cellulose; this condition can avoid in-can fast sedimentation. Considering the high shear rates region, all the samples reach a viscosity

value low enough to enable their application. The effect of the counterion is not detected here since SA02, AA02 and PA02 have an almost identical behavior.

During the application process it is important to prevent unwanted events like bad levelling and sagging [150]; this can be done studying the thixotropic response of a material. A generic definition of thixotropy is a time-dependent shear thinning behavior characterized by the recovery of the original structure after removing a load or a deformation [197]. 3ITT has been used as a prediction of this event. In fact, it has the power to predict the material recovery after a structural breakdown by simulating the application process in three intervals: the first and the latter intervals simulate the behavior at rest, and the middle interval simulates the structural breakdown that occurs during application

It is generally known that weak gel structures are easily deformed by a high shear rate; on the other hand, strong gel structures hardly changed their original network arrangement under a shear force.

The complexity of the rheological nature of paints requires the investigation of the viscosity recovery after a high shear step as well. Figure 6.12 (a) shows the 3ITT results under rotational conditions.

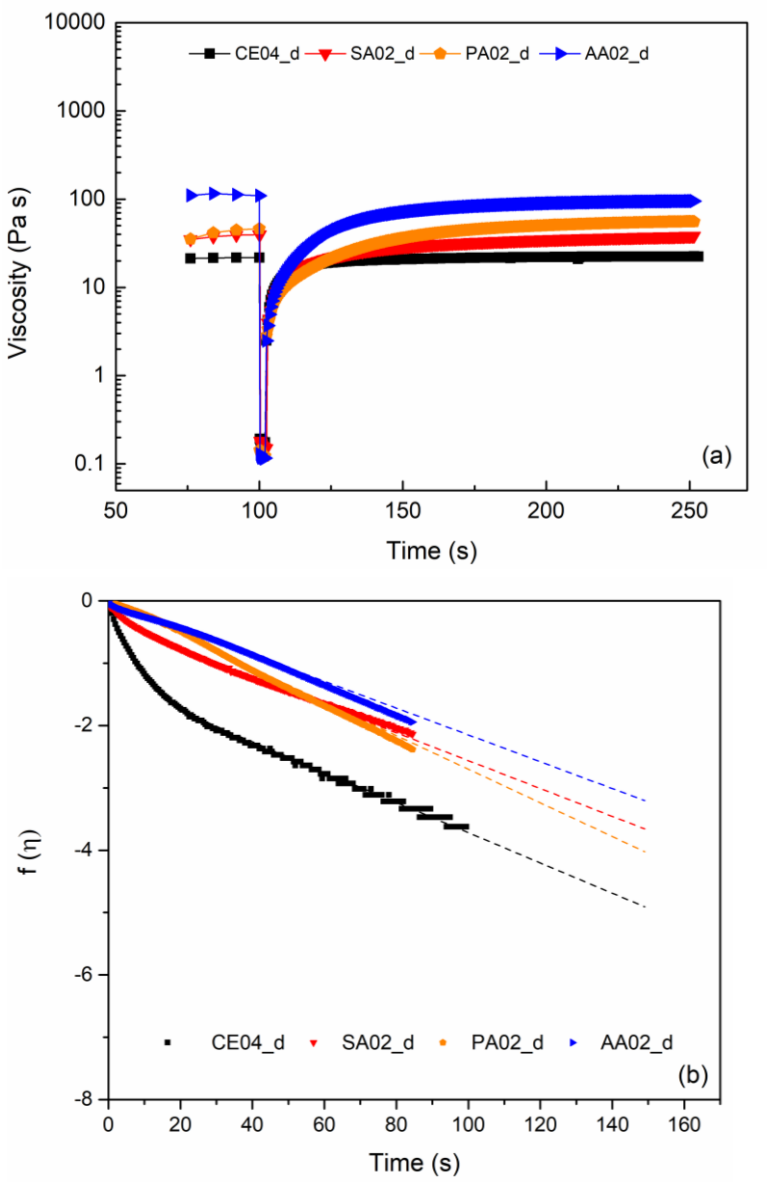

Figure 6.12 a) 3ITT of diluted formulations; comparison between standard CE04, SA02, PA02 and AA02 (b) Representation of the third interval of 3ITT as a logarithmic function of viscosity vs time. Experimental data (symbol), fitting data (line); comparison between standard CE04, SA02, PA02 and AA02

According to the 3ITT tests, the faster is the recovery, the better is the sagging resistance and the worse is the leveling; on the contrary, the slower is the recovery, the better is the leveling and the worse is the sagging effect [151]. CE04 shows a sharp and quick recovery. On the other hand, this behavior does not occur for, SA02, PA02 and AA02.

The viscosity values in the third step, after 20 and 60 seconds from the removing of the high shear, listed in Table 6.8 were chosen as reference values to confirm the previous qualitative analysis of the recovery step.

Table 6.8 Viscosity recovery and fitting parameters during the third interval of 3ITT

	Viscosity recovery (%)		**Fitting parameters**			
	20 s	**60 s**	**τ_1 (s)**	**τ_2 (s)**	**f**	**R^2**
CE04	86±1	100±1	4.5	41	0.72	0.9972
SA02	50±1	77±1	3.5	44	0.28	0.9976
AA02	33±1	67±1	-	36	0	0.9946
PA02	45±1	93±1	-	46	0	0.9984

What it is interesting to notice in Table 6.8 is that CE04 regains 86 % of its viscosity at rest within the first 20 seconds and completes the recovery after one minute. On the contrary, the three alginate paints show a lower percentage of recovery and a different behavior according to the type of basic gel involved. In fact, for 0.2 wt. % alginate samples, sodium-based formulation recovers its viscosity faster than potassium and ammonium after 20 seconds; on the other hand, after 60 seconds, PA02 regains almost the original viscosity value. To better explain the observed trend, the thixotropic behavior was mathematically evaluated by fitting the data of the third interval with the viscoelastic model reported in Eq. 6.1, which describes the increase of viscosity with an exponential recovery trend with two different relaxation times:

$$\left(\frac{\eta_{max}-\eta}{\eta_{max}-\eta_0}\right) = f\left(1-e^{-\frac{t}{\tau_1}}\right) + (1-f)\left(1-e^{-\frac{t}{\tau_2}}\right) \qquad (6.1)$$

where η is the viscosity measured in the third interval, η_{max} is the maximum value measured at $\dot{\gamma} = 0.1\ [s^{-1}]$, η_0 is the minimum viscosity in the high shear rate interval, τ_1 and τ_2 are characteristic times of the rebuilding process, f is a parameter connected to the relative weight of each characteristic time, ranging between 0 and 1.

By plotting a viscosity function f (η) expressed as ln [($\eta_{max} - \eta$)/($\eta_{max} - \eta_0$)] versus time ($t-t_0$), where t_0 represents the time at the beginning of the third step, Figure 6.12 (b) can be obtained.

Figure 6.12 (b) better describes the recovery behavior compared to the traditional 3ITT curve. CE04, and SA02 exhibit a smooth trend where two slopes are depicted. It is clear that two mechanisms with two-time scales are involved in the rebuilding of the internal structure; on the other hand, PA02 and AA02 have only one slope, thus one characteristic time.

After the high shear deformation step, all the polymeric chains have been stretched and oriented, while particles have been deformed and disaggregated. When the deformation is removed, they tend to come back to their original state. This event is strongly affected by the internal friction that occurs between the single

polymeric chains and between the polymeric chains and the particles dispersed in the system. For this reason, the characteristic time τ_1, the shortest time, probably described the ability to reorganize the original structure according to the occurrence of short-range interaction among the chains. τ_2 on the other hand, is the longest time and probably describes long range interaction including re-aggregation and stabilization of the dispersion. Those parameters are correlated with the type of thickener used to create the gel at the beginning of the paint manufacturing phase.

Cellulose acts as a non-associative thickener and its thickening mechanism is only related to chains entanglements [198]. After the high shear rate step, the internal friction among the chains is low and because there is no interaction between the polymer and, above all, the solid particles, τ_1 is fast, and f is high (0.72) while τ_2 is slow.

Alginates show two different behaviors, one for sodium and one for potassium and ammonium samples. Sodium exhibits two characteristics times, while potassium and ammonium only one. According to the amplitude sweep test, CE04 showed lower viscoelastic properties. Considering this, rheological profile, CE04 has the weakest solid character ascribable to weak gels; with these premises, weaker structure can be described by two characteristic times as cellulose does. Among the alginate samples only SA02 exhibit a low value of τ_1, while PA02 and AA02 do not show τ_1. However, a high value of τ_2 demonstrates that long range interactions are more important when the original microstructure is the result of a more complex thickening mechanism. Considering the yield stress values obtained from the viscosity curve in Figure 6.8 (b), it is reasonable to think that ammonium alginate builds the strongest network followed by potassium and sodium; for this reason, 3ITT results are in good agreement with the rheological results of basic formulations.

6.3.5. Conclusions

In this study paints formulations containing alginate as thickener were characterized; specifically, three different alginate salts of sodium, potassium and ammonium, were studied. The influence of the counterion was evaluated through rheology and tensile tests. Moreover, the stability and the applicability of the paint formulation were investigated.

Basic formulations were investigated to evaluate the rheological profile and the role of alginates counterions during storage and mixing conditions. Tensile tests were performed on dry film to investigate mechanical properties.

Viscosity curves both in a controlled shear and in a controlled stress approaches were performed. A shear thinning behavior was depicted for all the samples; moreover, a viscoplastic nature with a yield stress was identified. From the oscillatory test it was clear that the elastic part, G', predominates over the viscous part, G'', for all the samples. From the evaluation of the critical strain and the flow point, it resulted that alginate

built a stiffer network due to its interaction with mainly calcium carbonate. The counterion slightly influences the overall viscosity, the storage modulus and the loss modulus. However, it affects the yield stress and the viscoelastic parameters. In fact, the stiffness of the gel is correlated with the mechanism of interaction between the three alginate cations and calcium ions.

Tensile tests emphasized the plastic nature of the free-standing films. It is worth noticing that alginate samples exhibited different mechanical properties with respect to cellulose. Despite the presence of inner defects, the Young's modulus was similar among the samples. However, SA02 showed higher value of both the tensile parameters due to a more homogenous dispersion. The effect of the counterion here is related to the previously mentioned different mode of interaction with the surrounding system. Leading to a more or less homogeneous dispersion

According to the viscosity curve, diluted samples have a coherent rheological profile. CE04 showed the lowest shear thinning behavior; alginate samples exhibit a higher shear thinning behavior. Moreover, they did not exhibit a specific dependency on the counterion involved in the gel phase preparation.

During the recovery of diluted samples, 3ITT, the effect of the counterion is highlighted. Alginates showed a recovery trend for the viscosity that follows the order SA-PA-AA. These behaviors can be explained considering the different affinity of sodium, potassium and ammonium ions towards alginate chain, leading to a different interaction with calcium ions as well.

Considering all the results obtained, the formulation containing sodium alginate at 0.2 wt.% was chosen as optimal formulation for the development of an alginate based top architectural coating.

6.4 VALIDATION OF A SODIUM ALGINATE BASED PAINT: QUALITY ASSESSMENT

A validation of a paint formulation combines both tests regulated by international standards (ISO) and empirical tests connected to the knowledge of a paint formulator. According to the results obtained through the step-by-step approach, in this section the optimal formulation containing SA 0.2 wt. % will be described. Samples prepared with low viscosity alginate, potassium and ammonium alginate were tested as well and the results are reported in appendix A.

6.4.1. Materials and samples preparation

Alginate based paint was prepared with a high-speed disperser, Dispermat, equipped with a stainless-steel dispersion impeller; low speed was set during the mixing phase, while high speed was set during the grinding phase. According to the results obtained in Section 6.3 the optimal formulation is reported in Table 6.9.

Table 6.9 Optimal formulation for water based paint containing alginate as thickener

Component	Chemical	Concentration (wt. %)
Thickener	Sodium alginate (Algaia)	0.2
Additives	Fatty acid/acrylic based chemicals	0.6
Binder	Copolymeric vinyl emulsion	10
Pigment	Titanium dioxide	8
Solvent	Water	23.2
Filler	Calcium carbonate	58

6.4.2. Characterizations techniques

Specific weight

To measure the specific weight a stainless-steel pycnometer with a volume of 50 ml was used. The measurement was carried out at 20°C according to UNI EN ISO 2811-1.

pH measurement

The pH value of aqueous products is of decisive importance for the product properties and durability. pH value was measured using a pH-meter with a glass membrane electrode according to ISO 19396-1:2017.

Punctual viscosity, ICI cone and plate viscosity.

Cone and Plate viscometer are associated with high-shear flow. Good high-shear viscosity, referred to as ICI builders, is indicative of shear conditions as a paint or coating is being rolled or brushed on a particular surface. ISO 2884-1:1999. Shear rate was fixed at 12,000 s^{-1}.

In can stability

The in-can or storage stability of the paints was evaluated performing two tests after an accelerated aging cycle, keeping the samples in oven at T= 50 °C for one month inside glass cans. After cooling the samples at room temperature, and before any other test, the presence of syneresis, which is the separation between the liquid, upper part, and the gel, bottom part was evaluated. Particle settling was investigated according to ASTM D869; the test consisted in vertically submerging a stainless steel spatula in the paint and evaluating the appearance of its surface after vertically pulling up [199].

Application test

To evaluate the applicability and the occurrence of surface defects, paints were applied on a 50x50 cm gypsum board with a brush. The tests were performed starting from diluted paints, according to the practical application conditions (30 %V dilution). Samples were dried at room temperature for one week.

A Wild Heerbrugg M3Z stereo microscope was used for low magnification observation of the surface appearance of dry paints applied with synthetic brush on a gypsum board.

6.4.3. Results and discussion

Specific weight, pH and ICI viscosity results are summarized in Table 6.10. CE04 was used again as reference sample.

Table 6.10 Technical characterization and validation of CE04 and SA02 based paint

	Specific weight (g/cm^3)	**pH**	**ICI viscosity (P)**
CE04	1.7±0.1	8.0±0.1	2.6±0.1
SA02	1.7±0.1	8.0±0.1	1.6±0.1

Specific weight and pH results are in good agreement with the one obtained for the standard CE04. On the other hand, ICI viscosity is slightly lower for SA02 compared to CE04 but still acceptable to enable a good application.

After one month of storage at T=50°C and cooling at room temperature, syneresis, sedimentation and homogeneity of the samples were tested. To evaluate the presence of particle settling, before mixing, a stainless-steel spatula was immersed vertically in the can without any torsion and removed. CE04 evenly coated the spatula while SA02 exhibits a thinner film of coating with a non-uniform distribution of the product due to the formation of the stiff gel structure.

Since there is no sedimentation but the formation of a strong network it was impossible to rate the samples according to ASTM D869. Anyhow, the spatula test remains an efficient tool to evaluate the performances after storage and the effect of building up the gel network in alginates samples.

Images of the brush application of the diluted samples, captured under a stereo microscope, are reported in Figure 6.13.

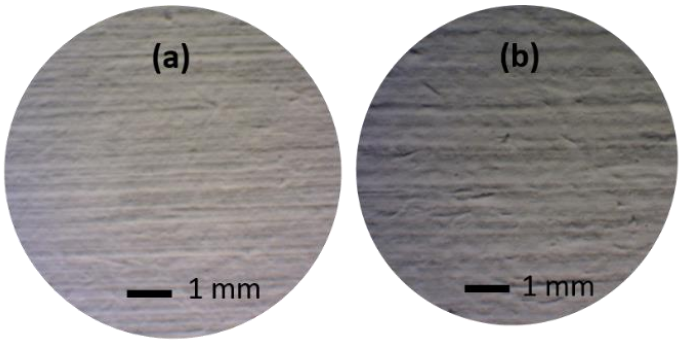

Figure 6.13 Stereomicroscope images: a) CE04; b) SA02

According to application on the gypsum board panels, all the samples showed irregular surfaces, in good agreement with the basic formulation involved in this work. The magnification highlights the surface defects; CE04 reminds the appearance of commercial products, the surface is almost even; SA02 exhibits as well good application with good leveling and no sagging.

6.4.4. Conclusions

In the coatings industry, the validation of a new formulation is an important step before the scale-up process. In this section, some of the traditional quality control techniques were used to investigate the suitability of an alginate-based formulation previously tested with non-traditional techniques i.e. oscillatory rheology.

According to the results obtained from the technical evaluation sodium alginate formulations SA02 exhibit a comparable specific weight and pH, a slightly lower ICI viscosity was depicted however, this value do not affect the application phase. The stiffer network built up by alginate avoid syneresis and sedimentation enabling good in-can stability performances.

7 NATURAL ZEOLITE AND WASTE-BASED AEROGEL AS THERMAL INSULATION FILLER: PREPARATION, CHARACTERIZATION AND DEVELOPMENT OF A THERMAL PLASTER FORMULATION

In this Chapter, natural zeolites and organic waste-based aerogels are deeply investigate. Initially, a physical and chemical characterization of the single raw materials is carried out, then thermal properties of plaster containing zeolites or aerogels are evaluated.

Giulia Gaggero

7.1 NATURAL ZEOLITE: CHARACTERIZATION AND SURFACE MODIFICATION

The use of zeolites in construction materials is not unusual. Today, in some part of the world, i.e. China, in the cement industry natural and synthetic zeolites are a very popular alternative to traditional natural pozzolanic materials [200,201]. With this regard, inside cement formulations, pozzolanic material reacts with portlandite in the presence of water, showing binding properties. For these reason they are known to increase the durability, lower the heat of hydration, increase the resistance to sulphate attack and reduce the energy cost per cement unit [202]. In all these applications, zeolite is used as pozzolanic material without considering the peculiar physiochemical properties that in other application fields define zeolite as essential. Modified zeolites with La(III) were investigated as functional pigment in the development of eco-friendly anticorrosive paints with some good inhibitory effects [203]. Indeed, zeolites can be doped with corrosion inhibitor and healing agents acting as carriers. If the coating is locally damaged due to scratches, the inhibitor entrapped in its framework structure is released promoting an active and self-healing process [204].

Zeolites are microporous materials which porosity depends on the framework type. If these multiple pores are filled with air, there is a chance that zeolites work as a thermal insulator material [205]. The thermal conductivity is an important parameter, however it is difficult to associate a specific value to each zeolite considering that depends on many factors like density, porosity and framework type. Generally speaking a wide range of thermal conductivity values have been reported in the literature with λ= 0.07- 4 W/m K [206–208].

In this section, natural zeolites were investigated as potential filler for plaster coatings. However, the peculiar water absorption ability makes the use of natural zeolites inside water-based media challenging. A surface modification with stearic acid was performed to enhance the hydrophobic nature of natural zeolites according to the adsorption of the carboxyl group of fatty acid molecules by hydrogen-bonding to the zeolite Al–OH–Si groups (Brönsted acid sites).

7.1.1. Materials

Two types of natural zeolites were used in this study:

- natural clinoptilolite, ZCL, with a content of 90% of clinoptilolite, was gently provided by ZEOCEL Italia;
- natural chabazite, ZCH, with a content of 65 % of chabazite was gently provided by Zeolite-Italia.

The chemicals used for the surface modification including stearic acid (95 %) and acetone, were obtained from Sigma-Aldrich.

7.1.2. Samples preparation

Zeolites were used as received and are identified with the code ZCL and ZCH for clinoptilolite and chabazite respectively. Surface modification with fatty acid esterification was carried out to enhance the hydrophobic character. Zeolites powders were first dried at 150 °C for 4 hours to remove all the excessive water. After that they were soaked in a stearic acid solution prepared by dissolving 1 g of stearic acid in 50 ml of acetone, in the ratio1:2 (powder: solution) for 4 hours and let dry overnight. Subsequently, they were dried at 150°C for 4 hours to promote the esterification between OH and COOH group [209]. Samples are identified with the code H-ZCL and H-ZCH for hydrophobic clinoptilolite and hydrophobic chabazite, respectively.

7.1.3. Characterizations techniques

Particle size

Considering the commercial nature of the zeolites, a Mastersizer 3000 particle size analyzer was used to obtain the complete particle size distribution curve. A sample of 0.3 g of powder was placed into a 25 mL vial with some drops of dispersant and distillate water. The dispersion was mixed with a magnetic stirrer to disperse the aggregates. The zeolite-water suspension was then added drop-by-drop to a 500 mL beaker of distilled water that was continuously stirred and pumped in the laser diffraction unit. Dispersed sample passes though the measurement area of the optical bench, where a laser beam illuminates the particles. A series of detectors then accurately measures the intensity of light scattered by the particles within the sample over a wide range of angles.

Spectroscopic characterization

Fourier – transform infrared spectroscopy (FTIR) spectra were measured at room temperature in the range 400–4000 cm^{-1} with a Bruker Vertex 70 instrument equipped with attenuated total reflectance (ATR) accessory with a resolution of 2 cm^{-1}.

Wetting ability

Contact angle measurement using the static sessile drop method was evaluated. Around 0.2 g of powder was pressed to form a pellet and a water drop of 15 µl was dripped onto its surface. The drop profile was allowed to stabilize before acquiring the measurement. Three repetitions were performed to ensure reproducibility.

7.1.4. Results and discussion

Size distribution

Laser diffractometry size analysis is based on the principle that particles of a given size diffract light through a given angle, the angle increasing with decreasing particle size.

The size distribution was measured while the suspension was continuously pumped around and is reported in Figure 7.1.

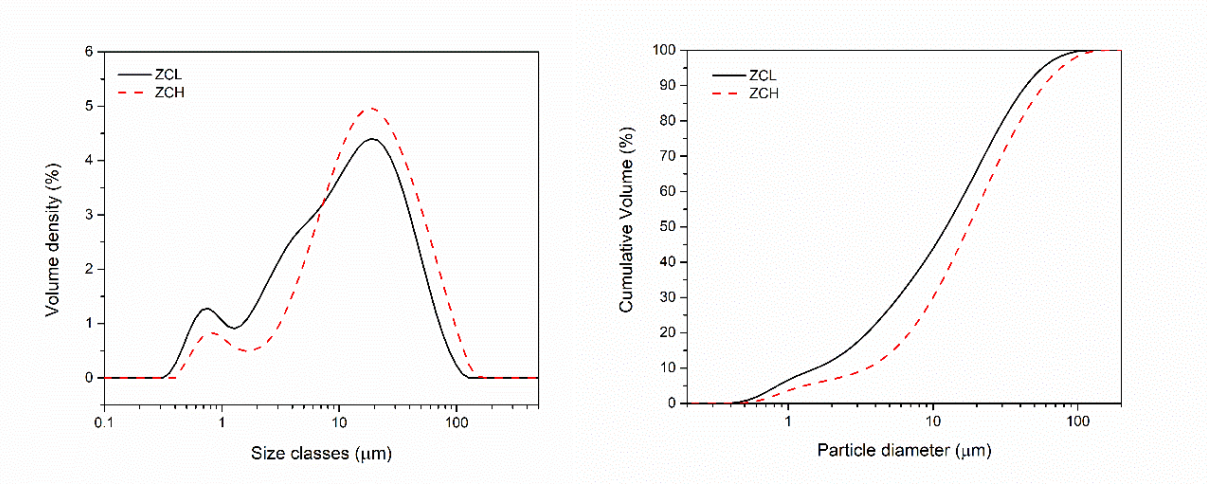

Figure 7.1 Size distribution curve of clinoptilolite ZCL, and chabazite ZCH

A multimodal distribution is depicted in Figure 7.1. Clinoptilolite, ZCL, exhibits a wide size distribution with two distinctive groups of data with a shoulder around 7 µm; on the other hand, chabazite, ZCH, shows a narrow distribution shifted to higher diameters. The average particle diameter corresponding to the 10, 50 and 90% of the total volume of material is reported in Table 7.1. It is evident that ZCL has smaller particles compared to ZCH. Knowing the size distribution curve is fundamental to predict the rheology of the powders in a water-based paint formulation. Indeed, a wider distribution enhances the packing ability of particles. Furthermore, particle size affects the rheology of a suspension. At the same concentration, the number of small particles increase resulting in an increase in the number of particle–particle interactions, thus exhibiting higher viscosity.

Table 7.1 Average diameter for 10, 50 and 90 % of the total particle volume of material.

	ZCL (µm)	**ZCH (µm)**
dx (10)	1.55	3.53
dx (50)	12.3	17.5
dx (90)	43.9	58.2

Spectroscopic characterization

A direct investigation of surface modification was carried out by means of infrared spectroscopic investigation. ATR spectra are reported in Figure 7.2.

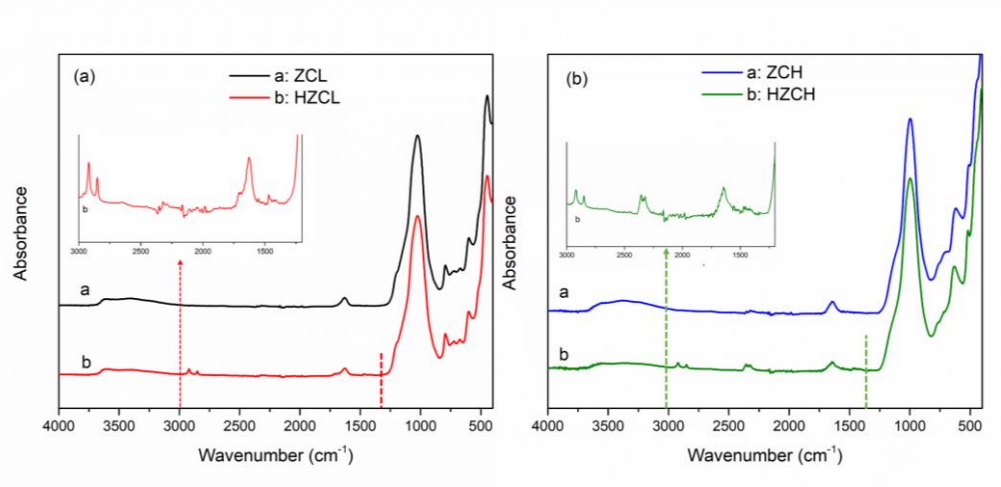

Figure 7.2 FTIR spectra collected in ATR mode of: a) pristine clinoptilolite (ZCL) and after stearic acid modification (HZCL); b) pristine chabazite (ZCH) and after stearic acid modification (HZCH)

FTIR spectrum of clinoptilolite, Figure 7.2 (a) shows the typical peaks of a hydrated material with a broad band at 3500-3300 cm^{-1} results from the vibration of OH water and a peak at 1628 cm^{-1} of the molecularly bound water in the structure. A broad band appears between 1058 and 810 cm^{-1} corresponding to asymmetric stretching vibration modes of internal T–O bonds in TO_4 tetrahedra (T = Si and Al) [210]. The shoulder at 1213 cm^{-1} is associated to the presence of Si-O-Si asymmetric stretching. Moreover, the 794 and 447 cm^{-1} bands are assigned to the symmetric stretching vibration modes of O–T–O groups [109].

The IR absorption bands associated with the chabazite framework vibrations are similar to those of clinoptilolite reported in Figure 7.2 (b). The broad band at 3500-3300 cm^{-1} is the results of the symmetric and asymmetric H_2O vibrations while at 1646 cm^{-1} bending vibration of H_2O molecules is depicted. A broad and intense peak at 1000 cm^{-1} with a shoulder at 1173 is associated to the O–T–O and specifically to Si-O-Si asymmetric stretching vibrations respectively [211].

Considering the spectra of modified zeolites, a zoom in of the region between 3000 and 1200 $cm^{-1}$is necessary to enhance the presence of organic compounds. Both HZCL and HZCH show two distinct peaks at 2919 and 2851 cm^{-1} associated to asymmetric and symmetric stretching of C-H respectively, correlated to the presence of stearic acid. Moreover, HZCL exhibits a small but characteristic band at 1709 cm^{-1} due to the asymmetric stretching of –C=O in the carboxyl group [212]. Therefore, the presence of fatty acid adsorption was confirmed for HZCL. On the other hand, HZCH spectrum enhances the presence of $-CH_2$, but no esterification reaction can be confirmed.

Wetting ability

Surface wetting ability was investigated through static contact angle measurement.

Natural zeolites are generally hydrophilic materials [213]; as a matter of fact, contact angles for ZCL and ZCH were not detectable, because both the pellets quickly adsorbed the water drop. However, modified

zeolites show both a contact angle of 100°±3 and 106°±4 for HZCL and HZCH respectively, as reported in Figure 7.3.

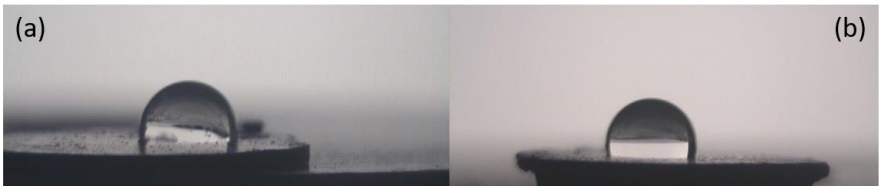

Figure 7.3 Investigation of surface wettability by contact angle measurement: (a) HZCL, (b) HZCH

The contact angle significantly increases, suggesting that the surface modification affects the surface wettability, thus the hydrophobic character.

7.1.5. Conclusions

Natural clinoptilolite and chabazite physical properties were characterized. Particle size distribution described a bimodal curve for both the zeolites. ATR-FTIR spectra showed the characteristic peaks of natural zeolites; moreover, along with the contact angle measurement, the spectra demonstrated, especially for HZCL, that fatty acid esterification modification worked onto zeolites surface, showing the characteristic peaks associated to asymmetric and symmetric stretching of C-H.

7.2 ORGANIC WASTE-BASED AEROGELS: PREPARATION, SURFACE MODIFICATION, AND CHARACTERIZATION

At the moment, silica aerogels with their extreme low thermal conductivity are the most promising thermal insulation functional filler available on the market in different form: as fiber, as matt and as panels. During the past years, cements [40] and plasters [42] containing silica aerogel were deeply investigated. As a consequence of the positive results, today silica-based aerogel plasters are available on the coatings market. The most interesting characteristic of aerogel plaster is that they can reach low value of thermal transmittance with thin layers of product, few cm in contrast with 12-15 cm of ETICS [214]. Even if they show to increase the energy efficiency of existing buildings, the cost of these products is still too high and limits its use. Cellulose aerogel has been tested as cost-effective alternative; despite the low thermal conductivity, several challenges still need to be overcome [215].

Traditionally, aerogel synthesis includes three main steps: gelation, solvent exchange, and drying as described in Section 4.3. In this work, the term aerogel refers to a new porous material obtained by organic wastes. Specifically, the term refers to a material that in its natural state has a high content of water with an intrinsic porous structure. This peculiar structure avoids the first traditional step of gelation. After the

solvent exchange and the drying step, we obtained a porous structure that resembles the traditional aerogels structures, hence the unconventional used of the term aerogel.

With these premises, in this section, organic waste-based aerogels from spent ground coffee and apple pomace were investigated as innovative lignocellulosic porous filler.

Coffee is one of the most consumed brewed beverage in the world; according to the International Coffee Organization ICO, world coffee consumption is projected to increase by 1.9% to 167.58 million bags in 2020/21 compared to 164.43 million bags for coffee year 2019/20 [216]; as a consequence of that, there is a high production of solid organic waste. Exhausted coffee or spent ground coffee is a lignocellulosic material, mainly disposed in landfills causing environmental issues [217]; several recent research were dedicated to reduce the environmental impact of coffee waste by implementing the cradle-to-cradle design. In fact, coffee has been used in biofuel production, as filler in the construction field and because of the presence of nutrients, as fertilizer [218,219].

Alongside coffee waste management, fruits and vegetables by-products are of great concern for the concept of circular economy. As a matter of fact, apple juice production contribute to the development of several tons per year of food waste known as apple pomace [220]. During juice extraction, 75 % of fruits weight is pressed and transformed to juice, while the other 25 % is pomace; apple pomace contains pulp, skin, seeds, and is normally used as animal feed or stock in landfills [221]. However, because of the presence of carbohydrates, proteins, lipids and fibers, several studies have been carried out on the extraction of valuable chemicals i.e. bakery yeast and pectin, and on the production of biogas out of sugars fermentation [222].

Since they are unconventional materials, basic physical properties and morphology were evaluated. Great attention was given to the hydrophilic nature of these fillers considering that the final goal of this project is to use aerogels in water media preventing the potential collapse of the porous structure. The consequences of the immersion in an aqueous environment were evaluated by immersing the aerogel in water for 24 hours. The morphology and the surface area were deeply affected by this test. In order to protect the surface and the inner structure from water adsorption, a silane-based surface modification technique was attempted. Both a liquid phase and a gas phase modification were tested to evaluate the best approach.

7.2.1. Materials

Ground coffee and apples were purchased from a local supermarket. Ethanol 99.8% was purchased from Sigma Aldrich, Germany. Tap water was used for the aging test. Methyltrimetoxysilane 97 % MTMS, was purchased from Sigma Aldrich.

7.2.2. Samples preparation

Coffee aerogels, CG, were prepared as follows. Wet spent ground coffee powder was rinsed with hot water until the supernatant was light brown. Solvent exchange was carried out by immersing the samples in ethanol/water mixture increasing the ethanol concentration, i.e., 60, 90, 100 wt. % of ethanol. The concentration of ethanol was checked by density-meter DMA 4500 (Anton Paar Company, Austria). When the final ethanol concentration was higher than 98 wt. %, samples were ready for supercritical CO_2 drying [223].

Apple aerogels, AG, were prepared by directly mixing apple pomace, without seeds, in ethanol. Solvent exchange and supercritical drying were carried out following the same procedure as used for coffee.

7.2.3. Samples surface modification

Silanes are well known hydrophobic agent for cellulose, they can form polysiloxane structures by reacting with a hydroxyl group of the cellulose fibers through a condensation reaction [224,225]. Because of their lignocellulosic nature, surface modification of both coffee and apple aerogel was done by silanization both in liquid and gas phase.

The liquid phase method, LPM, involved the samples before supercritical drying, thus at the end of the solvent exchange phase. The so prepared samples, known as alcogels, were filtered from pure ethanol to obtain 0.5 g of wet solid and immersed in 20 ml of a 5 wt. %. MTMS solution in ethanol 80 wt. % for 3 hours at 60°C. All the samples were washed with ethanol to remove the non-reacted silane.

The gas phase method, GPM, involved a technique known as chemical vapor deposition. Around 0.5 g of organic based aerogel was placed in a 100 ml bottle together with two small, opened vessels containing 2 ml of MTMS and 1 ml of deionized water, respectively. The bottle was then sealed and placed in an oven at 80 °C for 5 hours. After the reaction time, the bottle was quickly removed from the oven, and opened under a laboratory hood to remove the excess of silane. Samples were named $HCG_{(l)}$ and $HAA_{(l)}$ to indicate the hydrophobic modification of the aerogels in liquid phase, while $HCG_{(g)}$ and $HAG_{(g)}$ indicate the hydrophobic modification in gas phase.

7.2.4. Characterizations techniques

Microstructure of the samples was studied by scanning electron microscopy (Leo Gemini 1530, Zeiss, Oberkochen, Germany); samples were sputtered with a thin layer of gold to increase the conductivity.

Along with the investigation of the physical and chemical properties of pristine aerogel, hydrophobic modification was investigated.

Bulk density, ρ_b (g/ml), was measured using a graduated cylinder. Dry aerogels were poured in the cylinder up to a certain volume and weighted. The bulk density was calculated as a ratio of the particles weight and the occupied volume.

The water vapor uptake of the samples was measured at 20 °C by keeping the samples in a climate chamber with 80% humidity for 72 h. The water adsorption percentage was calculated according to Eq. (7.1).

$$V_u\ (\%) = \frac{w_t - w_d}{w_d} \cdot 100 \qquad (7.1)$$

Where V_u is the percentage of absorbed water vapor, w_t is the wet weight after 72 hours, w_d is the dry weight of the samples.

BET surface was measured with nitrogen adsorption (NOVA 4000e, Quantachrome Instrument; Anton Paar, Graz, Austria).

Contact angle measurement using the static sessile drop method was used. Around 0.2 g of powder were pressed to form a pellet and a water drop of 15 µl was dripped onto its surface. The drop profile was allowed to stabilize before acquiring the measurement.

IR spectra were measured at room temperature in the range 400–4000 cm^{-1} with a Bruker Vertex 70 instrument equipped with attenuated total reflectance (ATR) accessory with a resolution of 2 cm^{-1}.

Thermogravimetric analysis TGA, was performed with a STA PT 1600 Linseis, to investigate the thermal stability between 30 and 600 °C at a heating rate of 10°C/min in an inert atmosphere of nitrogen.

7.2.5. Results and discussion

Morphological analysis

Scanning electron microscopy was used to investigate the microstructure of coffee and apple aerogels. Two different magnifications were investigated and are reported Figure 7.4.

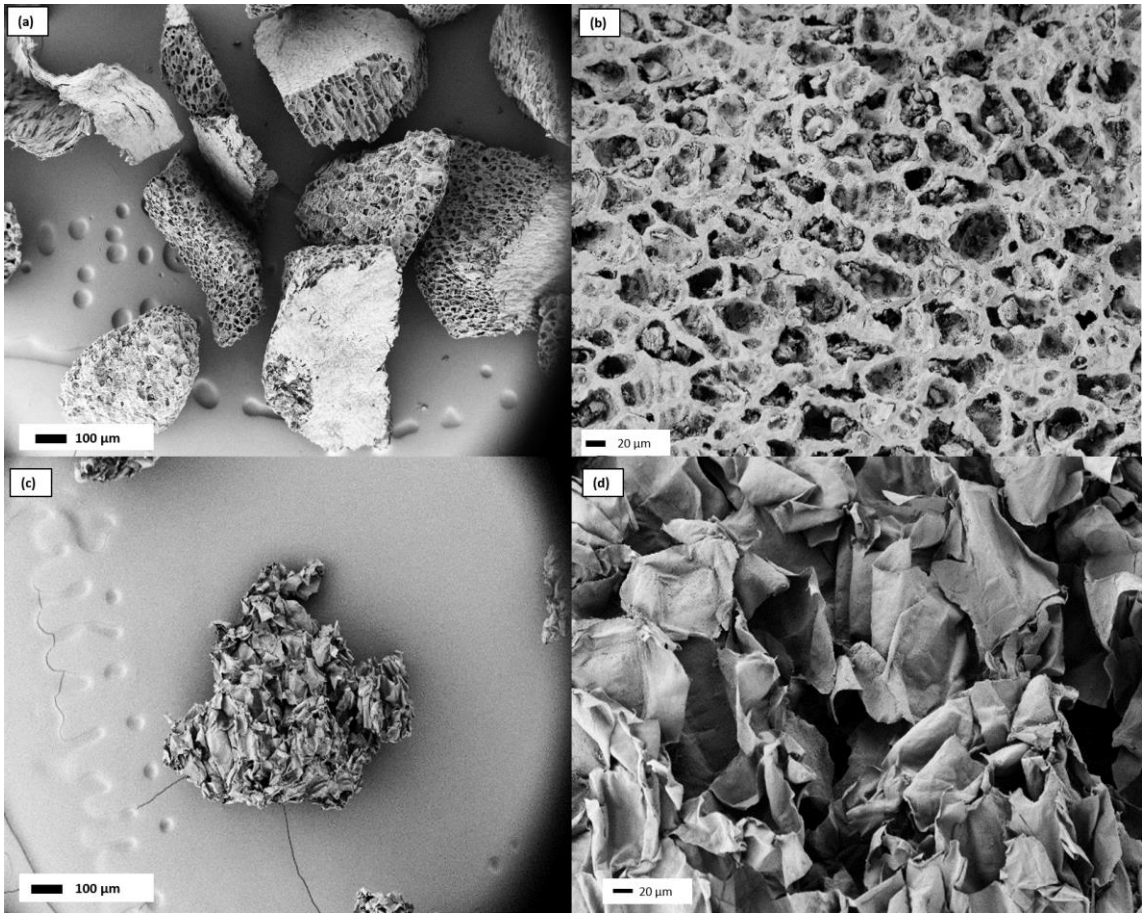

Figure 7.4 SEM micrographs of coffee aerogels at a) 100X magnification and b) 500X magnification SEM micrographs of apple aerogels at c) 100X magnification and d) 500X magnification

It is interesting to notice that both the organic raw materials have an intrinsic porosity when transformed into aerogels. Coffee aerogel, CG, Figure 7.4 presents a honeycomb like structure with a diffuse porosity (a); by increasing the magnification, it is possible to see smaller cavities inside the pores (b). On the other hand, apple aerogel AG, presents a sheet-like folded structure (c-d).

Since the main goal of this research is to use the air entrapped inside the pores as thermal insulator, the effect of water on the morphology and physical properties was investigated by immersing the aerogels in water for 24 hours and let it dry. In Figure 7.5 SEM micrographs of CG (e) and AG (f) after the water aging process are reported. CG surface morphology seems not affected by water; however, AG shows a collapse of the structure.

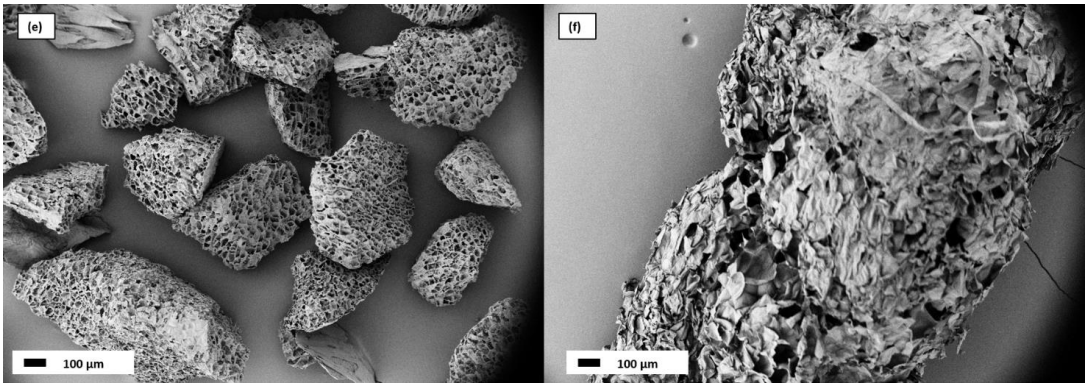

Figure 7.5 SEM micrographs at 100X magnification of: a) coffee aerogels after water immersion test, b) apple aerogels after water immersion test

Physical properties

Table 7.2 shows the bulk density and BET surface results of pristine aerogels and modified aerogels.

Table 7.2 Physical characterization of pristine coffee and apple aerogels (CG and AG), and after hydrophobic surface modification (HAC and HAG). N.d. means not detectable.

	S_{BET} (m^2/g)		**ρ (g/cm^3)**	
Treatment/sample	**CG**	**AG**	**CG**	**AG**
Pristine	229	208	0.191±0.004	0.016±0.001
After LPM	152	75	0.207±0.001	0.026±0.001
After GPM	n.d.	11	0.265±0.001	0.032±0.001

Considering the S_{BET} results, both pristine CG and AG have a reasonable high surface area. Moreover, the S_{BET} results, not reported here, of samples after being immersed in water for 24 hours present a not detectable surface area. A surface modification to prevent the collapse of the microstructure is necessary.

The results show that both LPM and GPM reduce the surface area; it is clear that $HCG_{(l)}$ and $HAG_{(l)}$ have a higher surface area compared to $HCG_{(g)}$ and $HAG_{(g)}$. This may be connected to the fact that MTMS, because of its dimension, not only covers the outer surface of the aerogel, but enter the pores resulting in a physical obstruction for the S_{BET} measurement.

By observing Table 7.2, CG has a higher bulk density then AG. Because of the novelty of this work, no direct comparison with other existing materials is possible, however both the aerogel have a bulk density comparable with traditional lightweight porous materials [226]. Moreover, it is interesting to notice that CG bulk density is slightly affected by LPM while after GPM, an increased value of ρ_b is shown. On the other hand, apple aerogels evidence an increased ρ_b after both the liquid and the gas phase modification.

An increase of the bulk density after silanization process can be linked to the direct presence of silane on the aerogel surface. The absence of humidity between the particles enhances the packing ability avoiding the formation of sticky big aggregates, thus increases the bulk density. Considering this hypothesis, surface modification worked better for apple then coffee. Moreover, because of the higher bulk density, gas phase modification seems to be more effective as modification technique.

Water vapor uptake

The influence of air humidity on the aerogel particles was tested at 80% RH. In fact, water vapor uptake is an important parameter, which affects degradation and induces changes in mechanical properties. Moreover, this test is a useful tool to evaluate the effectiveness of the hydrophobic modification. The results are reported in Table 7.3.

Table 7.3 Water vapor uptake after 72 h in a controlled humidity chamber at RH 80%

	Water absorption (%)	
Treatment/sample	**CG**	**AG**
Pristine	13	16
After LPM	15	22
After GPM	13	12

By weighing the samples before and after the humidity exposure, pristine aerogels, CG and AG, have an absorption of 13 and 16 %, respectively. With the LPM the absorption increases to 15% for $HCG_{(l)}$, and 22 % for $HAG_{(l)}$; this means that liquid phase modification has probably a negative impact on the structure of the aerogel. Moreover, it seems that hydrophobic character is damaged. On the contrary, samples modified by GPM exhibit an uptake of 13% for $HCG_{(g)}$, and 12% for $HAG_{(g)}$; this means that chemical vapor deposition has no effect on coffee, while it leads to better results for apple aerogels.

Wetting ability

Wettability behavior of pristine aerogels and modified aerogels was measured by means of water contact angle measurement and is shown in Figure 7.6. To better appreciate the hydrophilic/hydrophobic nature of the materials, two pictures were taken, at 5 s and 60 s after the contact of the drop with the surface.

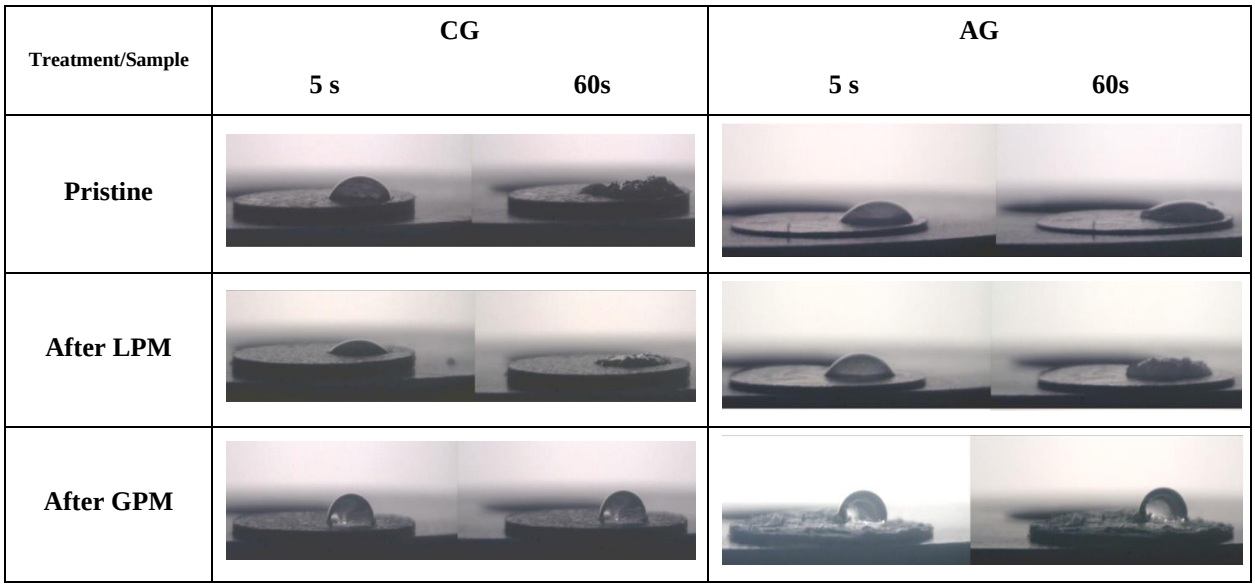

Figure 7.6 Investigation of surface wettability. Contact angle measurement after 5 and 60 seconds of pristine aerogels and after silanization in liquid phase (LPM), and in gas phase (GPM)

According to Figure 7.6 CG, AG, and their modification with LPM exhibit immediately a small contact angle; however, after 60 seconds, they exhibit a non-detectable contact angle due to adsorption of the water drops. On the other hand, the samples treated with the GPM demonstrate a good water repellence, by keeping a constant high contact angle. The results are reported in Table 7.4.

Table 7.4 Contact angle θ of of pristine aerogels and after silanization in liquid phase (LPM), and in gas phase (GPM) at t=0 s and after 60. n.d. stays for not detectable

	θ_{5s} (°)	θ_{60s} (°)	θ_{5s} (°)	θ_{60s} (°)
Treatment/Sample	**CG**		**AG**	
Pristine	50±2	n.d.	50±2	n.d.
After LPM	43±3	n.d.	49±2	n.d.
After GPM	97±3	97±3	100±3	100±3

ATR-FTIR Spectroscopy

The chemical composition and the interaction between aerogel and silane were investigated by ATR-FTIR spectroscopy. Figure 7.7 shows the absorbance spectra of the pure aerogel and the silane modified aerogel.

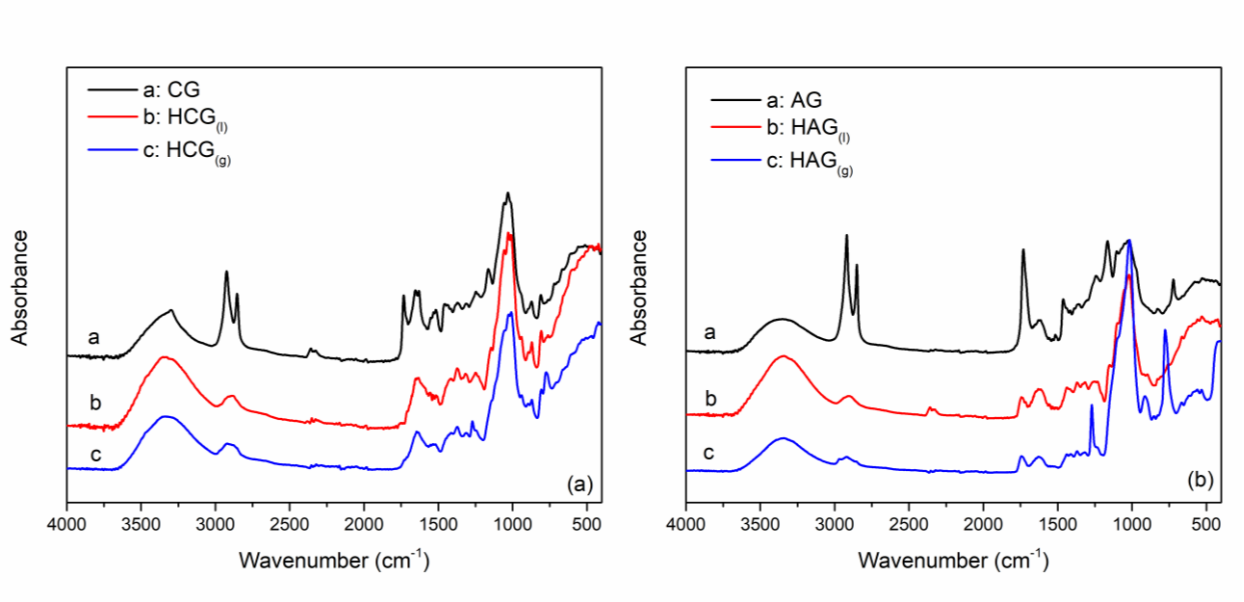

Figure 7.7 FTIR spectra collected in ATR mode of pristine aerogel (black curves), LPM silanization (red curves), and GPM silanization (blue curves). (a) CG, $HCG_{(l)}$ and $HCG_{(g)}$;(b) AG, $HAG_{(l)}$ and $HAG_{(g)}$

FTIR spectra of all the coffee aerogels, Figure 7.7 (a), show a broad peak between 3500 and 3000 cm^{-1} related to the hydroxyl group of O-H stretching vibration. Considering CG curve, the most representative peaks are at 2925 cm^{-1} and at 2855 cm^{-1} corresponding to the C-H stretching vibration of cellulose backbone, at 1733 cm^{-1} related to the C=O from carbonyl group in aliphatic esters. The small peak at 1655 cm^{-1} represents the carbonyl stretching from lignin moieties [227]. The wide peak at 1100–1300 cm^{-1} may be assigned to the C-C vibration of the cellulose [228]. What is interesting to notice for both $HCG_{(l)}$ and $HCG_{(g)}$, is that the broad band O-H stretching vibration band is shifted at 3351 cm^{-1}. Considering $HCA_{(l)}$, the two peaks at 2925 and 2855 are merged in a single peak with a lower absorbance that can be influenced by the presence of Si-CH_3 bond. Other characteristic peaks cannot be detected because of the strong overlapping between the two spectra. On the other hand, $HCG_{(g)}$ showed some significant differences compared to CG, the bending of the Si-CH_3 was observed with a peak at 1270 cm^{-1}, and the absorption bands related to the stretching vibrations of the Si–C bond and/or the stretching vibrations of the Si–O bond was observed at 776 cm^{-1} [229].

In the IR spectrum of apple aerogels, Figure 7.7 (b), the most representative peaks are associated to O-H stretching broad band at 3354 cm^{-1}, to the asymmetric and symmetric stretching vibration of C-H at 2918 and 2850 cm^{-1} respectively and to the characteristic vibration of carboxyl group C=O at 1731 cm^{-1}. A few complex bands in the range of 1000-1200 cm^{-1} are due to C-O and C=C stretching modes of the organic chain [230,231]. Considering $HAG_{(l)}$ and $HAG_{(g)}$, O-H characteristic peak is slightly shifted at 3340 cm^{-1}, the peaks at 2924 and 2854 are merged in a single smaller peak at 2911 cm^{-1}, the peak associated with the carboxyl group is shifted as well to 1746 cm^{-1}. Again, due to the overlapping of the region between 1200

and 1000 cm^{-1} it is difficult to see the characteristic peak of Si-O-Si. However, it is possible to identify the peak associated with the bending vibration of Si-CH_3 bond at 1250 cm^{-1} for $HAG_{(l)}$ and at 1271 cm^{-1} for $HAG_{(g)}$. Moreover, the latter exhibit specific peaks at 913 cm^{-1} attributed to the Si–OH bond stretching vibrations, and at 777 cm^{-1} related to the absorption bands of the stretching vibrations of the Si–C bond and/or the stretching vibrations of the Si–O bond [232,233].

The results confirmed the presence of an interaction between aerogels and MTMS. However, gas phase modification showed the best results, especially for apple aerogel. Coffee aerogel seems to be only slightly influenced by the presence of silanes.

Thermal stability

The thermal stability of all the samples was evaluated by thermo gravimetric assessment. Moreover, the presence of surface modification was investigated. In this sense, TGA allows only a qualitative assessment of the occurrence of surface modification. TGA and DTG curves are reported in Figure 7.8.

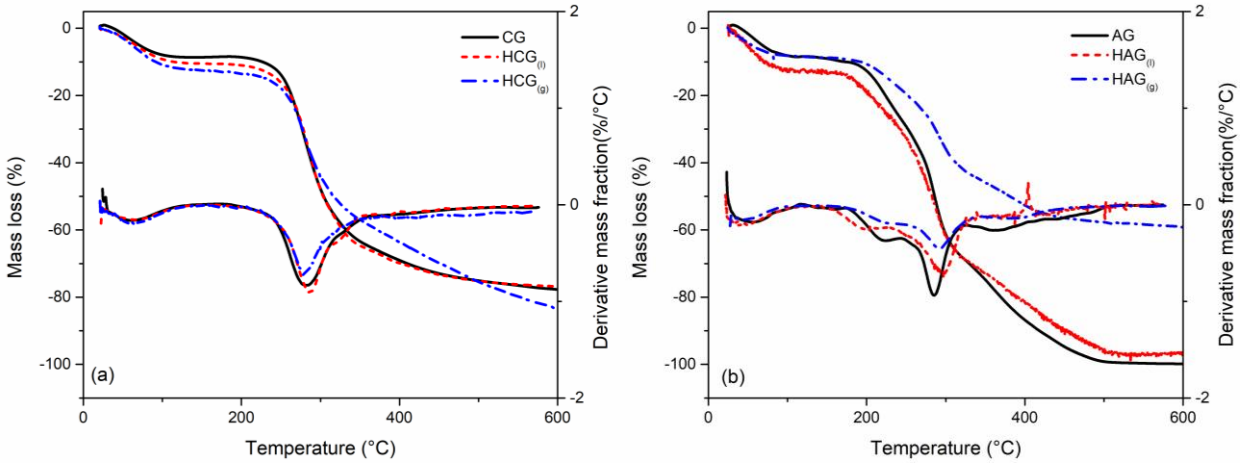

Figure 7.8 Thermal stability investigation. TGA and DTG profiles of pristine aerogel (black curves), LPM silanization (red curves), and GPM silanization (blue curves). (a) CG, pristine and after LPM and GPM treatment), (b) AG, pristine and after LPM and GPM treatment

Coffee aerogel curves show two clear degradation steps. The first one between 80 °C and 100 °C is the loss of moisture. The second one occurs between 200 °C and 400 °C, and describes the degradation of lignin and cellulose [144,234]. However, at the end of the thermal program, around 20% of the total mass remains as a solid residue. Considering the modified aerogel, $HCG_{(l)}$ has an almost identical curve, meaning that no additional elements are detected, i.e., surface silane group. On the other hand, $HCG_{(g)}$ shows a slower slope between 300 °C and 500 °C; this behavior can be related to an alteration of the structure during the GPM technique. From the DTG curves (derivative mass fraction %) the two steps degradation is

confirmed, the maximum of each peak describes the point of greatest rate of change on the weight loss curve. Two broad peaks with respectively a maximum at 65 °C and 281 °C are depicted for CG. However, the maximum of the peak associated with the lignocellulosic degradation is slightly shifted to 288°C and 279°C for $HCG_{(l)}$ and $HCG_{(g)}$, respectively.

The thermal decomposition of apple aerogels, Figure 7.8 (b), occurs in four steps. The first step ends around 100°C and can be attributed to moisture loss; the three degradation steps occurring between 200 and 500 °C are characteristic of the lignocellulosic compounds [231]. According to the literature, the weight loss that occurs at 200°C describes the degradation of lignin and hemicellulose; between 250 and 300°C also cellulose starts its pyrolysis, ending it around 500°C [235,236]. This behavior has been confirmed by the presence of four peaks in DTG curves at 40, 222, 285 and 362°C, respectively. Considering $HAG_{(l)}$ few differences with respect to the pristine AG are depicted: the thermal stability slightly improved after 300°C with a positive shift of the maximum correlated to the lignocellulosic degradation. However, no modification in the hydrophobic character can be detected. On the other hand, $HAG_{(g)}$ shows not only a better thermal stability all over the curve, but also a higher solid residual. These results can be strongly correlated to the presence of silane groups on the surface of apple aerogel.

7.2.6. Conclusions

Organic waste-based aerogels were prepared using spent ground coffee and apple pomace. Because of their innovative origin, physical and chemical characterizations were performed. Compared to traditional thermal insulating fillers, both CG and AG exhibited a good surface area and bulk density. A peculiar morphology was depicted by scanning electron microscopy: CG showed a honeycomb-like structure, while AG resembled a messy folded sheet structure. In order to use these materials inside a water-based coating formulation, two surface treatments by means of silanization were carried out: one following two a liquid phase modification, where MTMS was in ethanol solution, and another following a gas phase modification which involved pure MTMS in its gaseous state. CG modification was not entirely successful neither in liquid or gas phase, as showed by the bulk density, FTIR and TGA results. On the other hand, probably because of the different morphology and chemical structure, the silanization increased the hydrophobic character of AG, as confirmed by the bulk density, wetting ability, FTIR, and TGA results.

7.3 FORMULATION AND CHARACTERIZATION OF ZEOLITE AND AEROGEL BASED THERMAL INSULATING PLASTER

European households are responsible for 68% of the total final energy use in buildings, mainly related to heating, cooling, hot water, cooking and appliances [237] The refurbishment of existing buildings is a crucial point for the achievement of the energy and climate objectives of the European Union (EU) for 2020

and 2050 [83]. Multilayer external wall thermal insulation systems have been extensively used for the thermal retrofitting of building façades. These multilayers system is widely spread in Europe and consists of a base coat with a reinforcement glass fiber mesh, a thermal insulation board up to 10 cm typically of expanded polystyrene EPS, and finishing coat [238,239]. This solution however cannot be applied in every case. For example, the residential buildings of the historical city center of Genoa are close to each other connected by narrow street called "vicoli"; a thickness of 10 cm is not always available. Moreover, here in Italy, the refurbishment of the external façade must be proposed and accepted by all the people living in the building and is generally an expensive work. A recent alternative solution consists of using plasters or mortars with thermal insulation properties [240].

In this section, a plaster formulation based on natural zeolites and organic waste-based aerogels is developed and characterized. Thermal properties were evaluated focusing on thermal conductivity.

A qualitative assessment on the possibility of increasing building energy efficiency has been done.

7.3.1. Materials

Sodium alginate, viscosity 350-550 mPa s in 1% water at 20°C, was gently provided by Algaia; natural Clinoptilolite, ZCL, with a content of 90% of clinoptilolite, was gently provided by ZEOCEL Italia; natural chabazite, ZCH, with a content of 65 % of chabazite was gently provided by Zeolite Italia. Coffee and apple aerogels were prepared following the procedure described in section 7.2. All the other components, acrylic binder, organic additives, calcium carbonate and barium sulfate are commercial products provided by Boero Bartolomeo S.p.A.

7.3.2. Samples preparation

Thermal plaster formulations were prepared with a disperser, Dispermat, equipped with a stainless-steel dispersion impeller; low speed was set during the mixing phase, while high speed was set during the grinding phase. A butterfly impeller was used to incorporate aerogels.

Zeolites and aerogels concentration was chosen according to a qualitative rheology assessment by means of a spatula test. The concentration of each component is reported in Table 7.5.

Plaster samples were indicated with the type of filler used, followed by " –p", meaning "plaster". A mineral-based adhesive and skim coat consisting of cement, selected fine sands, hydraulic and synthetic binders was used as traditional reference sample, STD. Whereas a silica-based aerogel thermo plaster was also used as reference sample, STD-SG-p, considering it as the filler with the highest thermal performances on the market.

Table 7.5 Composition of plasters formulations (-p) containing aerogels (CG, AG) and zeolites (ZCL, ZCH)

	Concentration (wt. %)							
Sample/Component	**Thickener (SA)**	**Additives**	**Filler (d=1 mm)**	**Binder**	**Solvent**	**Filler (d=100 µm)**	**Zeolite**	**Aerogel**
ZCL-p	0.1	4.0	9	11	26	31	17	-
ZCH-p	0.1	4.0	9	11	26	25	23	-
HZCL-p	0.1	4.0	9	11	26	31	17	-
CG-p	0.1	4.0	10	11	30	31	-	13
AG-p	0.1	4.4	12	12	33	33.5	-	5
$HAG_{(g)}$-p	0.1	4.4	12	12	33	33.5	-	5

Each thermal plaster was applied on a fiber cement board 25x25 cm^2, with a variable dry thickness between 0.3 and 0.6 cm. The so prepared boards were let dry at room temperature for one week before testing their thermal properties. Considering the very low thickness and negligible thermal insulation properties of the architectural coating, the thermal characterization was done only on the plaster.

Top view and side view of some of the boards are shown in Figure 7.9.

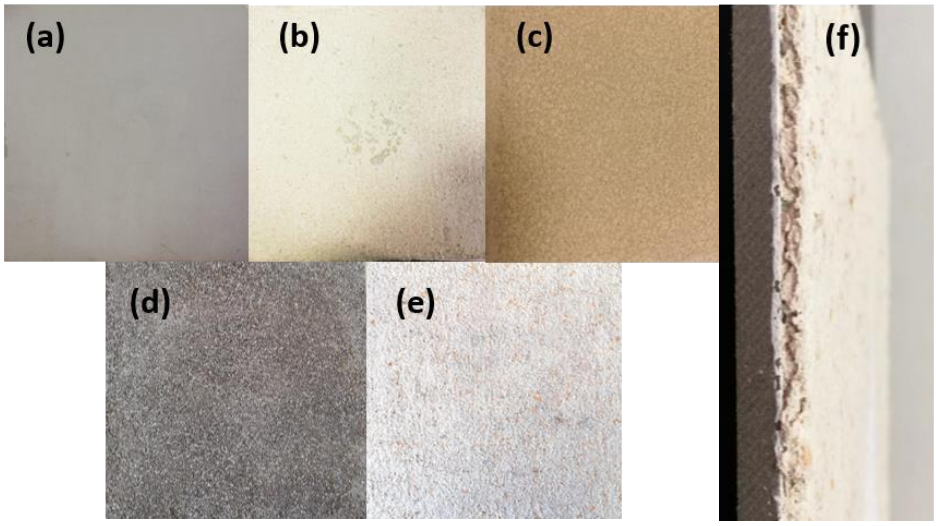

Figure 7.9 Thermal plaster applied onto fiber cement board. Top view of: a) STD, b) ZCL-p, c) ZCH-p, d) CG-p, e) AG-p. f) Side view of AG-p

7.3.3. Characterizations techniques

The maximum amount of thermal fillers was evaluated by slowly adding the raw material to a water-binder mixture (1:1) weighing the amount of filler until the physical appearance resembled a paste.

Specific weight was evaluated using a stainless steel, 50 ml, pycnometer at 20°C according to UNI EN ISO 2811-1.

The thermal properties of the plaster samples were investigated by means of the hot box method using an original instrument assembled following the UNIEN ISO 1934, described in Chapter 5.6.

7.3.4. Results and discussion

In the previous chapters, zeolites and aerogels were fully characterized. Considering the differences between the four raw materials, the concentration inside the thermal plaster formulations had to be optimized for each case.

Clinoptilolite showed a wider size distribution compared to chabazite, leading to a better packing ability. This means that between the two zeolites a lower amount of ZCL is probably necessary to obtain a suitable viscosity for the application.

Coffee aerogel had a higher density and a lower vapor uptake compared to apple aerogel; considering that coatings formulations are developed in weight percentage, it is reasonable to think that a higher amount of coffee can be added to the thermal plaster formulation.

The hypothesis were confirmed by the evaluation of the maximum amount of fillers that can be included still assuring a suitable viscosity. For ZCL, 17 wt. % was the optimal concentration, while for ZCH it was 23 wt. %.

Aerogels on the other hand, due to their stronger water adsorption, were included in the formulation in less quantity: coffee cannot exceed the 13 wt. %, while apple was present with5 wt. %.

The specific weight of the reference sample and of all the other thermal plasters, containing zeolites and aerogels, are reported in Table 7.6.

Table 7.6 Specific weight of thermal plaster

	Specific weight (g/cm^3)
STD	1.60±0.10
ZCL-p	1.65±0.30
ZCH-p	1.71±0.30
HZCL-p	1.56±0.30
CG-p	0.97±0.20
AG-p	1.13±0.20
HAG$_{(g)}$-p	1.18±0.30

Fillers are the components inside a paint formulation that mainly affect the specific weight. All the new thermal plasters show a suitable specific gravity. It is clear that ZCL-p and ZCH-p have the highest specific weight among the new thermal plasters as a consequence of the higher percentage of filler inside the formulation (Table 7.5); HZCL-p has a slightly lower specific weight, probably due to the presence of air inside the cavities of the zeolite. The aerogel based thermo plasters have a lower specific density compared to zeolites. The surface modification does not influence the specific weight of the thermal plaster containing $HAG_{(g)}$.

The procedure for the calculation of the thermal properties was suggested by the UNI EN ISO 6946. In this method, the total thermal resistance was obtained combining the thermal resistance of each part of a thermally homogeneous sample [241]. In order to separate the thermal contribution of the thermal plaster, $R_{p,}$ from the whole board, fiber cement supports were first characterized, determining R_{fc}.

Considering our multilayer system, the total thermal resistance is the sum of the two layers, i.e., fiber cement and thermal plaster. Since the equipment provided the total thermal resistance of the multilayer system, $R_{tot,}$ the calculation suggested by the standard was performed indirectly, subtracting the resistance value of the fiber cement alone (λ_{fc}=0.07 W/m K), as reported in Eq. (7.2):

$$R_{tp} = R_{tot} - R_{fc} \qquad (7.2)$$

Thermal conductivity λ_p, and thermal transmittance U_p, of the thermal plaster were then calculated as follows:

$$\lambda_{tp} = \frac{d_{tp}}{R_{tp}} \qquad (7.3)$$

$$U_{tp} = \frac{1}{R_{tp}} \qquad (7.4)$$

Where d_p is the plaster thickness. The resulting thermal characteristics are reported in

Table 7.7.

Table 7.7 Thermal properties of standard mineral based plaster, silica aerogel based plaster, zeolite and aerogel thermal plaster

	Coating thickness (mm)	**λ_p (W/m K)**	**U_p [W/m^2 K]**	**R_p [m^{2}K/W]**
STD	5	0.643	128.64	0.008
ZCL-p	5.5	0.240	43.65	0.023
ZCH-p	5.5	0.282	48.34	0.020
HZCL-p	3.9	0.236	48.12	0.021
STD-SG-p	4.9	0.032	6.54	0.154
CG-p	5.1	0.168	32.88	0.030
AG-p	3.7	0.223	60.36	0.017
HAG($_g$)-p	6.4	0.088	13.80	0.075

As expected, the mineral-based adhesive and skim coat reference sample has the highest value of λ and U, and the lowest thermal resistance, R whereas silica aerogel based plaster has the lowest value of λ. Both ZCL-p and ZCH-p have a lower value of λ compared to the reference sample STD, showing a reasonable insulation character. The surface stearic acid modification of the clinoptilolite did not affect the thermal insulation properties. Indeed, the thermal conductivity is almost the same.

Among the pristine aerogels, CG-p has the lowest value of λ = 0.168 W/mK. On the other hand, AG-p, has a λ = 0.223 W/mK, that is higher compared to CG-p, but similar to zeolites. Remarkably, hydrophobic AG showed the lowest value of the thermal conductivity, λ = 0.088 W/mK. According to the results, organic waste-based aerogels have the best thermal insulation properties.

Considering the natural origin and the innovative application, especially for organic waste-based aerogel, it is clear that it is hard to achieve the same value of λ of advanced materials already used as thermal fillers. [161]. However, they exhibit very promising results and can be used to improve the energy efficiency of building leading to an improvement in the thermal comfort conditions.

7.3.5. Conclusions

In conclusion, natural zeolites and waste-based aerogels were used as fillers to develop a plaster formulation with thermal insulation properties. The concentration of the fillers was theoretically evaluated according to the results obtained in Section 7.1 and Section 7.2. Specifically, size distribution, vapor uptake and bulk density were used as reference parameters for a qualitative assessment. The amount of filler used inside the formulations was practically investigated by weighing the filler needed to create a paste with a 1:1 mix of binder and water. Inside the concentration range identified with this approach, the optimum concentrations of the fillers are 17 wt. %, 23 wt. %, 13 wt. % and 5 wt. % for ZCL, ZCH, CG, and AG, respectively. Compared to the standard mineral plaster, all the samples exhibit acceptable specific gravity for application. Despite the impossibility of using our rheometer to investigate the rheological properties, all the samples exhibited good flow properties and partial adhesion to the trowel that is necessary for vertical applications, i.e. walls, and good drying properties without the formation of visible cracking.

The thermal properties of six innovative formulations containing ZCL, ZCH, HZCL, CG, AG, $HAG_{(g)}$ in the plaster, and two reference samples, a standard mineral commercial product, STD, and a silica aerogel based plaster, STD-SG-p, were measured by means of the hot box chamber, UNI ISO 1934. Compared with the mineral standard plaster, all the samples have better thermal insulation properties. However, they do not reach the low thermal properties of highly performing silica aerogels plaster.

8 CONCLUSIONS

The present Thesis was dedicated to setting the foundation for a new project in collaboration with Boero Bartolomeo S.p.A., an Italian paint manufacturer, aimed to investigate new environmentally friendly raw materials for coatings formulations and to enhance building energy efficiency by increasing the thermal insulation of the building envelope. To efficiently tackle these tasks, the solution here proposed consisted in developing an innovative multilayer coating cycle for interior walls made of an architectural coating and a plaster formulation.

In this context, alginate was selected as a potential thickener inside an architectural coating formulation due to its capacity to form from weak to strong gels in presence of bivalent and trivalent ions. Rheological properties of alginate-based coatings were fully investigated to evaluate the suitability of alginate as thickener. According to the results, alginate exhibited a high versatility. By tuning the molecular weight, the concentration and the counterion it is possible to obtain different rheological profiles. Finally, alginates based coatings proved to have good in-can stability and application properties.

In the second part of project, the attention was focused on the preparation and characterization of porous insulation fillers innovative for the building sector. Specifically, two natural zeolites, a clinoptilolite and a chabazite type, were used in this study. Unfortunately, the high water absorption capacity can reduce the insulating properties and turn the preparation of plasters into a very challenging procedure. To avoid this problem, a surface modification of the zeolites through stearic acid esterification was carried out.

Along with the use of natural inorganic resources, organic wastes were valorized to obtain porous materials. Specifically, spent ground coffee and apple pomace aerogels were prepared. Again, their hydrophilic character could damage their morphology, thus diminishing the thermal properties inside a water-based coating. In order to reduce this risk, the hydrophobic character of both coffee and apple aerogels was increased by means of silanization. Two different methods were investigated: a liquid phase modification and a gas phase modification. According to the results, coffee aerogels were slightly affected by silane modification. On the other hand, apple aerogels exhibited better hydrophobic character after gas phase modification.

Finally, after the preparation, surface modification, and characterization of the fillers, their thermal properties inside a plaster formulation were evaluated. A basic plaster formulation containing water as the solvent, an acrylic binder, alginate as a thickener, and barium sulfate as the main filler was prepared.

The thermal properties were measured. As expected, the standard mineral plaster STD exhibited the worst insulation properties, with high thermal conductivity, λ= 0.643 W/m K. On the other hand, silica based aerogel STD-SG-p showed outstanding thermal insulation properties, with ultra-low thermal conductivity, λ= 0.032 W/m K. For what concerns natural zeolites and organic waste-based aerogels, they showed promising thermal conductivities. Specifically, among the zeolites, ZCL-p exhibited the lowest

thermal conductivity, λ= 0.240 W/mK, and no significant differences were depicted between pristine and modified zeolite. By contrast, CG-p showed a lower λ among the pristine aerogels, λ= 0.168 W/m K, but the best thermal insulation properties were obtained for $HAG_{(g)}$-p the most promising material with a λ= 0.088 W/m K.

In conclusion, the formulations developed and optimized in this project represent an important first step towards the application of natural zeolite and organic waste-based aerogels as sustainable thermal insulation fillers. Indeed, organic waste-based aerogels are the most promising insulation materials. According to the results, it is clear that the type of biomass influences the thermal insulating performances.

A deeper investigation on the primary source of coffee (arabica, robusta) and apple (apple variety) is highly suggested to better understand the different results showed in this project.

Moreover, the hydrophilic character of both zeolites and aerogels is one of the major obstacles for their use as insulating filler in water media. For this reason, hydrophobic modifications with more sustainable chemicals and procedures should be investigated. However, hydrophobic modification of biobased materials is still a work-in-progress; cold plasma technology or wax dip-coating can inspire future methods of coffee and apple aerogel surface modification.

LIST OF FIGURES AND TABLES

List of figures

List of Tables

APPENDIX A

Alginate based formulations were tested as 0.4 wt. % as well. However, they exhibit higher viscosities and strong shear thinning behavior compared to cellulose, along with stronger elastic properties which results in a stiffer gel structure. Moreover, storage stability was poor, syenresis phenomena were evident and the paints were hardly mixable. The rheological profile and tensile properties of SA04, PA04, and AA04 are reported in the figures below.

A1) Viscosity curves, A2) amplitude sweep test, A3) tensile tests, A4) 3ITT curves and graphical presentation of the fitting model are reported in the figures below.

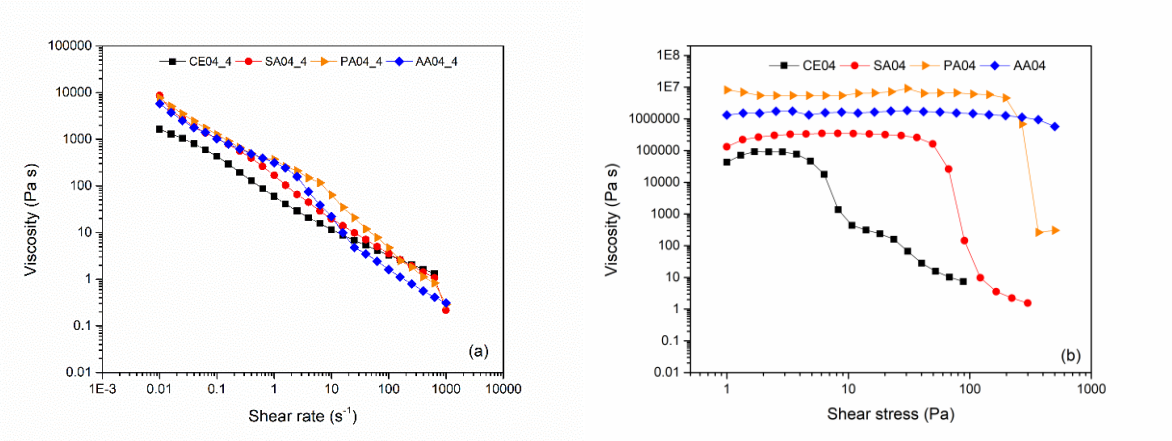

A1) Viscosity curves, shear rate controlled test, and b) shear stress controlled test

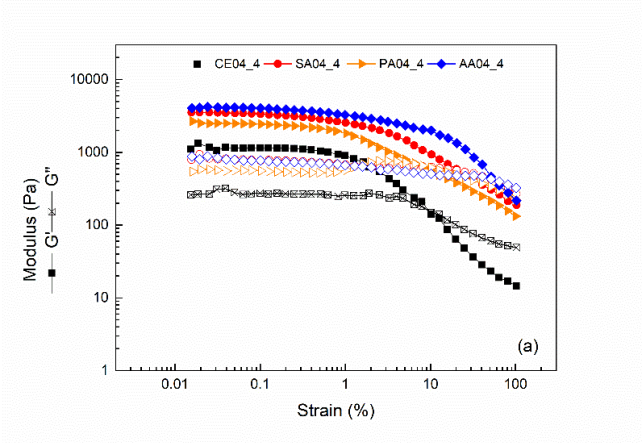

A2) Amplitude sweep test performed at f= 1Hz

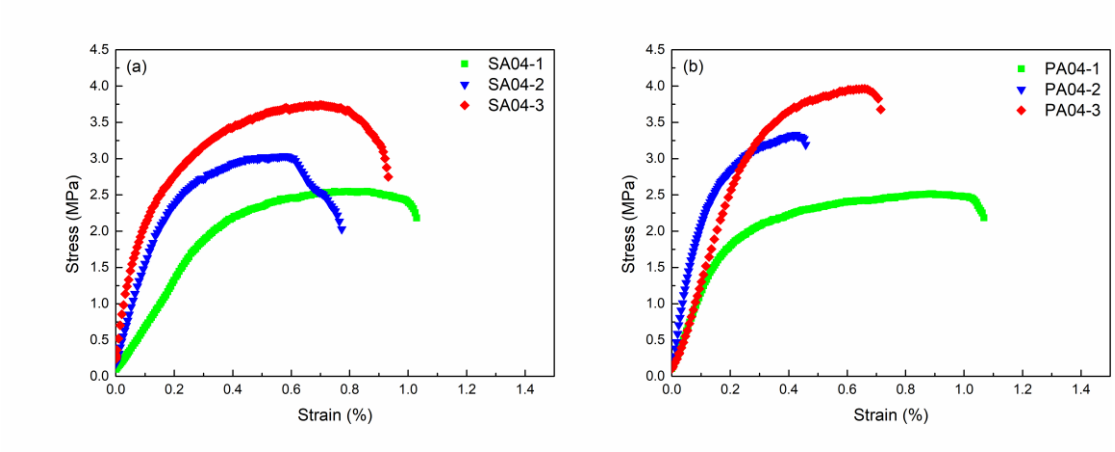

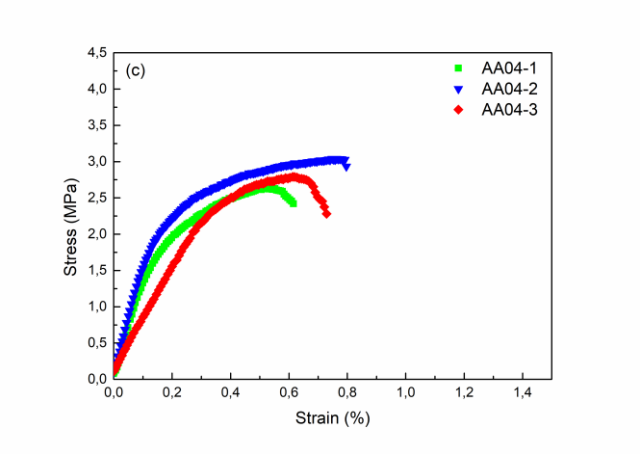

A3) Tensile test, stress vs strain

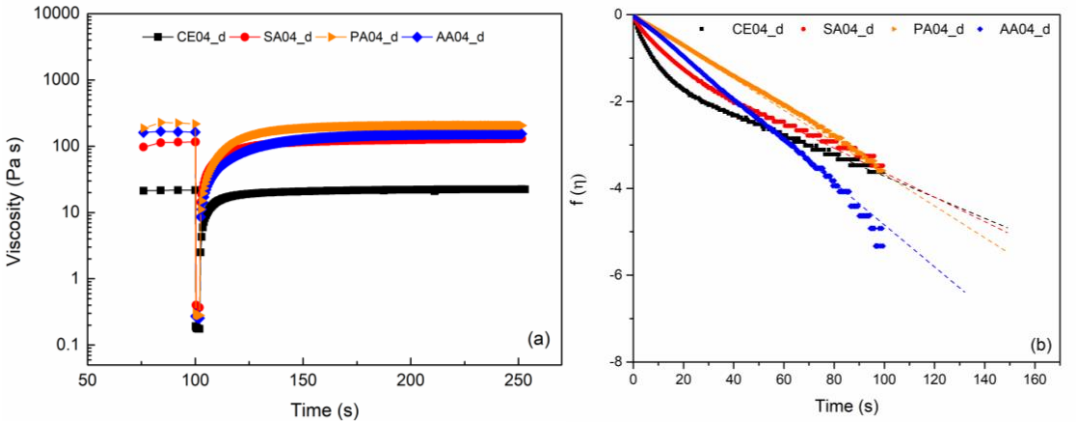

A4) a) 3ITT of diluted formulations and b) Representation of the third interval of 3ITT as a logarithmic function of viscosity vs time

Results of the validation of alginate based paint according to the industrial procedure described in Section 6.4.

	Specific weight (g/cm^3)	**pH**	**ICI viscosity (P)**
CE04	1.69±0.02	8.0±0.1	2.6±0.1
SAL02	1.73±0.01	8.0±0.1	0.89±0.1
SAL04	1.72±0.01	8.0±0. 1	1.68±0.1
PA02	1.71±0.05	8.0±0.1	1.5±0.1
AA02	1.71±0.05	8.0±0.1	1.6±0.1
SA04	1.73±0.02	7.8±0.1	2.5±0.1
PA04	1.73±0.01	7.8±0.1	2.4±0.1
AA04	1.72±0.01	7.8±0.1	2.5±0.1

APPENDIX B

International standards

ISO 14024: Environmental labels and declaration – Type I Environmental labeling – Principles and procedures

ISO 14021: Environmental labels and declarations – Self-declared environmental claims – Type II Environmental labelling

ISO 14025: Environmental labels and declarations – Type III Environmental declarations

ISO 8990: Thermal insulation - Determination of steady-state thermal transmission properties - Calibrated and guarded hot box

ISO 2811-1: Paints and varnishes - Determination of density - Part 1: Pycnometer method

ISO 19396-1: Paints and varnishes — Determination of pH value — Part 1: pH electrodes with glass membrane

ISO 2884-1: Paints and varnishes — Determination of viscosity using rotary viscometers — Part 1: Cone-and-plate viscometer operated at a high rate of shear

ISO 1934: Thermal performance of buildings - Determination of thermal resistance by hot box method using heat flow meter - Masonry

ASTM D869: Standard Test Method for Evaluating Degree of Settling of Paint

APPENDIX C

Scientific contribution

List of Publications:

- Gaggero, G.; Delucchi, M.; Allegretta, G.; Vicini, S.; Botter, R. *Interaction of sodium alginate thickener with components of architectural water-based coatings*. Progress in Organic Coatings, 151, 106116, **2021**.
- Dodero, A., Alberti, S., Gaggero, G., Ferretti, M., Botter, R., Vicini, S., Castellano, M., *An Up-to-Date Review on Alginate Nanoparticles and Nanofibers for Biomedical and Pharmaceutical Applications*. Advanced Material Interfaces, 8, 2100809, **2021.**
- Gaggero, G.; Delucchi, M.; Di Tanna, G.; Lagazzo, A.; Vicini, S.; Botterp, R. *Effect of different alginate salts on the rheological and tensile properties of waterborne paints.* Progress in Organic Coatings,163, 106676, **2022**.

Oral presentations:

- Gaggero, G., Delucchi, M., Vicini, S., Botter R. *A rheological evaluation of sodium alginate as thickener for waterborne paints: a focus on the application process*. MACROGIOVANI - Digital Edition, 26 June, **2020.**

Poster presentation:

- Gaggero, G., Delucchi, M., Allegretta, G., Vicini, S., Botter, R. *Sodium alginate as thickener in coatings formulations: investigation on its rheological properties.* XVI Convegno nazionale di reologia, 18-21 June, Rome, **2018**

REFERENCES

[1] S. Korkmaz, D. Erten, M. Syal, V. Potbhare, A Review of Green Building Movement Timelines in Developed and Developing Countries to Build an International Adoption Framework, Proc. Fifth Int. Conf. Constr. 21st Century Collab. Integr. Eng. Manag. Technol. (2009) 10.

[2] D.T. Doan, A. Ghaffarianhoseini, N. Naismith, T. Zhang, A. Ghaffarianhoseini, J. Tookey, A critical comparison of green building rating systems, Build. Environ. 123 (2017) 243–260. https://doi.org/10.1016/j.buildenv.2017.07.007.

[3] G. Bruntland, Our commmon future, World Comm. Environ. Oxf. Univ. Press. (1987) 45–65.

[4] B. Neyestani, A Review on Sustainable Building (Green Building), SSRN Electron. J. (2017). https://doi.org/10.2139/ssrn.2968885.

[5] S. Paraschiv, L.S. Paraschiv, A. Serban, Increasing the energy efficiency of a building by thermal insulation to reduce the thermal load of the micro-combined cooling, heating and power system, Energy Rep. 7 (2021) 286–298. https://doi.org/10.1016/j.egyr.2021.07.122.

[6] Q. Li, L. Zhang, L. Zhang, X. Wu, Optimizing energy efficiency and thermal comfort in building green retrofit, Energy. 237 (2021) 121509. https://doi.org/10.1016/j.energy.2021.121509.

[7] C. Yi, X. Bing, Building as Major Energy Consumer, in: Encycl. Sustain. Technol., Elsevier, 2017: pp. 137–148. https://doi.org/10.1016/B978-0-12-409548-9.10186-1.

[8] Energy performance of buildings directive. Last access January 2022. https://ec.europa.eu/energy/topics/energy-efficiency/energy-efficient-buildings/energy-performance-buildings-directive_it, (2022).

[9] T. Wilberforce, A.G. Olabi, E.T. Sayed, K. Elsaid, H.M. Maghrabie, M.A. Abdelkareem, A review on zero energy buildings – Pros and cons, Energy Built Environ. (2021) S2666123321000490. https://doi.org/10.1016/j.enbenv.2021.06.002.

[10] S.B. Husam Sameer, Life cycle input indicators of material resource use for enhancing sustainability assessment schemes of buildings, J. Build. Eng. 21 (2019) 230–242.

[11] S. Ferrari, M. Zoghi, T. Blázquez, G. Dall'O', New Level(s) framework: Assessing the affinity between the main international Green Building Rating Systems and the european scheme, Renew. Sustain. Energy Rev. (2021) 111924. https://doi.org/10.1016/j.rser.2021.111924.

[12] P. Anastas, N. Eghbali, Green Chemistry: Principles and Practice, Chem Soc Rev. 39 (2010) 301–312. https://doi.org/10.1039/B918763B.

[13] Environmental labels, ISO Publ. 2nd Ed. (2019) 12.

[14] R.E. Horne, Limits to labels: The role of eco-labels in the assessment of product sustainability and routes to sustainable consumption, Int. J. Consum. Stud. 33 (2009) 175–182. https://doi.org/10.1111/j.1470-6431.2009.00752.x.

[15] T. Kijek, Modelling Of Eco-innovation Diffusion: The EU Eco-label, Comp. Econ. Res. 18 (2015) 65–79. https://doi.org/10.1515/cer-2015-0004.

[16] F. Testa, I. Miroshnychenko, R. Barontini, M. Frey, Does it pay to be a greenwasher or a brownwasher?, Bus. Strategy Environ. 27 (2018) 1104–1116. https://doi.org/10.1002/bse.2058.

[17] M.R. Hall, D. Allinson, Heat and mass transport processes in building materials, in: Mater. Energy Effic. Therm. Comf. Build., Elsevier, 2010: pp. 3–53. https://doi.org/10.1533/9781845699277.1.3.

[18] M.S. Van Dusen, J.L. Finck, Heat transfer through building walls, Bur. Stand. J. Res. 6 (1931) 493. https://doi.org/10.6028/jres.006.033.

[19] M. Hamdani, S.M.E.A. Bekkouche, T. Benouaz, R. Belarbi, M.K. Cherier, Minimization of indoor temperatures and total solar insolation by optimizing the building orientation in hot climate, Eng. Struct. Technol. 6 (2014) 131–149. https://doi.org/10.3846/2029882X.2014.988756.

[20] D.A. Nield, A. Bejan, Convection in Porous Media, Springer International Publishing, Cham, Switzerland, 2017. https://doi.org/10.1007/978-3-319-49562-0.

[21] H.H. Humaish, Effect of porosity on thermal conductivity of porous materials, IOP Conf. Ser. Mater. Sci. Eng. 737 (2020) 012185. https://doi.org/10.1088/1757-899X/737/1/012185.

[22] D.S. Smith, A. Alzina, J. Bourret, B. Nait-Ali, F. Pennec, N. Tessier-Doyen, K. Otsu, H. Matsubara, P. Elser, U.T. Gonzenbach, Thermal conductivity of porous materials, J. Mater. Res. 28 (2013) 2260–2272. https://doi.org/10.1557/jmr.2013.179.

[23] H.-P. Ebert, Functional materials for energy-efficient buildings, EPJ Web Conf. 98 (2015) 08001. https://doi.org/10.1051/epjconf/20159808001.

[24] T. Shimizu, K. Matsuura, H. Furue, K. Matsuzak, Thermal conductivity of high porosity alumina refractory bricks made by a slurry gelation and foaming method, J. Eur. Ceram. Soc. 33 (2013) 3429–3435. https://doi.org/10.1016/j.jeurceramsoc.2013.07.001.

[25] D. Șova, M.D. Stanciu, S.V. Georgescu, Design of Thermal Insulation Materials with Different Geometries of Channels, Polymers. 13 (2021) 2217. https://doi.org/10.3390/polym13132217.

[26] B.P. Jelle, Traditional, state-of-the-art and future thermal building insulation materials and solutions – Properties, requirements and possibilities, Energy Build. 43 (2011) 2549–2563. https://doi.org/10.1016/j.enbuild.2011.05.015.

[27] N.F. Shahedan, M.M.A.B. Abdullah, N. Mahmed, A. Kusbiantoro, S. Tammas-Williams, L.-Y. Li, I.H. Aziz, P. Vizureanu, J.J. Wysłocki, K. Błoch, M. Nabiałek, Properties of a New Insulation Material Glass Bubble in Geopolymer Concrete, Materials. 14 (2021) 809. https://doi.org/10.3390/ma14040809.

[28] E. Barreira, V.P. de Freitas, External Thermal Insulation Composite Systems: Critical Parameters for Surface Hygrothermal Behaviour, Adv. Mater. Sci. Eng. 2014 (2014) 1–16. https://doi.org/10.1155/2014/650752.

[29] I. Zabalza Bribián, A. Valero Capilla, A. Aranda Usón, Life cycle assessment of building materials: Comparative analysis of energy and environmental impacts and evaluation of the eco-efficiency improvement potential, Build. Environ. 46 (2011) 1133–1140. https://doi.org/10.1016/j.buildenv.2010.12.002.

[30] T. Potrč, K.M. Rebec, F. Knez, R. Kunič, A. Legat, Environmental Footprint of External Thermal Insulation Composite Systems with Different Insulation Types, Energy Procedia. 96 (2016) 312–322. https://doi.org/10.1016/j.egypro.2016.09.154.

[31] A. Audenaert, S.H. De Cleyn, M. Buyle, LCA of low-energy flats using the Eco-indicator 99 method: Impact of insulation materials, Energy Build. 47 (2012) 68–73. https://doi.org/10.1016/j.enbuild.2011.11.028.

[32] J. Michalak, External Thermal Insulation Composite Systems (ETICS) from Industry and Academia Perspective, Sustainability. 13 (2021) 13705. https://doi.org/10.3390/su132413705.

[33] P. Moghaddam Fard, M.G. Alkhansari, Innovative fire and water insulation foam using recycled plastic bags and expanded polystyrene (EPS), Constr. Build. Mater. 305 (2021) 124785. https://doi.org/10.1016/j.conbuildmat.2021.124785.

[34] D.V. Marques, R.L. Barcelos, H.R.T. Silva, P. Egert, G.O.C. Parma, E. Girotto, D. Consoni, R. Benavides, L. Silva, R.F. Magnago, Recycled polyethylene terephthalate-based boards for thermal-acoustic insulation, J. Clean. Prod. 189 (2018) 251–262. https://doi.org/10.1016/j.jclepro.2018.04.069.

[35] P. Ricciardi, E. Belloni, F. Cotana, Innovative panels with recycled materials: Thermal and acoustic performance and Life Cycle Assessment, Appl. Energy. 134 (2014) 150–162. https://doi.org/10.1016/j.apenergy.2014.07.112.

[36] E. Cintura, L. Nunes, B. Esteves, P. Faria, Agro-industrial wastes as building insulation materials: A review and challenges for Euro-Mediterranean countries, Ind. Crops Prod. 171 (2021) 113833. https://doi.org/10.1016/j.indcrop.2021.113833.

[37] X. Cao, J. Liu, X. Cao, Q. Li, E. Hu, F. Fan, Study of the thermal insulation properties of the glass fiber board used for interior building envelope, Energy Build. 107 (2015) 49–58. https://doi.org/10.1016/j.enbuild.2015.08.007.

[38] X. Hu, Characteristics and Application of Thermal Mortar Materials in Building Materials, Mater. Today Proc. 22 (2020) 2539–2543. https://doi.org/10.1016/j.matpr.2020.03.383.

[39] S. Abidi, Y. Joliff, C. Favotto, Impact of perlite, vermiculite and cement on the Young modulus of a plaster composite material: Experimental, analytical and numerical approaches, Compos. Part B Eng. 92 (2016) 28–36. https://doi.org/10.1016/j.compositesb.2016.02.034.

[40] S.K. Adhikary, D.K. Ashish, Ž. Rudžionis, Aerogel based thermal insulating cementitious composites: A review, Energy Build. 245 (2021) 111058. https://doi.org/10.1016/j.enbuild.2021.111058.

[41] M. Gonçalves, N. Simões, C. Serra, I. Flores-Colen, A review of the challenges posed by the use of vacuum panels in external insulation finishing systems, Appl. Energy. 257 (2020) 114028. https://doi.org/10.1016/j.apenergy.2019.114028.

[42] M. Schuss, U. Pont, A. Mahdavi, Long-term experimental performance evaluation of aerogel insulation plaster, Energy Procedia. 132 (2017) 508–513. https://doi.org/10.1016/j.egypro.2017.09.696.

[43] O. Proskurnina, U.J. Pont, M. Kornicki, K. GmbH, A. Mahdavi, Application of aerogel-based plaster towards thermal retrofit of historical facades: A computational assessment, Conf. BSA2015 - Italy Conf. Bozental Bolzano Italy. (2015) 8.

[44] A. Uriarte, I. Garai, A. Ferdinando, A. Erkoreka, O. Nicolas, E. Barreiro, Vacuum insulation panels in construction solutions for energy efficient retrofitting of buildings. Two case studies in Spain and Sweden, Energy Build. 197 (2019) 131–139. https://doi.org/10.1016/j.enbuild.2019.05.039.

[45] F.N. Jones, M.E. Nichols, S.P. Pappas, Organic coatings: science and technology, 4th. ed, Wiley, Hoboken, New Jersey, 2017.

[46] J.H. Bieleman, Organic Thickeners for Water-Borne Paints, Chim. Int. J. Chem. 56 (2002) 163–169. https://doi.org/10.2533/000942902777680504.

[47] V. Alvarez, M. Paulis, Effect of acrylic binder type and calcium carbonate filler amount on the properties of paint-like blends, Prog. Org. Coat. 112 (2017) 210–218. https://doi.org/10.1016/j.porgcoat.2017.07.023.

[48] D. Stoye, W. Freitag, eds., Types of Paints and Coatings (Binders), in: Paints Coat. Solvents, Wiley-VCH Verlag GmbH, Weinheim, Germany, 1998: pp. 11–100. https://doi.org/10.1002/9783527611867.ch2.

[49] G. Wypych, Handbook of fillers, 4th edition, ChemTec Publishing, Toronto, 2016.

[50] J.V. Koleske, ed., Paint and coating testing manual: fifteenth edition of the Gardner-Sward handbook, ASTM International, West Conshohocken, PA, 2012.

[51] Detlef Gysau, Fillers for Paints Fundamentals and Applications, 3rd Revised Edition, European Coatings Library, Hanover: Vincentz Network, 2017.

[52] H.-J. Streitberger, A. Goldschmidt, BASF Handbook Basics of Coating Technology: 3rd Revised Edition, Vincentz Network, 2019. https://doi.org/10.1515/9783748600251.

[53] J.V. Koleske, R. Springate, D. Brezinski, Additives Handbook. Last access January 2022., HttpswwwpcimagcomextresourcesAdditivesHandbookPCI-Addit.-Defin.-2011-Secur.

[54] J.H. Bieleman, Organic Thickeners for Water-Borne Paints, Chim. Int. J. Chem. 56 (2002) 163–169. https://doi.org/10.2533/000942902777680504.

[55] G. Svanholm D., Associative thickeners: their adsorption behaviour onto latexes and the rheology of their solutions, Prog. Org. Coat. 30 (1997) 159–165. https://doi.org/10.1016/S0300-9440(96)00682-0.

[56] R. Lambourne, T.A. Strivens, Paint and surface coatings, Woodhead Publishing Limited, 1999. https://doi.org/10.1533/9781855737006.

[57] M. Carus, L. Dammer, The Circular Bioeconomy—Concepts, Opportunities, and Limitations, Ind. Biotechnol. 14 (2018) 83–91. https://doi.org/10.1089/ind.2018.29121.mca.

[58] P. Stegmann, M. Londo, M. Junginger, The circular bioeconomy: Its elements and role in European bioeconomy clusters, Resour. Conserv. Recycl. X. 6 (2020) 100029. https://doi.org/10.1016/j.rcrx.2019.100029.

[59] M.S. Gaikwad, V.V. Kusumkar, O.S. Yemul, D.G. Hundiwale, P.P. Mahulikar, Eco-friendly waterborne coating from bio-based polyester amide resin, Polym. Bull. 76 (2019) 2743–2763. https://doi.org/10.1007/s00289-018-2511-y.

[60] R.B. Lamorena, S.-G. Jung, G.-N. Bae, W. Lee, The formation of ultra-fine particles during ozone-initiated oxidations with terpenes emitted from natural paint, J. Hazard. Mater. 141 (2007) 245–251. https://doi.org/10.1016/j.jhazmat.2006.06.120.

[61] C. Veith, F. Diot-Néant, S.A. Miller, F. Allais, Synthesis and polymerization of bio-based acrylates: a review, Polym. Chem. 11 (2020) 7452–7470. https://doi.org/10.1039/D0PY01222J.

[62] J.G.H. Hermens, T. Freese, K.J. van den Berg, R. van Gemert, B.L. Feringa, A coating from nature, Sci. Adv. 6 (2020) eabe0026. https://doi.org/10.1126/sciadv.abe0026.

[63] S. Gogoi, N. Karak, Biobased Biodegradable Waterborne Hyperbranched Polyurethane as an Ecofriendly Sustainable Material, ACS Sustain. Chem. Eng. 2 (2014) 2730–2738. https://doi.org/10.1021/sc5006022.

[64] S.S. Panda, B.P. Panda, S. Mohanty, S.K. Nayak, Synthesis and properties of castor oil-based waterborne polyurethane cloisite 30B nanocomposite coatings, J. Coat. Technol. Res. 14 (2017) 377–394. https://doi.org/10.1007/s11998-016-9855-8.

[65] S.D. Rajput, D.G. Hundiwale, P.P. Mahulikar, V.V. Gite, Fatty acids based transparent polyurethane films and coatings, Prog. Org. Coat. 77 (2014) 1360–1368. https://doi.org/10.1016/j.porgcoat.2014.04.030.

[66] D.J. Kalita, I. Tarnavchyk, B.J. Chisholm, D.C. Webster, Novel bio-based epoxy resins from eugenol as an alternative to BPA epoxy and high throughput screening of the cured coatings, Polymer. 233 (2021) 124191. https://doi.org/10.1016/j.polymer.2021.124191.

[67] E.M. Petrie, The Evolution of Bio-Based Green Solvents, Met. Finish. 109 (2011) 33–36. https://doi.org/10.1016/S0026-0576(13)70009-6.

[68] Titanium dioxide proposed to be classified as suspected of causing cancer when inhaled. Last access January 2022, ECHA Eur. Chem. Agency. https://echa.europa.eu/it/-/titanium-dioxide-proposed-to-be-classified-as-suspected-of-causing-cancer-when-inhaled.

[69] M. Skocaj, M. Filipic, J. Petkovic, S. Novak, Titanium dioxide in our everyday life; is it safe?, Radiol. Oncol. 45 (2011) 227–247. https://doi.org/10.2478/v10019-011-0037-0.

[70] S. Middlemas, Z.Z. Fang, P. Fan, A new method for production of titanium dioxide pigment, Hydrometallurgy. 131–132 (2013) 107–113. https://doi.org/10.1016/j.hydromet.2012.11.002.

[71] N.A. Rowson, L.M. Grover, R.A. Choudhery, Low Carbon Footprint TiO2 Substitutes in Paint: A Review, Int. J. Chem. Eng. Appl. 6 (2015) 331–340. https://doi.org/10.7763/IJCEA.2015.V6.505.

[72] R. Narayan, K.V.S.N. Raju, The use of calcined clay as part replacement of titanium dioxide in latex paint formulations, J. Appl. Polym. Sci. 77 (2000) 1029–1036. https://doi.org/10.1002/1097-4628(20000801)77:5<1029::AID-APP9>3.0.CO;2-V.

[73] M.C.F. Karlsson, D. Corr, C. Forsgren, B.-M. Steenari, Recovery of titanium dioxide and other pigments from waste paint by pyrolysis, J. Coat. Technol. Res. 12 (2015) 1111–1122. https://doi.org/10.1007/s11998-015-9707-y.

[74] J. Kuusisto, T.C. Maloney, Preparation and characterization of corn starch–calcium carbonate hybrid pigments, Ind. Crops Prod. 83 (2016) 294–300. https://doi.org/10.1016/j.indcrop.2016.01.026.

[75] K.H. Mo, U.J. Alengaram, M.Z. Jumaat, S.C. Lee, W.I. Goh, C.W. Yuen, Recycling of seashell waste in concrete: A review, Constr. Build. Mater. 162 (2018) 751–764. https://doi.org/10.1016/j.conbuildmat.2017.12.009.

[76] S. Yoo, J.S. Hsieh, P. Zou, J. Kokoszka, Utilization of calcium carbonate particles from eggshell waste as coating pigments for ink-jet printing paper, Bioresour. Technol. 100 (2009) 6416–6421. https://doi.org/10.1016/j.biortech.2009.06.112.

[77] K.N. Onwukamike, S. Grelier, E. Grau, H. Cramail, M.A.R. Meier, Critical Review on Sustainable Homogeneous Cellulose Modification: Why Renewability Is Not Enough, ACS Sustain. Chem. Eng. 7 (2019) 1826–1840. https://doi.org/10.1021/acssuschemeng.8b04990.

[78] A.J. Gunorubon, U. Misel, Alternatives to natrosol as thickener in the production of emulsion paint, ARPN J. Eng. Appl. Sci. 9 (2014) 5.

[79] Rhône-Poulenc, Use of Xanthan Gum in water-based paints, Pigment Resin Technol. 16 (1987) 7–11. https://doi.org/10.1108/eb042346.

[80] D. Saha, S. Bhattacharya, Hydrocolloids as thickening and gelling agents in food: a critical review, J. Food Sci. Technol. 47 (2010) 587–597. https://doi.org/10.1007/s13197-010-0162-6.

[81] Y. Qin, Seaweed Hydrocolloids as Thickening, Gelling, and Emulsifying Agents in Functional Food Products, in: Bioact. Seaweeds Food Appl., Elsevier, 2018: pp. 135–152. https://doi.org/10.1016/B978-0-12-813312-5.00007-8.

[82] M. Kjellin, I. Johansson, eds., Surfactants from renewable resources, Wiley, Chichester, U.K, 2010.

[83] L. Bianco, V. Serra, S. Fantucci, M. Dutto, M. Massolino, Thermal insulating plaster as a solution for refurbishing historic building envelopes: First experimental results, Energy Build. 95 (2015) 86–91. https://doi.org/10.1016/j.enbuild.2014.11.016.

[84] J.P. Ingham, Mortar, plaster, and render, in: Geomaterials Microsc., Elsevier, 2013: pp. 137–162. https://doi.org/10.1016/B978-0-12-407230-5.50016-9.

[85] R. Nogueira, A.P. Ferreira Pinto, A. Gomes, Design and behavior of traditional lime-based plasters and renders. Review and critical appraisal of strengths and weaknesses, Cem. Concr. Compos. 89 (2018) 192–204. https://doi.org/10.1016/j.cemconcomp.2018.03.005.

[86] K.A.D.Y.T. Kahandawa Arachchi, A. Selvaratnam, J.C.P.H. Gamage, G.I.P. De Silva, Green composite plaster with modified morphology for enhanced thermal comfort in buildings, Case Stud. Constr. Mater. 15 (2021) e00611. https://doi.org/10.1016/j.cscm.2021.e00611.

[87] A.R.G. de Azevedo, J. Alexandre, E.B. Zanelato, M.T. Marvila, Influence of incorporation of glass waste on the rheological properties of adhesive mortar, Constr. Build. Mater. 148 (2017) 359–368. https://doi.org/10.1016/j.conbuildmat.2017.04.208.

[88] H. Du, K.H. Tan, Properties of high volume glass powder concrete, Cem. Concr. Compos. 75 (2017) 22–29. https://doi.org/10.1016/j.cemconcomp.2016.10.010.

[89] V. Corinaldesi, J. Donnini, A. Nardinocchi, Lightweight plasters containing plastic waste for sustainable and energy-efficient building, Constr. Build. Mater. 94 (2015) 337–345. https://doi.org/10.1016/j.conbuildmat.2015.07.069.

[90] G. Di Bella, V. Fiore, G. Galtieri, C. Borsellino, A. Valenza, Effects of natural fibres reinforcement in lime plasters (kenaf and sisal vs. Polypropylene), Constr. Build. Mater. 58 (2014) 159–165. https://doi.org/10.1016/j.conbuildmat.2014.02.026.

[91] A. Vishavkarma, K.V. Harish, Effect of rice husk ash on permeation characteristic of cementitious mortar, Mater. Today Proc. (2021) S2214785321069510. https://doi.org/10.1016/j.matpr.2021.10.448.

[92] K. Selvaranjan, S. Navaratnam, J.C.P.H. Gamage, J. Thamboo, R. Siddique, J. Zhang, G. Zhang, Thermal and environmental impact analysis of rice husk ash-based mortar as insulating wall plaster, Constr. Build. Mater. 283 (2021) 122744. https://doi.org/10.1016/j.conbuildmat.2021.122744.

[93] K.Y. Lee, D.J. Mooney, Alginate: Properties and biomedical applications, Prog. Polym. Sci. 37 (2012) 106–126. https://doi.org/10.1016/j.progpolymsci.2011.06.003.

[94] M. Szekalska, A. Puciłowska, E. Szymańska, P. Ciosek, K. Winnicka, Alginate: Current Use and Future Perspectives in Pharmaceutical and Biomedical Applications, Int. J. Polym. Sci. 2016 (2016) 1–17. https://doi.org/10.1155/2016/7697031.

[95] R. Ahmad Raus, W.M.F. Wan Nawawi, R.R. Nasaruddin, Alginate and alginate composites for biomedical applications, Asian J. Pharm. Sci. 16 (2021) 280–306. https://doi.org/10.1016/j.ajps.2020.10.001.

[96] A. Dodero, L. Pianella, S. Vicini, M. Alloisio, M. Ottonelli, M. Castellano, Alginate-based hydrogels prepared via ionic gelation: An experimental design approach to predict the crosslinking degree, Eur. Polym. J. 118 (2019) 586–594. https://doi.org/10.1016/j.eurpolymj.2019.06.028.

[97] S. Vicini, M. Mauri, S. Vita, M. Castellano, Alginate and alginate/hyaluronic acid membranes generated by electrospinning in wet conditions: Relationship between solution viscosity and spinnability: Research Article, J. Appl. Polym. Sci. 135 (2018) 46390. https://doi.org/10.1002/app.46390.

[98] Y. Li, J. Lu, X. Tian, Z. Xu, L. Huang, H. Xiao, X. Ren, Q. Kong, Alginate with citrus pectin and pterostilbene as healthy food packaging with antioxidant property, Int. J. Biol. Macromol. 193 (2021) 2093–2102. https://doi.org/10.1016/j.ijbiomac.2021.11.041.

[99] J.G. de Oliveira Filho, J.M. Rodrigues, A.C.F. Valadares, A.B. de Almeida, T.M. de Lima, K.P. Takeuchi, C.C.F. Alves, H.A. de F. Sousa, E.R. da Silva, F.H. Dyszy, M.B. Egea, Active food packaging: Alginate films with cottonseed protein hydrolysates, Food Hydrocoll. 92 (2019) 267–275. https://doi.org/10.1016/j.foodhyd.2019.01.052.

[100] Y. Fujiwara, R. Maeda, H. Takeshita, Y. Komohara, Alginates as food ingredients absorb extra salt in sodium chloride-treated mice, Heliyon. 7 (2021) e06551. https://doi.org/10.1016/j.heliyon.2021.e06551.

[101] Andrea Dodero, Stefano Alberti, G. Gaggero, M. Ferretti, R. Botter, S. Vicini, M. Castellano, An Up-to-Date Review on Alginate Nanoparticles and Nanofiber for Biomedical and Pharmaceutical Applications, Adv. Mater. Interfeces. 8 (2021) 2100809. https://doi.org/DOI: 10.1002/admi.202100809.

[102] J. Kozlowska, W. Prus, N. Stachowiak, Microparticles based on natural and synthetic polymers for cosmetic applications, Int. J. Biol. Macromol. 129 (2019) 952–956. https://doi.org/10.1016/j.ijbiomac.2019.02.091.

[103] S. Mitura, A. Sionkowska, A. Jaiswal, Biopolymers for hydrogels in cosmetics: review, J. Mater. Sci. Mater. Med. 31 (2020) 50. https://doi.org/10.1007/s10856-020-06390-w.

[104] A.E. Gaidoumi, A.C. Benabdallah, B.E. Bali, A. Kherbeche, Synthesis and Characterization of Zeolite HS Using Natural Pyrophyllite as New Clay Source, Arab. J. Sci. Eng. 43 (2018) 191–197. https://doi.org/10.1007/s13369-017-2768-8.

[105] B. Jha, D.N. Singh, Basics of Zeolites, in: Fly Ash Zeolites, Springer Singapore, Singapore, 2016: pp. 5–31. https://doi.org/10.1007/978-981-10-1404-8_2.

[106] Y.D.G. Edañol, K.A.S. Usman, S. Buenviaje Jr.C., M.E. Mantua, L. Payawan Jr.M., Utilizing Silica from Rice Hull for the Hydrothermal Synthesis of Zeolite Y, KIMIKA. 29 (2018) 17–21. https://doi.org/10.26534/kimika.v29i1.17-21.

[107] Z. Yuna, Review of the Natural, Modified, and Synthetic Zeolites for Heavy Metals Removal from Wastewater, Environ. Eng. Sci. 33 (2016) 443–454. https://doi.org/10.1089/ees.2015.0166.

[108] F.A. Mumpton, La roca magica: Uses of natural zeolites in agriculture and industry, Proc. Natl. Acad. Sci. 96 (1999) 3463–3470. https://doi.org/10.1073/pnas.96.7.3463.

[109] N. Mansouri, N. Rikhtegar, H.A. Panahi, F. Atabi, B.K. Shahraki, Porosity, characteriza-tion and structural properties of natural zeolite – clinoptilolite – as a sorbent, Environ. Prot. Eng. 39 (2013). https://doi.org/10.37190/epe130111.

[110] A. Jaskūnas, B. Subačius, R. Šlinkšienė, Adsorption of potassium ions on natural zeolite: kinetic and equilibrium studies, Chemija. 26 (2015) 69–78.

[111] M. Kong, Z. Liu, T. Vogt, Y. Lee, Chabazite structures with Li+, Na+, Ag+, K+, NH4+, Rb+ and Cs+ as extra-framework cations, Microporous Mesoporous Mater. 221 (2016) 253–263. https://doi.org/10.1016/j.micromeso.2015.09.031.

[112] A. Nakatsuka, N. Kawata, K. Fujiwara, Dehydration behavior of a natural hydrated Ca-chabazite studied by in-situ high-temperature single-crystal X-ray diffraction, Microporous Mesoporous Mater. 311 (2021) 110648. https://doi.org/10.1016/j.micromeso.2020.110648.

[113] Y. Li, L. Li, J. Yu, Applications of Zeolites in Sustainable Chemistry, Chem. 3 (2017) 928–949. https://doi.org/10.1016/j.chempr.2017.10.009.

[114] P. Cao, B. Li, W. Sun, L. Zhao, Understanding the zeolites catalyzed isobutane alkylation based on their topology effects on the reactants adsorption, Chem. Eng. Sci. 250 (2022) 117387. https://doi.org/10.1016/j.ces.2021.117387.

[115] T. Derbe, S. Temesgen, M. Bitew, A Short Review on Synthesis, Characterization, and Applications of Zeolites, Adv. Mater. Sci. Eng. 2021 (2021) 1–17. https://doi.org/10.1155/2021/6637898.

[116] C.G.S. Lima, E.Y.C. Jorge, L.G.S. Batinga, T. de M. Lima, M.W. Paixão, ZSM-5 zeolite as a promising catalyst for the preparation and upgrading of lignocellulosic biomass-derived chemicals, Curr. Opin. Green Sustain. Chem. 15 (2019) 13–19. https://doi.org/10.1016/j.cogsc.2018.08.001.

[117] A. Galadima, O. Muraza, Zeolite catalyst design for the conversion of glucose to furans and other renewable fuels, Fuel. 258 (2019) 115851. https://doi.org/10.1016/j.fuel.2019.115851.

[118] I. Rodríguez-Iznaga, G. Rodríguez-Fuentes, V. Petranovskii, Ammonium modified natural clinoptilolite to remove manganese, cobalt and nickel ions from wastewater: Favorable conditions to the modification and selectivity to the cations, Microporous Mesoporous Mater. 255 (2018) 200–210. https://doi.org/10.1016/j.micromeso.2017.07.034.

[119] A. Badeenezhad, A. Azhdarpoor, S. Bahrami, S. Yousefinejad, Removal of methylene blue dye from aqueous solutions by natural clinoptilolite and clinoptilolite modified by iron oxide nanoparticles, Mol. Simul. 45 (2019) 564–571. https://doi.org/10.1080/08927022.2018.1564077.

[120] J.-H. Shen, Y.-S. Wang, J.-P. Lin, S.-H. Wu, J.-J. Horng, Improving the indoor air quality of respiratory type of medical facility by zeolite filtering, J. Air Waste Manag. Assoc. 64 (2014) 13–18. https://doi.org/10.1080/10962247.2013.831798.

[121] L. Gao, X. Kong, D. Meng, S. Yang, W. Guo, X. Tang, M. Wang, H. Qiu, J. Li, B. Wang, Y. He, X. Pu, J. Zhu, Y. Zhang, Preparation of a novel zeolite Y-stainless-steel wire mesh honeycomb for VOC capture, Microporous Mesoporous Mater. 328 (2021) 111438. https://doi.org/10.1016/j.micromeso.2021.111438.

[122] V.S. Jakkula, S.P. Wani, Zeolites: Potential soil amendments for improving nutrient and water use efficiency and agriculture productivity, Sci. Rev. Chem. Commun. (2018) 1–15.

[123] H. Serati-Nouri, A. Jafari, L. Roshangar, M. Dadashpour, Y. Pilehvar-Soltanahmadi, N. Zarghami, Biomedical applications of zeolite-based materials: A review, Mater. Sci. Eng. C. 116 (2020) 111225. https://doi.org/10.1016/j.msec.2020.111225.

[124] G. Cerri, M. Degennaro, M. Bonferoni, C. Caramella, Zeolites in biomedical application: Zn-exchanged clinoptilolite-rich rock as active carrier for antibiotics in topical therapy, Appl. Clay Sci. 27 (2004) 141–150. https://doi.org/10.1016/j.clay.2004.04.004.

[125] T. Woignier, L. Duffours, Densification and Strengthening of Aerogels by Sintering Heat Treatments or Plastic Compression, Gels. 4 (2018) 12. https://doi.org/10.3390/gels4010012.

[126] H. Maleki, N. Hüsing, Aerogels as promising materials for environmental remediation—A broad insight into the environmental pollutants removal through adsorption and (photo)catalytic processes, in: New Polym. Nanocomposites Environ. Remediat., Elsevier, 2018: pp. 389–436. https://doi.org/10.1016/B978-0-12-811033-1.00016-0.

[127] Silica Aerogel, in: Mater. Res. Found., 1st ed., Materials Research Forum LLC, 2020: pp. 109–132. https://doi.org/10.21741/9781644900994-4.

[128] I. Smirnova, P. Gurikov, Aerogel production: Current status, research directions, and future opportunities, J. Supercrit. Fluids. 134 (2018) 228–233. https://doi.org/10.1016/j.supflu.2017.12.037.

[129] İ. Şahin, Y. Özbakır, Z. İnönü, Z. Ulker, C. Erkey, Kinetics of Supercritical Drying of Gels, Gels. 4 (2017) 3. https://doi.org/10.3390/gels4010003.

[130] J.L. Gurav, I.-K. Jung, H.-H. Park, E.S. Kang, D.Y. Nadargi, Silica Aerogel: Synthesis and Applications, J. Nanomater. 2010 (2010) 1–11. https://doi.org/10.1155/2010/409310.

[131] A. Lamy-Mendes, A.D.R. Pontinha, P. Alves, P. Santos, L. Durães, Progress in silica aerogel-containing materials for buildings' thermal insulation, Constr. Build. Mater. 286 (2021) 122815. https://doi.org/10.1016/j.conbuildmat.2021.122815.

[132] H. Zhang, C. Zhang, W. Ji, X. Wang, Y. Li, W. Tao, Experimental Characterization of the Thermal Conductivity and Microstructure of Opacifier-Fiber-Aerogel Composite, Molecules. 23 (2018) 2198. https://doi.org/10.3390/molecules23092198.

[133] E. Moretti, F. Merli, E. Cuce, C. Buratti, Thermal and Acoustic Properties of Aerogels: Preliminary Investigation of the Influence of Granule Size, Energy Procedia. 111 (2017) 472–480. https://doi.org/10.1016/j.egypro.2017.03.209.

[134] A. Verma, S. Thakur, G. Goel, J. Raj, V.K. Gupta, D. Roberts, V.K. Thakur, Bio-based sustainable aerogels: New sensation in CO2 capture, Curr. Res. Green Sustain. Chem. 3 (2020) 100027. https://doi.org/10.1016/j.crgsc.2020.100027.

[135] K. Ganesan, T. Budtova, L. Ratke, P. Gurikov, V. Baudron, I. Preibisch, P. Niemeyer, I. Smirnova, B. Milow, Review on the Production of Polysaccharide Aerogel Particles, Materials. 11 (2018) 2144. https://doi.org/10.3390/ma11112144.

[136] H. Cai, S. Sharma, W. Liu, W. Mu, W. Liu, X. Zhang, Y. Deng, Aerogel Microspheres from Natural Cellulose Nanofibrils and Their Application as Cell Culture Scaffold, Biomacromolecules. 15 (2014) 2540–2547. https://doi.org/10.1021/bm5003976.

[137] S. Wei, Y.C. Ching, C.H. Chuah, Synthesis of chitosan aerogels as promising carriers for drug delivery: A review, Carbohydr. Polym. 231 (2020) 115744. https://doi.org/10.1016/j.carbpol.2019.115744.

[138] E.G. Deze, S.K. Papageorgiou, E.P. Favvas, F.K. Katsaros, Porous alginate aerogel beads for effective and rapid heavy metal sorption from aqueous solutions: Effect of porosity in Cu2+ and Cd2+ ion sorption, Chem. Eng. J. 209 (2012) 537–546. https://doi.org/10.1016/j.cej.2012.07.133.

[139] Z. Li, L. Shao, Z. Ruan, W. Hu, L. Lu, Y. Chen, Converting untreated waste office paper and chitosan into aerogel adsorbent for the removal of heavy metal ions, Carbohydr. Polym. 193 (2018) 221–227. https://doi.org/10.1016/j.carbpol.2018.04.003.

[140] M. He, Md.K. Alam, H. Liu, M. Zheng, J. Zhao, L. Wang, L. Liu, X. Qin, J. Yu, Textile waste derived cellulose based composite aerogel for efficient solar steam generation, Compos. Commun. 28 (2021) 100936. https://doi.org/10.1016/j.coco.2021.100936.

[141] X. Yue, T. Zhang, D. Yang, F. Qiu, Z. Li, Hybrid aerogels derived from banana peel and waste paper for efficient oil absorption and emulsion separation, J. Clean. Prod. 199 (2018) 411–419. https://doi.org/10.1016/j.jclepro.2018.07.181.

[142] X.-L. Wu, T. Wen, H.-L. Guo, S. Yang, X. Wang, A.-W. Xu, Biomass-Derived Sponge-like Carbonaceous Hydrogels and Aerogels for Supercapacitors, ACS Nano. 7 (2013) 3589–3597. https://doi.org/10.1021/nn400566d.

[143] L. Zhu, Y. Wang, Y. Wang, L. You, X. Shen, S. Li, An environmentally friendly carbon aerogels derived from waste pomelo peels for the removal of organic pollutants/oils, Microporous Mesoporous Mater. 241 (2017) 285–292. https://doi.org/10.1016/j.micromeso.2016.12.033.

[144] X. Zhang, L.P. Kwek, D.K. Le, M.S. Tan, H.M. Duong, Fabrication and Properties of Hybrid Coffee-Cellulose Aerogels from Spent Coffee Grounds, Polymers. 11 (2019) 1942. https://doi.org/10.3390/polym11121942.

[145] F. Irgens, Rheology and Non-Newtonian Fluids, Springer International Publishing, Cham, 2014. https://doi.org/10.1007/978-3-319-01053-3.

[146] G. Schramm, A Practical Approach to Rheology and Rheometry, 2nd Edition, Gebrueder HAAKE GmbH, Karlsruhe, Federal Republic of Germany, 1998.

[147] J.W. Goodwin, R.W. Hughes, Rheology for chemists: an introduction, 2nd ed, RSC publ, Cambridge, 2008.

[148] R.R. Eley, Rheology in Coatings, Principles and Method, in: R.A. Meyers (Ed.), Paint Coat. Test. Man. 14th Ed., John Wiley & Sons, Ltd, Chichester, UK, 2006: p. a0611. https://doi.org/10.1002/9780470027318.a0611.

[149] A. Ramkrishnan, S. Kumar, Electrohydrodynamic effects in the leveling of coatings, Chem. Eng. Sci. 101 (2013) 785–799. https://doi.org/10.1016/j.ces.2013.06.024.

[150] R. Bhavsar, S. Shreepathi, Evolving empirical rheological limits to predict flow-levelling and sag resistance of waterborne architectural paints, Prog. Org. Coat. 101 (2016) 15–23. https://doi.org/10.1016/j.porgcoat.2016.07.016.

[151] T.G. Mezger, The Rheology Handbook: 4th Edition, Vincentz Network, Hannover, Germany, 2019.

[152] N.N. Daéid, Forensic Science | Systematic Drug Identification, in: Encycl. Anal. Sci., 2nd Edition, Elsevier, 2005: pp. 471–480. https://doi.org/10.1016/B0-12-369397-7/00197-7.

[153] A. Ramírez-Hernández, C. Aguilar-Flores, A. Aparicio-Saguilán, Fingerprint analysis of FTIR spectra of polymers containing vinyl acetate, DYNA. 86 (2019) 198–205. https://doi.org/10.15446/dyna.v86n209.77513.

[154] A.B.D. Nandiyanto, R. Oktiani, R. Ragadhita, How to Read and Interpret FTIR Spectroscope of Organic Material, Indones. J. Sci. Technol. 4 (2019) 97. https://doi.org/10.17509/ijost.v4i1.15806.

[155] A.K. Kota, J.M. Mabry, A. Tuteja, Superoleophobic surfaces: design criteria and recent studies, Surf. Innov. 1 (2013) 71–83. https://doi.org/10.1680/si.12.00017.

[156] K.-Y. Law, Definitions for Hydrophilicity, Hydrophobicity, and Superhydrophobicity: Getting the Basics Right, J. Phys. Chem. Lett. 5 (2014) 686–688. https://doi.org/10.1021/jz402762h.

[157] K.R. Rajisha, B. Deepa, L.A. Pothan, S. Thomas, Thermomechanical and spectroscopic characterization of natural fibre composites, in: Interface Eng. Nat. Fibre Compos. Maximum Perform., Elsevier, 2011: pp. 241–274. https://doi.org/10.1533/9780857092281.2.241.

[158] Laurence Podgorski, M. de Meijer, J.-D. Lanvin, Influence of Coating Formulation on Its Mechanical Properties and Cracking Resistance, Coatings. 7 (2017) 163. https://doi.org/10.3390/coatings7100163.

[159] C.G. Munger, L.D. Vincent, Corrosion prevention by protective coatings, 3. ed, NACE International, Houston, Tex, 2014.

[160] K.G. Wakili, C. Tanner, U-value of a dried wall made of perforated porous clay bricks Hot box measurement versus numerical analysis, Energy Build. (2003) 6.

[161] A. Comite, E.S. Cozza, G. Di Tanna, C. Mandolfino, F. Milella, S. Vicini, Thermal barrier coatings based on alumina microparticles, Prog. Org. Coat. 78 (2015) 124–132. https://doi.org/10.1016/j.porgcoat.2014.10.001.

[162] R. Russo, M. Malinconico, G. Santagata, Effect of Cross-Linking with Calcium Ions on the Physical Properties of Alginate Films, Biomacromolecules. 8 (2007) 3193–3197. https://doi.org/10.1021/bm700565h.

[163] S. Vicini, M. Mauri, J. Wichert, M. Castellano, Alginate gelling process: Use of bivalent ions rich microspheres, Polym. Eng. Sci. 57 (2017) 531–536. https://doi.org/10.1002/pen.24552.

[164] L. Wang, F. Zhu, D. Lu, Rheological properties of sodium alginate and xanthan pastes on cotton with reactive dye in screen printing, Text. Res. J. 83 (2013) 1873–1884. https://doi.org/10.1177/0040517513481873.

[165] F. Saad, A.L. Mohamed, M. Mosaad, H.A. Othman, A.G. Hassabo, Enhancing the rheological properties of aloe vera polysaccharide gel for use as an eco-friendly thickening agent in textile printing paste, Carbohydr. Polym. Technol. Appl. 2 (2021) 100132. https://doi.org/10.1016/j.carpta.2021.100132.

[166] Bouillon L., Ecological paint composition, useful for substrates including plastic, concrete, wood and cement used in buildings, comprises a load of algae with one or more alga having mineral structure, FR2998576A1, 2017.

[167] K. Mazur, R. Buchner, M. Bonn, J. Hunger, Hydration of Sodium Alginate in Aqueous Solution, Macromolecules. 47 (2014) 771–776. https://doi.org/10.1021/ma4023873.

[168] C.M. Keary, Characterization of METHOCEL cellulose ethers by aqueous SEC with multiple detectors, Carbohydr. Polym. 45 (2001) 293–303. https://doi.org/10.1016/S0144-8617(00)00263-0.

[169] A. Dodero, S. Vicini, M. Alloisio, M. Castellano, Sodium alginate solutions: correlation between rheological properties and spinnability, J. Mater. Sci. 54 (2019) 8034–8046. https://doi.org/10.1007/s10853-019-03446-3.

[170] W. Graessley, Polymer chain dimensions and the dependence of viscoelastic properties on concentration, molecular weight and solvent power, Polymer. 21 (1980) 258–262. https://doi.org/10.1016/0032-3861(80)90266-9.

[171] R.Y. Lochhead, The Use of Polymers in Cosmetic Products, in: Cosmet. Sci. Technol., Elsevier, 2017: pp. 171–221.

[172] S. Saalah, L.C. Abdullah, M.M. Aung, M.Z. Salleh, D.R. Awang Biak, M. Basri, E.R. Jusoh, S. Mamat, Colloidal stability and rheology of jatropha oil-based waterborne polyurethane (JPU) dispersion, Prog. Org. Coat. 125 (2018) 348–357. https://doi.org/10.1016/j.porgcoat.2018.09.018.

[173] S.R. Derkach, Rheology of emulsions, Adv. Colloid Interface Sci. 151 (2009) 1–23. https://doi.org/10.1016/j.cis.2009.07.001.

[174] E. Kostansek, Controlling particle dispersion in latex paints containing associative thickeners, J. Coat. Technol. Res. 4 (2007) 375–388. https://doi.org/10.1007/s11998-007-9037-9.

[175] M.M.M.G.P.G. Mantilaka, R.M.G. Rajapakse, D.G.G.P. Karunaratne, H.M.T.G.A. Pitawala, Preparation of amorphous calcium carbonate nanoparticles from impure dolomitic marble with the aid of poly(acrylic acid) as a stabilizer, Adv. Powder Technol. 25 (2014) 591–598. https://doi.org/10.1016/j.apt.2013.09.008.

[176] S.M.H. Dabiri, A. Lagazzo, F. Barberis, M. Farokhi, E. Finochio, L. Pastorino, Characterization of alginate-brushite in-situ hydrogel composites, Mater. Sci. Eng. C. 67 (2016) 502–510. https://doi.org/10.1016/j.msec.2016.04.104.

[177] W.-P. Voo, B.-B. Lee, A. Idris, A. Islam, B.-T. Tey, E.-S. Chan, Production of ultra-high concentration calcium alginate beads with prolonged dissolution profile, RSC Adv. 5 (2015) 36687–36695. https://doi.org/10.1039/C5RA03862F.

[178] W. Chen, Q. Feng, G. Zhang, Q. Yang, C. Zhang, The effect of sodium alginate on the flotation separation of scheelite from calcite and fluorite, Miner. Eng. 113 (2017) 1–7. https://doi.org/10.1016/j.mineng.2017.07.016.

[179] Y. Ma, Q. Feng, Alginate hydrogel-mediated crystallization of calcium carbonate, J. Solid State Chem. 184 (2011) 1008–1015. https://doi.org/10.1016/j.jssc.2011.03.008.

[180] L. Fuks, D. Filipiuk, M. Majdan, Transition metal complexes with alginate biosorbent, J. Mol. Struct. 792–793 (2006) 104–109. https://doi.org/10.1016/j.molstruc.2005.12.053.

[181] M. Rashidzadeh, Synthesis of High-Thermal Stable Titanium Dioxide Nanoparticles, Int. J. Photoenergy. 2008 (2008) 1–4. https://doi.org/10.1155/2008/245981.

[182] F. Loosli, L. Vitorazi, J.-F. Berret, S. Stoll, Towards a better understanding on agglomeration mechanisms and thermodynamic properties of TiO2 nanoparticles interacting with natural organic matter, Water Res. 80 (2015) 139–148. https://doi.org/10.1016/j.watres.2015.05.009.

[183] A. Overbeek, F. Bückmann, E. Martin, P. Steenwinkel, T. Annable, New generation decorative paint technology, Prog. Org. Coat. 48 (2003) 125–139. https://doi.org/10.1016/S0300-9440(03)00101-2.

[184] R.R. Eley, Applied rheology and architectural coating performance, J. Coat. Technol. Res. (2019). https://doi.org/10.1007/s11998-019-00187-5.

[185] A. Rodd, Rheological characterisation of "weak gel" carrageenan stabilised milks, Food Hydrocoll. 14 (2000) 445–454. https://doi.org/10.1016/S0268-005X(00)00024-2.

[186] H. Emady, M. Caggioni, P. Spicer, Colloidal microstructure effects on particle sedimentation in yield stress fluids, J. Rheol. 57 (2013) 1761–1772. https://doi.org/10.1122/1.4824471.

[187] P.C.F. Møller, J. Mewis, D. Bonn, Yield stress and thixotropy: on the difficulty of measuring yield stresses in practice, Soft Matter. 2 (2006) 274. https://doi.org/10.1039/b517840a.

[188] J.P. Paques, E. van der Linden, C.J.M. van Rijn, L.M.C. Sagis, Preparation methods of alginate nanoparticles, Adv. Colloid Interface Sci. 209 (2014) 163–171. https://doi.org/10.1016/j.cis.2014.03.009.

[189] K. Backfolk, S. Lagerge, J.B. Rosenholm, D. Eklund, Aspects on the Interaction between Sodium Carboxymethylcellulose and Calcium Carbonate and the Relationship to Specific Site Adsorption, J. Colloid Interface Sci. 248 (2002) 5–12. https://doi.org/10.1006/jcis.2001.8195.

[190] G. Pan, G. Zhang, Q. Shi, W. Chen, The Effect of Sodium Alginate on Chlorite and Serpentine in Chalcopyrite Flotation, (2019) 16.

[191] R. Bhavsar, R. Raj, R. Parmar, Studies of sedimentation behaviour of high pigmented alkyd primer: A rheological approach, Prog. Org. Coat. 76 (2013) 852–857. https://doi.org/10.1016/j.porgcoat.2013.02.009.

[192] T. Kusano, Rheological behavior of concentrated slurry and wet granules for lithium ion battery electrodes, Adv. Powder Technolgy. 31 (2020) 4491–4499. https://doi.org/10.1016/j.apt.2020.09.023.

[193] M. Youssry, F.Z. Kamand, M.I. Magzoub, M.S. Nasser, Aqueous dispersions of carbon black and its hybrid with carbon nanofibers, RSC Adv. 8 (2018) 32119–32131. https://doi.org/10.1039/C8RA05446K.

[194] K.I. Draget, K. Steinsvåg, E. Onsøyen, O. Smidsrød, Na- and K-alginate; effect on Ca2+-gelation, Carbohydr. Polym. 35 (1998) 1–6. https://doi.org/10.1016/S0144-8617(97)00237-3.

[195] G. Gaggero, M. Delucchi, G. Allegretta, S. Vicini, R. Botter, Interaction of sodium alginate thickener with components of architectural water-based coatings, Prog. Org. Coat. 151 (2021) 106016. https://doi.org/10.1016/j.porgcoat.2020.106016.

[196] J.V. Koleske, Mechanical Properties of Solid Coatings, in: R.A. Meyers (Ed.), Encycl. Anal. Chem., John Wiley & Sons, Ltd, Chichester, UK, 2006: p. a0608. https://doi.org/10.1002/9780470027318.a0608.

[197] R.G. Larson, Y. Wei, A review of thixotropy and its rheological modeling, J. Rheol. 63 (2019) 477–501. https://doi.org/10.1122/1.5055031.

[198] A. Maestro, C. González, J.M. Gutiérrez, Rheological behavior of hydrophobically modified hydroxyethyl cellulose solutions: A linear viscoelastic model, J. Rheol. 46 (2002) 127–143. https://doi.org/10.1122/1.1427910.

[199] A. Deka, N. Dey, Rheological studies of two component high build epoxy and polyurethane based high performance coatings, J. Coat. Technol. Res. 10 (2013) 305–315. https://doi.org/10.1007/s11998-012-9445-3.

[200] B.B. Raggiotti, M.J. Positieri, F. Locati, J. Murra, S. Marfil, Zeolite, Study of Aptitude as a Natural Pozzolan Applied to Structural Concrete, Rev. Constr. 14 (2015) 14–20. https://doi.org/10.4067/S0718-915X2015000200002.

[201] P. Frontera, S. Marchese, F. Crea, R. Aiello, J.B. Nagy, The strength effects of synthetic zeolites on properties of high performance concrete, in: High Perform. Struct. Mater. III, WIT Press, Ostend, Belgium, 2006: pp. 449–458. https://doi.org/10.2495/HPSM06044.

[202] G. Mertens, R. Snellings, K. Van Balen, B. Bicer-Simsir, P. Verlooy, J. Elsen, Pozzolanic reactions of common natural zeolites with lime and parameters affecting their reactivity, Cem. Concr. Res. 39 (2009) 233–240. https://doi.org/10.1016/j.cemconres.2008.11.008.

[203] O. D'Alessandro, C.E. Byrne, G. Selmi, C. Deyá, Anticorrosive paint with a modified zeolite as functional pigment for SAE 1010 steel protection, Pigment Resin Technol. 50 (2021) 136–145. https://doi.org/10.1108/PRT-05-2020-0052.

[204] L. Calabrese, E. Proverbio, A Brief Overview on the Anticorrosion Performances of Sol-Gel Zeolite Coatings, Coatings. 9 (2019) 409. https://doi.org/10.3390/coatings9060409.

[205] H. Song, N. Zheng, F. Xue, F. Cheng, Study on Thermal Insulation Zeolite by Coal Fly Ash, J. Nanomater. 2014 (2014) 1–6. https://doi.org/10.1155/2014/875940.

[206] S.K. Schnell, T.J.H. Vlugt, Thermal Conductivity in Zeolites Studied by Non-equilibrium Molecular Dynamics Simulations, Int. J. Thermophys. 34 (2013) 1197–1213. https://doi.org/10.1007/s10765-013-1467-2.

[207] A. Griesinger, K. Spindler, E. Hahne, Measurements and theoretical modelling of the e€ ective thermal conductivity of zeolites, Int J Heat Mass Transf. (1999) 12.

[208] T. Shimonosono, Y. Hirata, K. Nishikawa, S. Sameshima, K. Sodeyama, T. Masunaga, Y. Yoshimura, Thermal Properties of Zeolite-Containing Composites, Materials. 11 (2018) 420. https://doi.org/10.3390/ma11030420.

[209] A.P. Osonio, E.M. Olegario-Sanchez, Hydrophobic surface functionalization of Philippine natural zeolite for a targeted oil remediation application, AIP Conf. Proc. 1901 (2017) 080003. https://doi.org/10.1063/1.5010518.

[210] A. Zendelska, M. Golomeova, Š. Jakupi, K. Lisičkov, S. Kuvendžiev, M. Marinkovski, Characterization and application of clinoptilolite for removal of heavy metal ions from water resources, GEOME 2. 32 (2018) 21–32.

[211] L.T. Dimowa, I. Piroeva, S. Atanasova-Vladimirova, R. Rusew, B.L. Shivachev, Structural peculiarities of natural chabazite modified by ZnCl2 and NiCl2, Bulg. Chem. Commun. 50 (2018) 114–122.

[212] W. Guo, Y. Zhu, Y. Han, B. Luo, Y. Wei, Separation Mechanism of Fatty Acids from Waste Cooking Oil and Its Flotation Performance in Iron Ore Desiliconization, Minerals. 7 (2017) 244. https://doi.org/10.3390/min7120244.

[213] S. Wang, Y. Peng, Natural zeolites as effective adsorbents in water and wastewater treatment, Chem. Eng. J. 156 (2010) 11–24. https://doi.org/10.1016/j.cej.2009.10.029.

[214] D. Del Curto, V. Cinieri, Aerogel-Based Plasters and Energy Efficiency of Historic Buildings. Literature Review and Guidelines for Manufacturing Specimens Destined for Thermal Tests, Sustainability. 12 (2020) 9457. https://doi.org/10.3390/su12229457.

[215] D. Illera, J. Mesa, H. Gomez, H. Maury, Cellulose Aerogels for Thermal Insulation in Buildings: Trends and Challenges, Coatings. 8 (2018) 345. https://doi.org/10.3390/coatings8100345.

[216] International Coffee Organization, Last access September 2021,https://www.ico.org.

[217] N.E. Dávila-Guzmán, F. de Jesús Cerino-Córdova, E. Soto-Regalado, J.R. Rangel-Mendez, P.E. Díaz-Flores, M.T. Garza-Gonzalez, J.A. Loredo-Medrano, Copper Biosorption by Spent Coffee Ground: Equilibrium, Kinetics, and Mechanism, CLEAN - Soil Air Water. 41 (2013) 557–564. https://doi.org/10.1002/clen.201200109.

[218] D. García-García, A. Carbonell, M.D. Samper, D. García-Sanoguera, R. Balart, Green composites based on polypropylene matrix and hydrophobized spend coffee ground (SCG) powder, Compos. Part B Eng. 78 (2015) 256–265. https://doi.org/10.1016/j.compositesb.2015.03.080.

[219] T.-A. Kua, A. Arulrajah, S. Horpibulsuk, Y.-J. Du, C. Suksiripattanapong, Engineering and environmental evaluation of spent coffee grounds stabilized with industrial by-products as a road subgrade material, Clean Technol. Environ. Policy. 19 (2017) 63–75. https://doi.org/10.1007/s10098-016-1188-x.

[220] M. Yates, M.R. Gomez, M.A. Martin-Luengo, V.Z. Ibañez, A.M. Martinez Serrano, Multivalorization of apple pomace towards materials and chemicals. Waste to wealth, J. Clean. Prod. 143 (2017) 847–853. https://doi.org/10.1016/j.jclepro.2016.12.036.

[221] S. Vidović, A. Tepić Horecki, J. Vladić, Z. Šumić, A. Gavarić, A. Vakula, Apple, in: Valorization Fruit Process. -Prod., Elsevier, 2020: pp. 17–42. https://doi.org/10.1016/B978-0-12-817106-6.00002-2.

[222] M.L. Sudha, Apple Pomace (By-Product of Fruit Juice Industry) as a Flour Fortification Strategy, in: Flour Breads Their Fortif. Health Dis. Prev., Elsevier, 2011: pp. 395–405. https://doi.org/10.1016/B978-0-12-380886-8.10036-4.

[223] B. Schroeter, V.P. Yonkova, N.A.M. Niemeyer, I. Jung, I. Preibisch, P. Gurikov, I. Smirnova, Cellulose aerogel particles: control of particle and textural properties in jet cutting process, Cellulose. 28 (2021) 223–239. https://doi.org/10.1007/s10570-020-03555-2.

[224] M. Odalanowska, M. Woźniak, I. Ratajczak, D. Zielińska, G. Cofta, S. Borysiak, Propolis and Organosilanes as Innovative Hybrid Modifiers in Wood-Based Polymer Composites, Materials. 14 (2021) 464. https://doi.org/10.3390/ma14020464.

[225] S. Hokkanen, M. Sillanpää, Nano- and microcellulose-based adsorption materials in water treatment, in: Adv. Water Treat., Elsevier, 2020: pp. 1–83. https://doi.org/10.1016/B978-0-12-819216-0.00001-1.

[226] L.-Y. Long, Y.-X. Weng, Y.-Z. Wang, Cellulose Aerogels: Synthesis, Applications, and Prospects, Polymers. 10 (2018) 623. https://doi.org/10.3390/polym10060623.

[227] D. Pujol, C. Liu, J. Gominho, M.À. Olivella, N. Fiol, I. Villaescusa, H. Pereira, The chemical composition of exhausted coffee waste, Ind. Crops Prod. 50 (2013) 423–429. https://doi.org/10.1016/j.indcrop.2013.07.056.

[228] N.E. Dávila-Guzmán, F. de Jesús Cerino-Córdova, E. Soto-Regalado, J.R. Rangel-Mendez, P.E. Díaz-Flores, M.T. Garza-Gonzalez, J.A. Loredo-Medrano, Copper Biosorption by Spent Coffee Ground: Equilibrium, Kinetics, and Mechanism, CLEAN - Soil Air Water. 41 (2013) 557–564. https://doi.org/10.1002/clen.201200109.

[229] M. Zanini, A. Lavoratti, L.K. Lazzari, D. Galiotto, M. Pagnocelli, C. Baldasso, A.J. Zattera, Producing aerogels from silanized cellulose nanofiber suspension, Cellulose. 24 (2017) 769–779. https://doi.org/10.1007/s10570-016-1142-4.

[230] M. Yates, M.R. Gomez, M.A. Martin-Luengo, V.Z. Ibañez, A.M. Martinez Serrano, Multivalorization of apple pomace towards materials and chemicals. Waste to wealth, J. Clean. Prod. 143 (2017) 847–853. https://doi.org/10.1016/j.jclepro.2016.12.036.

[231] A.C. Gowman, M.C. Picard, A. Rodriguez-Uribe, M. Misra, H. Khalil, M. Thimmanagari, A.K. Mohanty, Physicochemical Analysis of Apple and Grape Pomaces, BioResources. 14 (2019) 3210–3230.

[232] Q. Liao, X. Su, W. Zhu, W. Hua, Z. Qian, L. Liu, J. Yao, Flexible and durable cellulose aerogels for highly effective oil/water separation, RSC Adv. 6 (2016) 63773–63781. https://doi.org/10.1039/C6RA12356B.

[233] L.-Y. Wu, Y.-L. Guo, L.-L. Cao, S. Jin, H.-Z. Lin, M.-Y. Wu, J.-K. Lin, J.-H. Ye, Application of NaOH-HCl-Modified Apple Pomace to Binding Epigallocatechin Gallate, Food Bioprocess Technol. 9 (2016) 917–923. https://doi.org/10.1007/s11947-016-1683-4.

[234] N. Zarrinbakhsh, T. Wang, A. Rodriguez-Uribe, M. Misra, A.K. Mohanty, Characterization of Wastes and Coproducts from the Coffee Industry for Composite Material Production, BioResources. 11 (2016) 7637–7653. https://doi.org/10.15376/biores.11.3.7637-7653.

[235] M.R.B. Guerrero, M. Marques da Silva Paula, M.M. Zaragoza, J.S. Gutiérrez, V.G. Velderrain, A.L. Ortiz, V. Collins-Martínez, Thermogravimetric study on the pyrolysis kinetics of apple pomace as waste biomass, Int. J. Hydrog. Energy. 39 (2014) 16619–16627. https://doi.org/10.1016/j.ijhydene.2014.06.012.

[236] A. Baldinelli, X. Dou, D. Buchholz, M. Marinaro, S. Passerini, L. Barelli, Addressing the energy sustainability of biowaste-derived hard carbon materials for battery electrodes, Green Chem. 20 (2018) 1527–1537. https://doi.org/10.1039/C8GC00085A.

[237] E. Lucchi, F. Becherini, M.C. Di Tuccio, A. Troi, J. Frick, F. Roberti, C. Hermann, I. Fairnington, G. Mezzasalma, L. Pockelé, A. Bernardi, Thermal performance evaluation and comfort assessment of advanced aerogel as blown-in insulation for historic buildings, Build. Environ. 122 (2017) 258–268. https://doi.org/10.1016/j.buildenv.2017.06.019.

[238] T. Kvande, N. Bakken, E. Bergheim, J. Thue, Durability of ETICS with Rendering in Norway—Experimental and Field Investigations, Buildings. 8 (2018) 93. https://doi.org/10.3390/buildings8070093.

[239] J.L. Parracha, G. Borsoi, I. Flores-Colen, R. Veiga, L. Nunes, Impact of natural and artificial ageing on the properties of multilayer external wall thermal insulation systems, Constr. Build. Mater. 317 (2022) 125834. https://doi.org/10.1016/j.conbuildmat.2021.125834.

[240] B. Maleki, A. Khadang, H. Maddah, M. Alizadeh, A. Kazemian, H.M. Ali, Development and thermal performance of nanoencapsulated PCM/ plaster wallboard for thermal energy storage in buildings, J. Build. Eng. 32 (2020) 101727. https://doi.org/10.1016/j.jobe.2020.101727.

[241] L. Evangelisti, C. Guattari, F. Asdrubali, Comparison between heat-flow meter and Air-Surface Temperature Ratio techniques for assembled panels thermal characterization, Energy Build. 203 (2019) 109441. https://doi.org/10.1016/j.enbuild.2019.109441.